Katholieke
Universiteit
Leuven

Faculteit Wetenschappen
Centrum voor Plasma-Astrofysica

Velocity shear induced phenomena in solar and astrophysical flows

Alexander G. Tevzadze

A thesis submitted for
Doctor in de Wetenschappen

Supervisors:
Prof. Dr. Marcel Goossens
Dr. George D. Chagelishvili

Leuven, April 2006.

Thanks

The present dissertation is a summary of the work that I have conducted in Centre for Plasma Astrophysics, (CPA, K.U.Leuven) and Abastumani Astrophysical Observatory (AbAO, Georgia).
I would like to thank George Chagelishvili who introduced me into the subject of the presented study and for continuous support.
Marcel Goossens was my supervisor in CPA and among many other things I would like to thank him for his patience during the last 5 years.
Andria Rogava has led me in navigation to the Belgium. I thank him for help and support.
At CPA I enjoyed hospitality for which I thank Stefaan Poedts and Arnold Debosscher. For friendly and stimulating atmosphere in the CPA I thank Anik De Groof, Jesse Andries, Bart van der Holst, Yuriy Voitenko and Jovo Vranje who are presently in CPA, as well as Balazs Pinter, Istvan Ballai, Eva Robbrecht, Petra Vanlommel, Olena Sirenko, Dipankar Banerjee, Arpad Csik, Hans De Sterck, Birendra Pandey, Yusef Zhugzhda, Ronald Van der Linden and Inigo Arregui who have already left CPA.
Special thanks to Bidzina Shergelashvili, my PhD-mate, who also helped a lot with administrative details.
I would like to thank Gianluigi Bodo and Paola Rossi from Osservatorio di Torino for introducing me into the field of numerical simulations.
I would like to thank all my colleagues in AbAO while I have no opportunity to list the names.
While the bulk of the thesis is based on the studies conducted at CPA and AbAO, there is a contribution from my earlier period spent at Space Research Institute in Moscow. I would like to thank people with whom I have interacted in SRI: S. Moiseev, N. Erokhin, O. Chkhetiani and my friends and colleagues when staying at SRI - Sandro Taktakishvili, George Khujadze and Grigol Gogoberidze. I would like to thank director of the AbAO from that period Jumber Lominadze for the support and opportunities I had.
I would like to remember Elguja Tsikarishvili, who have introduced me into the field of astrophysics when I was still doing my undergraduate studies.

Contents

Chapter 1

Introduction

The subject of the present thesis is a study of the dynamics of inhomogeneous flows. In particular, we carry out a theoretical and numerical investigation of the linear perturbations of flows with inhomogeneous velocity profiles.
Inhomogeneity of mean flow is a basic source of energy and affects all possible motions and processes that take place in these flows at kinematic scales. Velocity shear modifies existing and originates new phenomena. Flows with inhomogeneous velocity affected by gravity, rotation and electro-magnetic forces exhibit a variety of phenomena that are not yet fully understood. Thus, the investigation of shear flow dynamics is an important topic in astrophysics. A contribution in this direction is attempted by the present thesis.

1.1 Shear flows in nature

Flows in nature are all inhomogeneous to some extent. In reality, there are a variety of factors that define how important the velocity shear of the flow is. Therefore, we call a flow a shear flow if the velocity inhomogeneity exerts a noticeable effect on processes taking place in the flow. Below are some examples of shear flows – flows where processes are driven and sometimes energetically supported by the velocity inhomogeneity.

Solar flows

The Sun is a sphere of self-gravitating hot plasma in almost perfect hydrostatic equilibrium. It is usual star with the only difference that it is in close vicinity of the Earth. This remarkable natural laboratory gives us an excellent opportunity to study various highly energetic flows at different temporal and spatial scales in a complex environment. Indeed,

a closer look on the Sun reveals that it sustains violent flows that exhibit strong inhomogeneities.

It has long been known from observations of sunspots that the surface of the Sun rotates differentially. The solar equator rotates almost 30% faster than regions closer to the poles. The solar surface exhibits a global shear in the latitudinal direction. Recent observations of solar acoustic oscillations made it possible to infer the internal structure of the rotation. The Sun rotates differentially throughout the convection zone, while the deeper interior rotates rigidly (radiative zone and core). The strong turbulent flows in the convection zone continuously redistribute the angular momentum leading to a profound radial and latitudinal differential rotation of the matter within the solar convective envelope. The dependence of the solar rotation rate on the radial distance, as well as on latitude is illustrated in Fig. 1.1. The global latitudinal differential rotation is uniform within the convection zone, while the zones of the strong radial shear in the rotation rate are concentrated at the top and the bottom of the convection zone. The layer of extreme differential rotation at the base of the convection zone, where the nearly rigid body rotation in the radiative zone adjusts itself to the differential pattern in the convection zone is called the solar tachocline. This is the layer where the differential rotation is thought to play a crucial role in fuelling the dynamo that generates the solar magnetic fields.

Together with this global shearing the Sun exhibits numerous small-scale flows with strongly inhomogeneous velocity profiles in different physical conditions. Local shear flows are formed in the convection zone (see Fig. 1.2), where the rising flows of hotter and descending flows of cooler material create velocity gradients that trigger small scale turbulence and the production of solar acoustic oscillations.

Even more complex flows are found in the solar atmosphere. This low density magnetized environment is highly structured and sustains a variety of inhomogeneous flows that occur on different time scales.

Velocity shear is also thought to be an important factor in defining the dynamics of the solar wind.

Astrophysical disk flows

Many astrophysical objects are structured into disks rotating around the gravitating center. Kepler's law determines the rotation angular velocity of any given mass around the central object. When the matter rotating around the center is not bounded gravitationally into isolated dense formations (planets or stars), but is distributed and can exchange momentum, it may be well considered as a continuous medium and a global flow around the centre. In these flows every fluid parcel rotates on its own Keplerian orbit. Hence fluid parcels situated on two different orbits

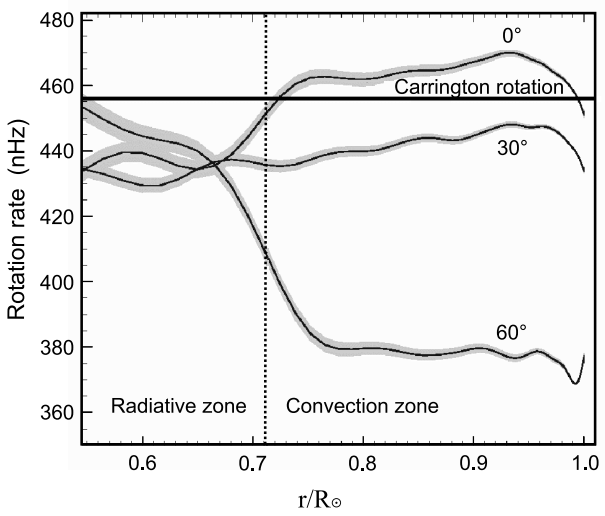

Figure 1.1: Solar rotation rate as function of radius at three different latitudes: 0°, 30° and 60° (as inferred from the MDI SOHO data). The formal errors are indicated by shaded regions. The dotted vertical line marks the lower boundary of the convection zone. The solid horizontal line marks the Carrington rotation rate, which matches the rotation rate of the solar sunspots at approximately 20° latitude and is usually used as a reference frame. It appears that the latitudinal differential rotation is observed throughout the whole height of the convective envelope. The radial shear in the rotation rate occurs at the top, and most remarkably at the bottom of the convection zone where it forms the solar tachocline. [Adapted from Kosovichev et al. 1997]

are continuously shifted with respect to each other. In other words, Kepler's law introduces a strong differential rotation in the radial direction. Keplerian rotation differs from solid body rotation and is characterized by radial shear flow in the co-rotating frame. This kind of flows occur on different scales such as planetary rings, protoplanetary disks, segments of galactic disks, circumstellar and accretion disks around normal stars and compact objects. In astrophysical disks with differential rotation the radial velocity inhomogeneity of the flow is energetically fed by the gravitational potential. Hence, differentially rotating astrophysical flows are characterized by a persistent velocity shear. This indicates how important shear induced processes in such environment are. In particular, processes driven by velocity inhomogeneity are thought to play a key role in supporting the turbulence in accretion disks, affect small scale dynamics of perturbations and the momentum transport in general as well as the process of the planet formation in protoplanetary disks.

Sometimes, disk flows are accompanied by rapid outflows, directed per-

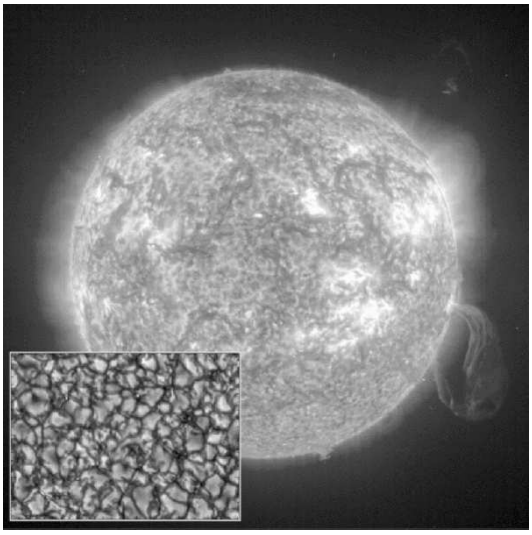

Figure 1.2: The Sun. This is the SOHO satellite image taken by the Extreme ultraviolet Imaging Telescope at 304Å wavelength when the observed bright material is at $6 \div 8 \cdot 10^4$K temperature. The image reveals the inhomogeneity and high complexity of flows in the solar atmosphere. The granulation pattern observed on the top of the convection zone is shown in the left bottom corner of the figure. The field of 20×14.5 Mm^2 is shown. This image is restored from the ground based observations of the German Vacuum Tower Telescope. The bright granular structures correspond to the hot rising material, while dark lanes in between the granules are the cooler downflows. The strong shear flows in the vertical direction are observed.

pendicular to the disk plane. These are astrophysical jets. These highly energetic flows are often beaming at extremely high speeds and are excellent objects for the study of the strongly inhomogeneous flows at relativistic speeds.

An important class of shear flows may be found in the planetary atmospheres. These include the spectacular shear flows, such as the Jovian zonal flows that support a number of vortices, including the Great Red Spot, as well as some minor but not less intriguing examples of the vortices and violent transient flows that may be observed on surfaces of planetary atmospheres.

Other examples of shear flows in astrophysics are flows in molecular clouds, inhomogeneities in the stellar winds and atmospheres, pulsar magnetosphere, etc.

Terrestrial flows

The best studied example of shear flows in nature are probably those that occurr in the Earth's atmosphere and oceans. Analysis of the terrestrial shear flow is closely related to studies in climate dynamics, various atmospheric phenomena and ocean dynamics. The velocity shear is an important factor in the balances in the Earth's core magma flows, where it is thought to support the terrestrial dynamo that generates the planet's magnetic field.

Research in shear flows is an important subject in different laboratory applications as well as technical flows such as oil/gas tubes; convective shear flows; biological flows; rheological flows and shear effect on polymer chains; multi-phase and other complex flows.

Analysis of inhomogeneous flows is the essence of the boundary layer research (where velocity shear and viscosity are intrinsically persistent), as well as of the analysis of turbulent flows in general.

1.2 Shear flow analysis

The importance of shear flows has been understood long ago and the investigation of these flows has occupied human attention fore more than a century. Nevertheless, shear flows are still not completely understood. Problems arise already in the linear stability analysis.

For a long time the research of shear flows was focused on the stability analysis, focusing on flows with an equilibrium velocity profile having an inflection point, where the second spatial derivative of the velocity changes sign in a particular point. This was due to the fact that according to the classical Rayleigh's theory the existence of an inflection point in the equilibrium velocity profile is a necessary condition for the occurrence of a spectral instability (see Fjørtøft 1950). It was accepted that extraction of the mean flow energy by perturbations was possible only when the flow velocity profile had an infection point. However, as it was found in 1990s, this argument was not completely correct and the presence of an inflection point was not the only crucial fact in the dynamics of shear flows. It was found that smooth shear flows without an inflection point in the velocity profiles exhibit a lot of energetic processes – processes of mean flow energy extraction, energy exchange between perturbations, etc., while according to the classical theory they are spectrally stable and consequently "relaxed." In the present thesis we concentrate particularly on these non-classical effects in smooth shear flows. This emphasis is due to the following two facts: firstly, it is of prime interest in theoretical hydrodynamics, and secondly, most of the flows in astrophysical objects are sheared with smooth velocity profiles, without any inflection point.

The traditional way for the investigation of dynamical processes in a

continuous medium is the modal analysis by eigenmodes and eigenvalues. This method consists of the following two steps: a) linearization about a stationary background solution and b) using the spectral expansion of perturbations and study of eigenvalues of the linear problem. The flow is found to be unstable if the linear eigenvalue spectrum has a positive imaginary part, which corresponds to exponentially growing solutions. This method was useful in the study of many fundamental instabilities that reveal themselves in the eigenvalue spectrum. However, there is increasing number of cases where results predicted by this modal analysis lead to controversy.

Already Couette (1890) noticed that the flow between the counter-rotating cylinders becomes turbulent when perturbations are spectrally stable and no exponentially growing linear perturbations are present. Later extended observations by Coles (1965) have confirmed that turbulent regimes may be observed in both, counter rotating as well as in co-rotating cylinders. No linear instability is known for plane Couette flow, while experimental results indicate that it becomes turbulent at Reynolds numbers (Re) about 1300 (see e.g. Dauchot and Daviaud 1995, Bottin et al. 1998). Pipe Poiseuille flow is linearly stable and becomes turbulent when Re is larger than about 2000. Interesting is the case of the plane Poiseuille flow which becomes linearly unstable at $Re = 5772$ (see Lin 1946, Orszag 1971), while experiments show well developed turbulent state already at $Re = 1000$. This is a strong indication that the mechanism of transition to turbulence in these flows must be different from an eigenvalue instability. Attempts to resolve these problems referred to the nonlinear dynamics of the system and thus questioned the step a) of the modal analysis rather than the validity of the linear eigenmode analysis itself.

It was recently Reddy et al. (1993) (see also Trefethen et al. 1993) who have revealed the essence of the difficulties of the modal approach. It appears that the eigenmode analysis is not fit for a self-consistent analysis of dynamics of shear flows. The operators that appear in the modal analysis of shear flows (for instance plane Couette or Poiseuille flows) are not self-adjoint. The eigenfunctions of such operators are not mutually orthogonal. In this case the system is called non-normal. In non-normal systems the eigenvalue analysis does not give an adequate description of the dynamics of the system. It omits the interference processes due to the non-orthogonality of the solutions. As a result, even when all eigensolutions decay monotonically in time a particular solution may undergo a large relative growth in a limited time interval. We demonstrate the transient growth of a non-modal solution for a simple 2D non-normal system in Fig. 1.3. Hence, the use of a spectral expansion of perturbations and the study of the eigenmodes does not gives an adequate description of the shear flow dynamics. In short, knowledge

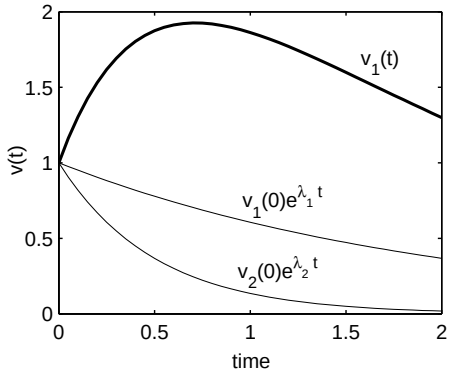

Figure 1.3: Illustration of the non-modal growth in the simplified two dimensional model system: $\partial_t \mathbf{v} = \mathbf{L}\mathbf{v}$, where $\mathbf{L} = \begin{pmatrix} \lambda_1 & A \\ 0 & \lambda_2 \end{pmatrix}$ is a non-normal matrix. The figure is plotted for the following set of parameters and initial values of $\mathbf{v}(t)$: $\lambda_1 = -0.5$, $\lambda_2 = -2$, $A = -4$, $v_1(0) = 1$ $v_2(0) = 1$. Eigenvalues of the matrix L are λ_1 and λ_2. Hence the modal analysis predicts the following simple exponential solutions: $v_1(0)\exp(\lambda_1 t)$ and $v_2(0)\exp(\lambda_2 t)$ (see the bottom two graphs on the figure). However, eigenvectors of this non-normal matrix are not orthogonal: $u_1 = \begin{pmatrix} 1 \\ 0 \end{pmatrix}$ and $u_2 = \begin{pmatrix} A/\Delta\lambda \\ 1 \end{pmatrix}$, where $\Delta\lambda = \lambda_1 - \lambda_2$. Hence, the correct solution of the system will be a result of the superposition of the modal solutions: $v_1(t) = \left[v_1(0) - \frac{A}{\Delta\lambda} v_2(0)\right] e^{\lambda_1 t} + \frac{A}{\Delta\lambda} v_2(0) e^{\lambda_2 t}$ and $v_2(t) = v_2(0)e^{\lambda_2 t}$. The top (heavy) curve of the figure $v_1(t)$ reveals the transient amplification on finite times before the asymptotic modal behavior of the exponential decrease. The amplitude of the transient growth is proportional to the measure of the non-normality A. This transient amplification is not anticipated by the eigenvalues (spectral characteristics) of the system but is completely attributed to the non-normal behavior of the system.

obtained by modal analysis of the non-normal system (shear flow) is valid only asymptotically, for long times, while it omits eigenmode interference that takes place transiently, during limited time intervals.
Once it was understood that the modal analysis leads to the difficulties new alternative methods were developed. The notion of the pseudospectrum was developed in order to include non-normal effects of transient amplification in the spectral characteristics of the flow (see Trefethen 1997). Numerical calculations of the pseudospectrum have been carried out for several different shear flows in order to specify more accurately its stability characteristics. The transient amplification phenomenon was also recognized by Gustavsson and Hultgren (1980), who performed a numerical study of the Orr-Sommerfeld equation. The non-exponential character of the non-modal amplification phenomenon was probably best

understood by Landahl (1980) who, by means of the partial integration of the equation of motion, demonstrated that perturbations in a spectrally stable shear flow can be amplified and introduced the notation of an algebraic instability.
However, probably the most efficient method was designed well before the understanding of the non-normality of shear flows. Lord Kelvin (1886) was the first to find modes that describe transiently growing solutions in an inviscid incompressible parallel shear flow. The method was extended and applied to galactic disk shear flows by Goldreich and Lynden-Bell (1965) and has been used extensively during the last decade. The essence of the method, which is normally referred as a non-modal approach, lies in the following two steps. Transformation of variables to the co-moving frame (sometimes called "shearing sheet") and further study of the spatial Fourier harmonics (SFH) without spectral expansion in time. Such a method leads to an initial value problem in contrast to a boundary value problem obtained in modal analysis and fits best for the description of the transient non-normal phenomena.
The non-modal formalism is well described in case of bounded compressible parallel shear flows in Criminale and Drazin (1990). Butler and Farrell (1992) have introduced the notion of optimal perturbations – perturbations that are best fit to be maximally amplified by the non-normal mechanism (see also Farrell, Ioannou 1993). Stochastic non-normal systems have been numerically investigated by Farrell and Ioannou (1994). They have specified the non-modal amplification rates of such system and found that the variance maintained by the stochastic forcing in the spectrally stable shear flow may be increased with power of the Reynolds number between 1,5 and 3.
The non-modal approach greatly simplifies the mathematical description of the shear flow dynamics and helps to grasp phenomena that are overlooked by the modal analysis. This analysis has been instrumental in revealing two novel channels of energy exchange in shear flows:

(i) The energy exchange between the background flow and perturbations

(ii) The energy exchange between different perturbation modes

The first channel describes the transient amplification of vortical perturbations and the non-modal energy exchange between the wave modes and the mean shear flow. The same process accounts for the shear flow stabilization of the spectral instabilities. The transient growth phenomenon is largely responsible for the development of the new conjecture of the linear subcritical transition to the turbulence.
The second channel describes the energy exchange between the different modes during their linear stage of the evolution. Shear flow couples

linear modes and leads to their transformations. The bulk of the present thesis reflects the study of the energy exchange processes between the modes in shear flows present in various astrophysical situations.

1.3 Outline of the thesis

The purpose of this thesis is to investigate shear flows and study velocity shear induced phenomena in different astrophysical applications. The thesis is organized as follows:

In the first chapter we shortly outline the importance of the study and describe different astrophysical environments where the inhomogeneity of the flow velocity plays an important role in the global dynamics of the system. We describe the theoretical methods of shear flow analysis: the modal analysis and difficulties which arise when it is applied to shear flows. We introduce the non-modal method. We describe advantages of this method and progress that has been achieved using it.

In the second chapter we analyze basic properties of shear flows using the non-modal method. We demonstrate the formalism of the non-modal analysis and also characteristic features of flows with velocity shear. Particularly, we consider linear perturbations and analyze the vortex and wave modes separately.

The third chapter is devoted to the study of mode conversion. We analyze the dynamics of spatial Fourier harmonics of the compressible linear perturbations in shear flows and study the excitation of acoustic waves due to shear induced vortex-wave conversion. We also demonstrate the phenomenon using the direct numerical simulations of the initially localized vortex modes.

In chapter 4 we study compressible perturbations in a magnetized shear flow. Using the MHD approximation we demonstrate that fast magnetosonic waves may be excited from vortex mode perturbations due to the background velocity shear.

In chapter 5 we investigate unstably stratified shear flows. We study the shear flow effects on gravity modified acoustic waves, vortices and the convectively unstable buoyancy perturbations on their linear stage of evolution. Particularly, we study the phenomenon of the conversion of convection into the acoustic waves.

We study the dynamics of astrophysical disks in chapter 6. In particular we analyze linear perturbations in a differentially rotating medium. We study the growth of barotropic vortices due to the transient amplification mechanism, and effects of the velocity shear on the acoustic and density-spiral waves in the medium. We study the excitation of the density-spiral and double excitation of the both wave modes due to the shear flow. We discuss the importance of our findings in view of the transition to the

turbulence and momentum transport in accretion disk flows.
We study the dynamics of the MHD waves in parallel shear flows in chapter 7. We analyze the linear perturbation modes individually and study cases when the resonant phenomenon of wave transformations may occur. We study the phenomenon for double and triple transformations. In chapter 8 we give a summarizing discussion of the presented investigation.

Chapter 2

General properties of shear flows

In this chapter we focus on simple shear flows aiming to describe the non-modal method as well as the basic properties of flows with inhomogeneous velocity fields. We start with the equations of magnetohydrodynamics and then study the linear perturbations of the non-magnetized equilibrium state. We illustrate the mathematical formalism of the non-modal method for a parallel flow with a constant linear velocity shear. In order to demonstrate the effect of the background shear flow on the perturbation modes individually we consider limiting cases separately. In particular, we analyze the effects of shear flow on the vortical and compressible perturbations when simple analytic solutions may be obtained. Finally, we estimate the possible values of the velocity shear that may occur in equilibrium flows and introduce the convention used further throughout the thesis.

2.1 Basic equations

The basic MHD equations are the conservation laws for mass, momentum and energy. Conservation of the mass is described by the continuity equation:

$$\left\{\frac{\partial}{\partial t} + \mathbf{V}\cdot\nabla\right\}\rho + \rho(\nabla\cdot\mathbf{V}) = 0. \tag{2.1}$$

Momentum conservation is written as the equation of motion:

$$\rho\left\{\frac{\partial}{\partial t} + \mathbf{V}\cdot\nabla\right\}\mathbf{V} = -\nabla P + \mathbf{F}_B + \sum_n \mathbf{F}_n, \tag{2.2}$$

where we have neglected all dissipative effects and assume that the flow is inviscid. The sum of external forces $\mathbf{F}_n$ includes the inertial Coriolis force in the case of rotating medium and the gravity force in the case of the flow affected by gravity. The effect of the magnetic field in the equation of motion may be described by the Lorenz force:

$$\mathbf{F}_B = \frac{1}{4\pi}(\nabla \times \mathbf{B}) \times \mathbf{B}. \tag{2.3}$$

The complete description of the magnetized flow needs additional equations for the evaluation of the magnetic field. For this purpose we employ the ideal magnetohydrodynamic (MHD) approximation. It uses the magnetic induction equation for the description of the field dynamics:

$$\frac{\partial \mathbf{B}}{\partial t} = \nabla \times (\mathbf{V} \times \mathbf{B}), \tag{2.4}$$

where the magnetic diffusivity is neglected. In this ideal case the magnetic flux is "frozen" into the fluid flow. The magnetic field follows the solenoidal condition which excludes the existence of the magnetic monopoles:

$$\nabla \cdot \mathbf{B} = 0. \tag{2.5}$$

The energy conservation law may be written for the entropy of the flow as:

$$\left\{ \frac{\partial}{\partial t} + \mathbf{V} \cdot \nabla \right\} S = 0, \tag{2.6}$$

where we assume that the flow is isentropic. This is a well justified approximation when the effects of heat conductivity and emission or absorption of radiation are negligible.
For the description of the thermodynamic equilibrium state we can use the equation of entropy in the ideal gas approximation:

$$S = c_{\mathrm{v}} \ln \frac{P}{\rho^{\gamma}} + \text{constant}, \tag{2.7}$$

where γ is the adiabatic index and c_{v} is the specific heat. In many cases it is useful to employ the dynamical equation for the hydrodynamic pressure which can be derived from Eqs. (2.1,6,7):

$$\left\{ \frac{\partial}{\partial t} + \mathbf{V} \cdot \nabla \right\} P + \gamma P (\nabla \cdot \mathbf{V}) = 0. \tag{2.8}$$

Eqs. (2.1)-(2.7) are the set of equations that describe MHD flow influenced by the Coriolis and gravity forces. In this chapter we focus on non-rotating flows, we neglect gravity and magnetic field, and focus on hydrodynamics in order to describe the basic properties of flows with velocity shear.

2.2 Shear flow equilibrium and linear perturbations

Let us consider an unbounded inviscid hydrodynamic flow. The basic properties of shear flows may be studied for 2D flows. Thus we consider the simplest possible inhomogeneous flow, namely a 2D flow with constant linear shear of velocity and homogeneous pressure and density (plane Couette flow):

$$\mathrm{V}_0 = (Ay, 0), \quad P_0 = \text{constant}, \quad \rho_0 = \text{constant}. \tag{2.9}$$

A is the constant parameter of the velocity shear, which is assumed to be positive (see Fig. 2.1). This gives an exact time independent equilibrium solution of Eqs. (2.1), (2.2) and (2.8). However, realistic flows are much more complicated. For their analysis we may employ the perturbative method. We distinguish the equilibrium and perturbed parts in various physical quantities and study the perturbations on a known equilibrium flow. Formally:

$$\mathbf{V} = \mathbf{V}_0 + \mathbf{V}', \quad P = P_0 + P', \quad \rho = \rho_0 + \rho', \tag{2.10}$$

where $\mathbf{V}'$, P' and ρ' are perturbations of the velocity, pressure and density, respectively. When the perturbations are much smaller in amplitude than the corresponding equilibrium quantities we can neglect terms that are higher than the first order in the perturbations and analyze the linear problem.
Substitution of the variables (2.10) into the Eqs. (2.1), (2.2) and (2.8) and linearization leads to the following system of partial differential equations:

$$\left\{\frac{\partial}{\partial t} + Ay\frac{\partial}{\partial x}\right\} V_x' = -AV_y' - \frac{1}{\rho_0}\frac{\partial P'}{\partial x}, \tag{2.11}$$

$$\left\{\frac{\partial}{\partial t} + Ay\frac{\partial}{\partial x}\right\} V_y' = -\frac{1}{\rho_0}\frac{\partial P'}{\partial y}, \tag{2.12}$$

$$\left\{\frac{\partial}{\partial t} + Ay\frac{\partial}{\partial x}\right\} \rho' + \rho_0 \left(\nabla \cdot \mathbf{V}'\right) = 0, \tag{2.13}$$

$$\left\{\frac{\partial}{\partial t} + Ay\frac{\partial}{\partial x}\right\} P' + \gamma P_0 \left(\nabla \cdot \mathbf{V}'\right) = 0. \tag{2.14}$$

The effect of the background shear flow enters through the explicit coordinate dependence in the convective derivative.
The principal advantage of linear analysis is that it is possible to identify the perturbation spectrum. The linear character of the governing equations permits any solution to be expanded into a linear superposition of different modes.

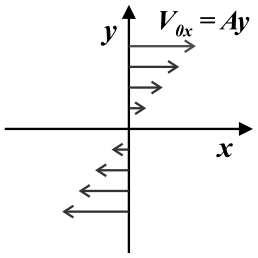

Figure 2.1: Shear flow with constant linear velocity profile $\mathbf{V}_0 = (Ay, 0)$. This is a simplest example of the incompressible flow with parallel streamlines and non-zero vorticity: curl$\mathbf{V}_0 = -A$.

It is straightforward to define the linear spectrum in the limiting case of a static background, when $\mathbf{V}_0 = 0$ ($A = 0$). In this case Eqs. (2.11) - (2.14) are homogeneous in time as well as in space. Hence, the corresponding solutions may be expressed in terms of harmonic functions of coordinate and time variables and may be found prescribing the same $(\mathbf{r}, t)$ dependence to all physical variables:

$$\mathbf{V}'(\mathbf{r}, t) \propto \exp(\mathrm{i}k_x x + \mathrm{i}k_y y - \mathrm{i}\omega t). \tag{2.15}$$

Substitution of this into Eqs. (2.11-14) in the case of $A = 0$ leads to the well known dispersion equation:

$$\omega^2(\omega^2 - c_s^2 k^2) = 0, \tag{2.16}$$

where $k^2 = k_x^2 + k_y^2$ and $c_s^2 = \gamma P_0/\rho_0$ is the sound speed. This dispersion describes two types of perturbations:

- Acoustic wave mode with $\omega^2 = c_s^2 k^2$, which corresponds to the oscillating compressible perturbations with purely potential velocity field: $P', \rho' \neq 0$, $\nabla \times \mathbf{V}' = 0$.
- Vortex mode with $\omega = 0$, which corresponds to the aperiodic incompressible perturbations with purely vortical velocity field: $P', \rho' = 0$, $\nabla \times \mathbf{V}' \neq 0$.

The different linear modes have clearly distinguishable eigenfrequencies and do not posses any similar feature in this shearless limit ($A = 0$). New effects are introduced when the background flow is sheared ($A \neq 0$) and the mean velocity has nonzero vorticity ($\nabla \times \mathbf{V}_0 \neq 0$).[1] In this case the two modes have a mixed character: the acoustic wave mode acquires vortical features, while the vortex mode become compressible.
To understand how a shearing (vortical) background flow affects a linear mode we calculate the contribution of the linear perturbations to the total velocity circulation of the flow. After straightforward manipulations

[1]Please, note that we use $\nabla \times \mathbf{F}$ notation for the rotation of a vector in the general case, not specifying the dimension of the vector $\mathbf{F}$ (3D or 2D). While we employ curl$\mathbf{F}$ notation only in the 2D case, stressing therewith that the product of this operator is a scalar quantity.

of Eqs. (2.11) - (2.14) we obtain:

$$\left\{\frac{\partial}{\partial t} + Ay\frac{\partial}{\partial x}\right\}\left[\left(\frac{\partial V_y'}{\partial x} - \frac{\partial V_y'}{\partial x}\right) - A\frac{\rho'}{\rho_0}\right] = 0. \tag{2.17}$$

We can somewhat generalize this equation in the case of a 2D flow with constant velocity shear: [1]

$$\left\{\frac{\partial}{\partial t} + (\mathbf{V}_0 \cdot \nabla)\right\}\left[\frac{\mathrm{curl}\mathbf{V}'}{\rho_0} + \frac{\rho'\ \mathrm{curl}\mathbf{V}_0}{\rho_0^2}\right] = 0, \tag{2.18}$$

Hence, the linear perturbations of the potential vorticity $\mathrm{curl}\mathbf{V}/\rho$ are convected with the equilibrium flow.
This is the basic property of vorticity which helps us to identify the vortical modes in simple hydrodynamic situation. However, this conservation law has its limitations. For instance, the flow viscosity leads to the decrease of potential vorticity through the thermal dissipation. Potential vorticity also varies in baroclinic flows: perturbations of $\nabla P \times \nabla\rho$ act as the source or the sink of potential vorticity depending on the thermodynamic properties of the background flow. Most profound is the action of magnetic field, when Lorenz force leads to the oscillatory behavior of the potential vorticity. Neglecting all these factors in the present section allows us to consider potential vorticity conservation and analyze its consequences for the vortex and acoustic modes in shear flows.
The term in the square brackets of Eq. (2.18) remains constant in Lagrangian coordinates (moves together with fluid) and actually determines the contribution of perturbations to the total velocity circulation of the flow. Consequently, perturbations that do not change the circulation of the background flow velocity should obey the following condition:

$$\rho_0\mathrm{curl}\mathbf{V}' + \rho'\mathrm{curl}\mathbf{V}_0 = 0. \tag{2.19}$$

Hence purely compressible perturbations ($\rho' \neq 0$, $\mathrm{curl}\mathbf{V}' = 0$) may not be expressed as a superposition of only acoustic wave perturbations. Linear perturbations of the density (or pressure) contribute to the potential vorticity by the background vortical momentum $\rho'\mathrm{curl}\mathbf{V}_0$. This means that acoustic wave modes acquire a vortical nature in flows with inhomogeneous velocity profiles. Perturbations of acoustic vorticity will propagate with the sound wave frequency:

$$\mathrm{curl}\mathbf{V}'(t) = -\mathrm{curl}\mathbf{V}_0\frac{\rho'(t)}{\rho_0}.$$

[1] The same equation may be obtained by the direct calculation of the linear perturbation of velocity circulation in Eq. (2.18) having in mind that $\rho'/\rho_0 = \int_{S'} \mathrm{d}f / \int_{S_0} \mathrm{d}f$, where S_0 and S' are mean and perturbed components of the area over which the vorticity is integrated. Note, that in this 2D case $\mathrm{d}f$ is a scalar quantity.

On the other hand vortex modes loose their purely vortical nature and acquire compressible nature: $\mathrm{curl}\mathbf{V}' = 0,\ \rho' \neq 0$ necessarily contains the vortex mode perturbations, since the resulting contribution into the total velocity circulation is non-zero. This vortex mode perturbations of density (and pressure) do not propagate and behave aperiodically[2]. In other words, vortical or compressible perturbations are not uniquely associated with vortex and acoustic wave modes, respectively.
For this simplified 2D hydrodynamic example we have seen that the vortical character of the equilibrium flow affects basic characteristics of the perturbation. The effect increases with the velocity shear parameter $A = -\mathrm{curl}\mathbf{V}_0$. As we will see later, this is the crucial factor that determines the necessary conditions for different modes to interact in the linear regime.
It is helpful to reduce the system of partial differential equations to a set of ordinary differential equations. The common approach to this problem has been modal analysis. It employs an expansion of the physical variables in Fourier modes with predefined temporal and x-spatial structure and study of the boundary value problem with respect to the y coordinate. For the reasons discussed in the introduction we do not use the modal analysis but employ an alternative method.

2.3 Non-modal formalism

For shortness of notation we introduce the generalized vector:

$$\Psi'(\mathbf{r},t) \equiv \begin{pmatrix} \mathbf{V}'(\mathbf{r},t) \\ \rho'(\mathbf{r},t) \\ P'(\mathbf{r},t) \end{pmatrix}. \tag{2.20}$$

In the non-modal method, we use a transformation of variables from the stationary to the co-moving frame, a so-called shearing sheet transformation:

$$x' \equiv x - Ayt, \quad y' \equiv y, \quad t' \equiv t. \tag{2.21}$$

This substitution of variables transforms the spatial inhomogeneity of the equations (2.8-12) into a inhomogeneity:

$$\frac{\partial}{\partial t} + Ay\frac{\partial}{\partial x} = \frac{\partial}{\partial t'}, \quad \frac{\partial}{\partial x} = \frac{\partial}{\partial x'}, \quad \frac{\partial}{\partial y} = \frac{\partial}{\partial y'} - At'\frac{\partial}{\partial x'}. \tag{2.22}$$

Hence, the full *spatial* Fourier expansion is straightforward:

$$\Psi'(\mathbf{r}',t') = \int\int_{-\infty}^{+\infty} \psi(\mathbf{k}',t') \exp\left(\mathrm{i}k_x'x' + \mathrm{i}k_y'y'\right) \mathrm{d}k_x'\mathrm{d}k_y', \tag{2.23}$$

[2]This density perturbations are sometimes referred as a pseudo-sound in hydrodynamic literature.

where

$$\psi(\mathbf{k},t) \equiv \begin{pmatrix} \mathbf{v}(\mathbf{k},t) \\ \varrho(\mathbf{k},t) \\ p(\mathbf{k},t) \end{pmatrix}. \tag{2.24}$$

Similarly, we may choose a particular form of the spatial harmonics and analyze perturbations in the laboratory frame. Substitution of (2.21) into the Fourier expansion (2.23) gives us an understanding of the intrinsic shape of the spatial harmonics (SFH) of the perturbed quantities in shear flows: $\exp(\mathrm{i}\mathbf{k}'\mathbf{r}') = \exp[\mathrm{i}k'_x x + \mathrm{i}(k'_y - Atk'_x)y]$. Hence we seek solutions of Eqs. (2.11)-(2.14) of the form:

$$\Psi'(\mathbf{r},t) \propto \psi(\mathbf{k}(t),t)\exp(\mathrm{i}\mathbf{k}(t),\mathbf{r}), \tag{2.25}$$

$$\mathbf{k}(t) = (k_x, k_y(t)), \quad k_y(t) = k_y(0) - Ak_x t. \tag{2.26}$$

The expansion in spatial harmonics with time dependent wave-numbers cancels the explicit coordinate dependence in the original equations. This leads to a system of ordinary differential equations for the perturbation SFH in time:

$$\frac{\mathrm{d}v_x}{\mathrm{d}t} + Av_y + \mathrm{i}k_x\frac{p}{\rho_0} = 0, \tag{2.27}$$

$$\frac{\mathrm{d}v_y}{\mathrm{d}t} + \mathrm{i}k_y(t)p = 0, \tag{2.28}$$

$$\frac{\mathrm{d}\varrho}{\mathrm{d}t} + \mathrm{i}\rho_0(k_x v_x + k_y(t)v_y) = 0, \tag{2.29}$$

$$\frac{\mathrm{d}p}{\mathrm{d}t} + \mathrm{i}\gamma P_0(k_x v_x + k_y(t)v_y) = 0, \tag{2.30}$$

Eqs. (2.27) - (2.30) pose an initial value problem. The solution of this initial value problem describes the temporal evolution of the SFH in shear flows. Note that the perturbations are described by the individual SFH obtained from the solution of the above initial value problem, and also by the fact that every harmonic linearly drifts in the wave-number space (**k**-space): $\mathbf{k} = \mathbf{k}(t)$. The behavior of the perturbations in the **r**-space is determined by the combined effect of the amplitude of SFHs and their drift in **k**-space. The linear drift of the SFH in a shear flow is easy to understand. It reveals the fact, that the shearing background flow stretches the wave-crests in the direction of the streamlines. Linear drift of SFH is an important property of all perturbations of shear flows. It reveals an inherent anisotropy of the linear process of energy redistribution in the **k**-space, the background trend of the energy transport between the different spatial scales. Temporal characteristics of perturbation modes are defined by their spatial characteristis – wave-numbers.

Therefore, the time dependence of the wave-numbers indicates the temporal variation of the effective frequencies of the perturbation SFH in shear flows:

$$\omega = \omega(\mathbf{k}), \quad k_y = k_y(t): \quad \omega = \omega(t)\ . \tag{2.31}$$

A more detailed description of this process will be given later for particular examples.
Let us consider two limiting cases where simple solutions for sound waves and vortical perturbations are obtained. This will help us to get a general insight into the influence of velocity shear on the dynamics.

2.4 Vortex mode perturbations

First we look at the limiting case of a 2D incompressible flow to study purely vortical perturbations. We neglect the perturbation of the fluid density $\varrho \equiv 0$ and adopt a divergence free velocity field:

$$\nabla \cdot \mathbf{V} = 0. \tag{2.32}$$

We can rewrite Eqs. (2.27)-(2.30) to the following:

$$\frac{\mathrm{d}v_x}{\mathrm{d}t} + Av_y + \mathrm{i}k_x\frac{p}{\rho_0} = 0, \tag{2.33}$$

$$\frac{\mathrm{d}v_y}{\mathrm{d}t} + \mathrm{i}k_y(t)\frac{p}{\rho_0} = 0, \tag{2.34}$$

$$k_x v_x + k_y(t)v_y = 0. \tag{2.35}$$

After straightforward manipulations we obtain the following solution of the system:

$$v_x(t) = -\frac{k_y(t)}{k_x k^2(t)}C, \tag{2.36}$$

$$v_y(t) = \frac{C}{k^2(t)}, \tag{2.37}$$

$$\frac{\mathrm{i}p(t)}{\rho_0} = -2A\frac{k_x}{k^4(t)}C, \tag{2.38}$$

where C is a constant of integration. This aperiodic mode is sometimes called the Kelvin mode, with reference to the pioneering paper by Lord Kelvin 1887. The solution describes a transient amplification of the vortical SFH in shear flow. The pressure SFH is complex due to the $\pi/2$ phase difference between the velocity and pressure perturbations. In the incompressible limit the total spectral energy density of perturbations is only due to kinetic terms and may be written as:

$$E_{\mathbf{k}}(t) = \frac{\rho_0}{2}(|v_x(t)|^2 + |v_y(t)|^2) = \frac{C^2\rho_0}{2k_x^2k^2(t)} \tag{2.39}$$

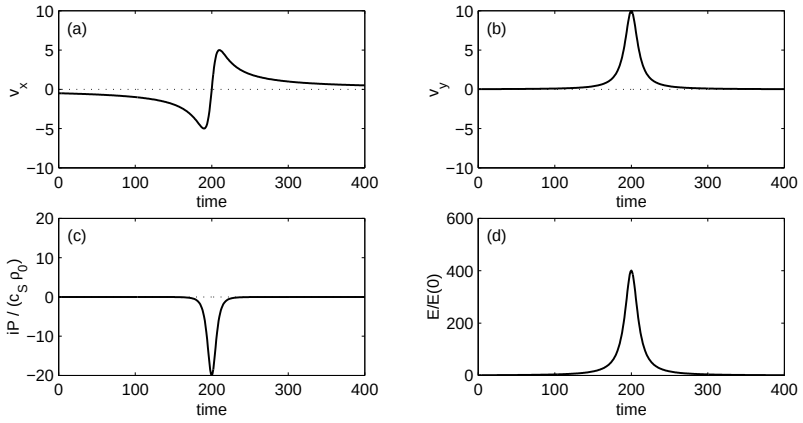

Figure 2.2: Transient amplification of the vortical perturbation SFH in shear flows. $k_x = 1$, $k_y = 20$, $C = 10$ and $A = 0.1$. The velocity $v_x(t)$, $v_y(t)$, pressure $\mathrm{i}p(t)/(c_s\rho_0)$, and normalized spectral energy $E_{\mathbf{k}}(t)/E_{\mathbf{k}}(0)$ of SFH are shown on the a,b,c and d graphs, respectively.

This solution is plotted on Fig. 2.2. It seems that the vortical perturbations are able to extract energy from the mean shear flow and are amplified by several orders of magnitude (by factor of 400 in the considered case). The maximal amplification is reached when the wave-number in the direction of the flow velocity shear is zero: in the present case – at $t = t^* = 200$, when $k_y(t^*) = k_y(0) - Ak_x t^* = 0$.

The character of the evolution of SFH is defined by its wave-number. Namely, SFH with $k_y/Ak_x > 0$ undergoes amplification and SFH with $k_y/Ak_x \leq 0$ looses energy to the background flow and decreases in amplitude.

This amplification phenomenon is a direct consequence of the eigenmode interference and has a transient character. As we shall see later, the transient amplification may be realized not only for aperiodic vortex modes. It can also occur for oscillating wave perturbations. The condition in the latter case is that the oscillating solution has a period much longer than the time scales on which the amplification occurs.

From a physical point of view, the growth of the energy of perturbations is due to the anisotropic character of the momentum exchange of the SFH with specific phases affected by the background velocity shear.

2.5 Acoustic wave mode perturbations

Combining Eqs. (2.13)-(2.14) we obtain the dynamical equation for the pressure and density perturbations:

$$\frac{\mathrm{d}P'}{\mathrm{d}t} = c_s^2 \frac{\mathrm{d}\rho'}{\mathrm{d}t} \ . \tag{2.40}$$

For the study of acoustic waves it is useful to assume that there are no stationary (constant) pressure and density perturbations in the flow. Stationary perturbations can always be removed by including them into the mean flow, e.g. by renormalization of the equilibrium flow. Hence, we may reduce the Eq. (2.39) to the following algebraic form

$$p = c_s^2 \varrho. \tag{2.41}$$

The perturbations are adiabatically compressible. Hence, the equations that govern the compressible SFH in a 2D unbounded shear flow are:

$$\frac{\mathrm{d}v_x}{\mathrm{d}t} + Av_y + \mathrm{i}k_x c_s^2 \frac{\varrho}{\rho_0} = 0 \ , \tag{2.42}$$

$$\frac{\mathrm{d}v_y}{\mathrm{d}t} + \mathrm{i}k_y(t) c_s^2 \frac{\varrho}{\rho_0} = 0 \ , \tag{2.43}$$

$$\frac{\mathrm{d}\varrho}{\mathrm{d}t} + \mathrm{i}\rho_0 \left(k_x v_x + k_y(t) v_y\right) = 0 \ . \tag{2.44}$$

These equations describe both, the acoustic (sound) waves as well as the vortex mode, which we have studied in the incompressible limit. In order to study the purely acoustic modes we should select the initial perturbations so that the vortex mode is excluded from the consideration.
Eqs. (2.42)-(2.44) allow for the following invariant form in time:

$$\frac{\mathrm{d}I}{\mathrm{d}t} = 0: \quad I(\mathbf{k}) = k_x v_y - k_y(t) v_x + A\frac{\mathrm{i}\varrho}{\rho_0}, \tag{2.45}$$

Referring to the Eq. (2.18) we may deduce that I($\mathbf{k}$) is a spectral form of the potential vorticity of the SFH. In order to remove the vortex mode from the analysis we select initial conditions with zero potential vorticity:

$$I(\mathbf{k}) \equiv 0. \tag{2.46}$$

Using this initial condition in Eqs. (2.42)-(2.44) we derive the second order differential equation that governs the acoustic wave mode:

$$\frac{\mathrm{d}^2 v_x}{\mathrm{d}t^2} + c_s^2 k^2(t) v_x = 0. \tag{2.47}$$

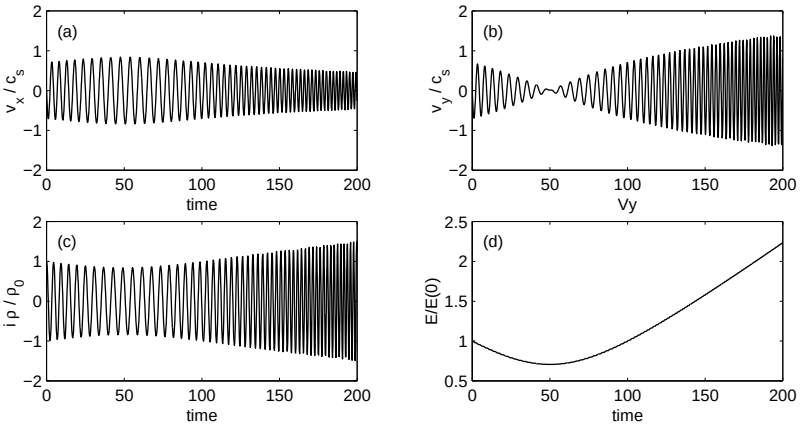

Figure 2.3: Evolution of the acoustic SFH of perturbations in shear flow. $k_x = 1$, $k_y = 1$, and $A = 0.02$. The velocity $v_x(t)$, $v_y(t)$, density $\mathrm{i}\varrho(t)/\rho_0$, and normalized spectral energy $E_{\mathbf{k}}(t)/E_{\mathbf{k}}(0)$ of the harmonic are shown on the a,b,c and d graphs, respectively. Oscillations of the velocity and density show the variation of the its frequency, which is apparently increased at longer times.

To get more insight into the qualitative behaviour of the perturbations we consider flows with low shear and solve Eq. (2.47) approximately, rather than trying to find the exact solution in the general case. When the time dependent parameters of the second order system are varying adiabatically, the system may be considered as an oscillatory system with a varying frequency

$$\omega^2(t) = c_s^2 k^2(t), \tag{2.48}$$

provided that the adiabatic condition of the slow variation is satisfied:

$$\left| \frac{\mathrm{d}\omega(t)}{\mathrm{d}t} \right| \ll \omega^2(t). \tag{2.49}$$

Hence, the velocity shear affects the acoustic wave frequency due to the wave-number variation. During the evolution in shear flows the frequency of the acoustic waves is increased or decreased, depending on the phase of the SFH. Conservation of the adiabatic invariant in such system reveals the characteristic behavior of the wave energy:

$$E_{\mathbf{k}}(t) \propto \omega(t) \propto |\mathbf{k}(t)|. \tag{2.50}$$

These effects are readily illustrated on Fig. 2.3 where we present the exact numerical solution of Eqs. (2.42) - (2.44) for specific initial conditions. On the other hand, the analytical solution of this system in the

WKB approximation is:

$$\mathrm{i}\varrho(t)/\rho_0 = A_\rho(t)\exp\left[\mathrm{i}\phi(t)\right] \ , \tag{2.51}$$

$$v_x(t) = A_{vx}(t)\exp\left[\mathrm{i}(\phi(t)+\phi_{vx}(t))\right] \ , \tag{2.52}$$

$$v_y(t) = A_{vy}(t)\exp\left[\mathrm{i}(\phi(t)+\phi_{vy}(t))\right] \ , \tag{2.53}$$

where

$$\phi(t) = \phi_0 + \int_0^t \omega(t)\mathrm{d}t \ . \tag{2.54}$$

$A_{vx}(t)$, $A_{vy}(t)$, $A_\rho(t)$ are amplitudes and $\phi_{vy}(t)$, $\phi_\rho(t)$ time dependent phase differences between the $v_x(t)$, $v_y(t)$ and $\varrho(t)$, respectively (We do not analyze the acoustic wave properties in detail here and refer the reader to Chagelishvili et al. 1994, 1997 for more details). We rather emphasize the characteristic properties of the acoustic waves that are inherent to waves influenced by a mean shear flow.

First of all, as we have already seen in the incompressible limit, the perturbations exchange energy with the background shear flow. The character of this process is largely defined by the velocity shear parameter and the character of perturbations. At low shear rates the equation describing the evolution of SFH are analogous to an oscillatory equation with a time dependent frequency. Therefore the shear induced temporal variation of the mode frequency is due to the time dependence of the SFH wave-numbers, the linear drift in $\mathbf{k}$-space. $\omega(t) = \omega(\mathbf{k}(t))$. The adiabatic character of the system then defines the character of energy exchange between perturbations and the background flow: $E_{\mathbf{k}}(t) \propto \omega(\mathbf{k}(t))$.

Shear of the flow also affects energy transfer by waves. In the simple case of uniform flow the energy transport of wave package may be estimated by the group velocity. However, in the present case the definition of the group velocity becomes problematic.

Indeed, when we use the classical definition of group velocity (cf. Lighthill 1978) and use Eq. (2.54) we obtain:

$$\mathbf{U} = \frac{\partial\omega(\mathbf{k})}{\partial\mathbf{k}} = \frac{\partial^2\phi(\mathbf{k},t)}{\partial\mathbf{k}\ \partial t} \tag{2.55}$$

However, the phase difference between the SFH of the different physical quantities (see Eqs. 2.51 - 2.53) is time dependent: the density and velocity perturbations evolve with their corresponding phases. Therefore, the group velocity calculated for different physical quantities is different:

$$\mathbf{U}_\rho = \mathbf{U} \ , \tag{2.56}$$

$$\mathbf{U}_{vx} = \mathbf{U} + \frac{\partial^2\phi_{vx}(\mathbf{k},t)}{\partial\mathbf{k}\ \partial t} \ , \tag{2.57}$$

$$\mathbf{U}_{vy} = \mathbf{U} + \frac{\partial^2 \phi_{vy}(\mathbf{k}, t)}{\partial \mathbf{k}\, \partial t} \ . \tag{2.58}$$

So, the compressible energy is transported with a different group velocity than the kinetic one. Even the definition of the kinetic energy is problematic, since the harmonics of different polarization transport the energy at different speeds. Two otherwise identical waves with different velocity components projected along the x and y directions have different mean group velocities due to the difference between $\mathbf{U}_{vx}$ and $\mathbf{U}_{vy}$. Hence, even the definition of the average group velocity becomes a subject of approximation. This property is generally inherent to all waves in shear flows, but is most profound during the non-adiabatic stage of the wave evolution, when the phases of different physical quantities significantly diverge. For the considered sound waves non-adiabaticity is profound when $k_y(t)/(Ak_x) < 1$ (see Chagelishvili et al. 1997).

2.6 Velocity shear rate

The dynamics of sheared flows crucially depends on the type of the velocity inhomogeneity. A major concern in this respect is the stability of a given flow. In fact, there are several different factors that may lead to exponential destabilization of the laminar shear flow. Flow may be fundamentally unstable due to the large amplitude or the specific geometry of the velocity shear. For instance, a powerful instability may occur in a flow that has an inflection point in the velocity profile. In the present thesis we study flows with smooth shear of velocity, i.e., velocity profile without an infection point and sufficiently smooth to be approximated by a linear profile locally. Therefore, we do not consider effects related to the flow velocity profile, but simply estimate the largest possible velocity shear that may occur in a spectrally stable flow.
The influence of the velocity shear is different on perturbations of different characteristic length-scales. We have already seen that a sheared flow results in a temporal variation of the wave-numbers thereby stretching the initial pattern into the direction of the streamlines. Therefore, for an adequate description of the effect of the shearing background on the perturbations, it is useful to introduce the non-dimensional shear rate:

$$R \equiv A/c_s k_{\|}, \tag{2.59}$$

where $k_{\|}$ is the characteristic wave-number of the perturbation along the flow. The value of the velocity shear rate may be estimated from several different points of view. The first natural question in this respect: what is the value of the shear rate R which does not lead to kinematic shocks. The latter process may occur when the variation of the flow velocity over a dissipative length scales is of the same order as the sound speed of the

medium c_s. The shear parameter A defines the velocity variation over a unit length scale. Thus the formation of extreme velocity gradients necessary for the formation of shock waves is possible when

$$Al_\nu/c_s \geq 1, \tag{2.60}$$

where l_ν is the characteristic dissipative length scale of the flow. Having in mind that $l_\parallel \sim 1/k_\parallel$ and using Eq. (2.59) we can rewrite Eq. (2.60) as:

$$R \geq l_\parallel/l_\nu. \tag{2.61}$$

The length scales of the dynamical perturbations are longer than the dissipative ones: $l_\parallel > l_\nu$. Therefore, the critical value of the velocity shear rate necessary for the formation of shock waves in a laminar flow should obey the following condition:

$$R > 1. \tag{2.62}$$

Note that the stability threshold may be much higher ($R \gg 1$) for large scale perturbations ($l_\parallel \gg l_\nu$). Our further analysis is restricted by the maximal value of the velocity shear rate for small scale perturbations: $l_\parallel \geq l_\nu$. Hence, we define the velocity shear rate to be low when $R \leq 0.1$, moderate when $0.1 < R < 1$, and high when $R \geq 1$.

Chapter 3

Linear mode conversion: excitation of acoustic waves

3.1 Introduction

The interaction of vorticity and acoustic waves has a long history of investigation. Indeed, starting from the pioneering papers by Lighthill (1952, 1954) intense research has been carried out in this field (see e.g., review by Ffowcs Williams 1977). The basic approach in this respect is the acoustic analogy. This approach employs the second order inhomogeneous equation that may be directly obtained from Eqs. (2.1,2):

$$\frac{\partial^2 \rho}{\partial t^2} - c_s^2 \nabla^2 \rho = Sr. \tag{3.1}$$

The solution of the homogeneous equation ($Sr = 0$) describes the acoustic waves, while the inhomogeneous term Sr is assumed to be the source of the wave excitation. In the present chapter we concentrate on the aerodynamic excitation of acoustic waves, which means that we study flows that are not influenced by rigid boundaries. In this case (neglecting viscosity) the source term is due to the Reynolds stress:

$$Sr = \frac{\partial^2 \rho V_i V_j}{\partial x_i \partial x_j}, \quad \text{where} \quad i, j = (x, y, z). \tag{3.2}$$

Hence, in the framework of the acoustic analogy the fluctuations of the Reynolds stress stochastically excite the oscillations of the acoustic waves. In order to analyze the acoustic production in various hydrodynamic situations several acoustic analogies have been developed (see

Howe 1975, Phillips 1960, Ffowcs Williams 1963, Lilley 1972, Crighton 1981). The basic approximation is that the process of sound generation is treated as the excitation of a *linear* acoustic field by the *nonlinear* process of turbulence. Specific to this method is that results strongly depend on the form of the analogy equation as well as the aero-acoustic variable chosen to analyze the process. This is more so when the convective terms (terms describing the background flow) are important which is the case in shear flows.

The positive effect of the inhomogeneity of the background velocity on the increase of the acoustic emission in the aerodynamic situation has been appreciated from the early stages of acoustic research (see Lighthill 1954). In fact, the velocity inhomogeneity leads to the existence of linear terms in the inhomogeneous part of the analogy equations (in our notations: $\mathbf{V} = (Ay, 0) + \mathbf{v}: \ Sr = 2A\partial v_y/\partial x$). An attempt to analyze the shear flow noise in the local parallel flow limit using the modal approximation may be found in Pao 1973. However, due to the non-normality of the operators in shear flows, modal solutions do not describe the acoustic emission adequately. In addition, the latter study still bears the artifact of the nonlinear analysis and attributes the source terms to the turbulent fluctuations in general. This leads to an incorrect choice of the form of the acoustic analogy equation and acoustic variable in shear flows.

Within the acoustic analogy the wave excitation rate is calculated by the use of estimates of the amplitude of the source terms $|Sr|$. We show that in shear flows the source term may not uniquely define the sound production rate. In the present chapter we employ the non-modal method and analyze the linear perturbation modes in flows with velocity inhomogeneity. Using this method we present an unambiguous separation of the inhomogeneous term from the convection effect and give a self-consistence treatment of the wave excitation process in the linear limit. We identify a vortex mode as the source of the acoustic waves rather than the inhomogeneity of the acoustic analogy equation. In fact, the vortex mode is a product of a balance between the inhomogeneous and homogeneous terms of the equation. Hence, we trace the vortex mode and identify the generated waves as the result of the velocity shear induced linear mode conversion. We employ direct numerical analysis and demonstrate the properties of the vortex-acoustic mode conversion in real space for different initial sets of perturbations.

This Chapter is organized as follows: In Sec. 2 we present the mathematics and necessary definitions of our 2D investigation. In Sec. 3 we analyze the dynamics of SFH of linear perturbations in the framework of non-modal analysis and study the coupling of vortex and acoustic wave modes in the linear regime. We use numerical analysis to reveal the details of the linear aerodynamic sound generation and study the phenomenon in wave-number space in terms of the SFH. Further we

evaluate the initial amplitude of the generated acoustic wave SFH using extrapolation of the numerical data. In Sec. 4 and 5 we present the results of direct numerical simulations of the 2D compressible hydrodynamic equations in the case of a smooth shear flow. The equations of our direct numerical simulations are nonlinear. However, the phenomenon of acoustic wave generation by vortices is linear by nature – embedding small amplitude initial perturbations in the equations, we minimize the actions of nonlinear terms and describe the phenomenon as it occurs during the linear stage of evolution. In Sec. 4 we study a localized (in real and wave-number spaces) packet of vortex mode perturbations and demonstrate the linear aerodynamic sound generation by identifying the tracers of the emitted sound waves. In general, we verify the results obtained with the non-modal method and show the global appearance of the phenomenon. Conclusions and discussion are given in Sec. 6.

3.2 Linear analysis

Let us consider a 2D compressible flow with uniform pressure and density ($P_0, \rho_0 = \text{const.}$) and linear shear of velocity: $\mathbf{V}_0 = (Ay, 0, 0)$. The equations that govern the dynamics of linear adiabatic ($p = c_s^2 \varrho$) perturbation harmonics within the non-modal method are the following (see Eqs. 2.27-30):

$$\frac{\mathrm{d}}{\mathrm{d}t} v_x(t) + A v_y(t) + k_x c_s^2 \frac{\mathrm{i}\varrho(t)}{\rho_0} = 0, \tag{3.3}$$

$$\frac{\mathrm{d}}{\mathrm{d}t} v_y(t) + k_y(t) c_s^2 \frac{\mathrm{i}\varrho(t)}{\rho_0} = 0, \tag{3.4}$$

$$\frac{\mathrm{d}}{\mathrm{d}t} \frac{\mathrm{i}\varrho(t)}{\rho_0} - k_x v_x(t) - k_y(t) v_y(t) = 0, \tag{3.5}$$

were $k_y(t) = k_y - A k_x t$. The conservation law of the potential vorticity of this system is:

$$I = k_x v_y(t) - k_y(t) v_x(t) + A \frac{\mathrm{i}\varrho}{\rho_0}. \tag{3.6}$$

For further analysis we rewrite Eqs. (3.3-6) in the form of wave equations:

$$\frac{\mathrm{d}^2}{\mathrm{d}t^2} v_x(t) + c_s^2 k^2(t) v_x(t) = c_s^2 k_y(t) I, \tag{3.7}$$

$$\frac{\mathrm{d}^2}{\mathrm{d}t^2} v_y(t) + \frac{2Ak_x}{c_s^2 k^2(t)} \frac{\mathrm{d}}{\mathrm{d}t} v_y(t) + c_s^2 k^2(t) v_y(t) = -c_s^2 k_x I, \tag{3.8}$$

$$\frac{\mathrm{d}^2}{\mathrm{d}t^2} \frac{\mathrm{i}\varrho(t)}{\rho_0} + \frac{2Ak_x k_y(t)}{c_s^2 k^2(t)} \frac{\mathrm{d}}{\mathrm{d}t} \frac{\mathrm{i}\varrho(t)}{\rho_0} + \left(c_s^2 k^2(t) + \frac{2A^2 k_x^2}{c_s^2 k^2(t)} \right) \frac{\mathrm{i}\varrho(t)}{\rho_0} = \frac{2Ak_x^2}{k^2(t)} I. \tag{3.9}$$

Any of these equations may be used for the analysis of the vortex-acoustic interaction. For obvious simplicity we employ Eq. (3.7) in order to describe the phenomenon qualitatively. We can find the remaining physical quantities by using the solution for $v_x(t)$ and the potential vorticity given by initial perturbations:

$$v_y(t) = \frac{1}{c_s^2 k_x^2 + A^2}\left(c_s^2 k_x (k_y(t)v_x(t) - I) - A\frac{\mathrm{d}v_x(t)}{\mathrm{d}t}\right), \tag{3.10}$$

$$\varrho(t) = \frac{\mathrm{i}\rho_0}{c_s^2 k_x^2 + A^2}\left(A(I - k_y(t)v_x(t)) - k_x\frac{\mathrm{d}v_x(t)}{\mathrm{d}t}\right). \tag{3.11}$$

The total spectral energy density of each SFH in **k**-space is defined as follows:

$$E_k(t) \equiv \frac{\rho_0}{2}\left(|v_x(t)|^2 + |v_y(t)|^2 + c_s^2\left|\frac{\mathrm{i}\varrho(t)}{\rho_0}\right|^2\right), \tag{3.12}$$

Note that $\mathrm{d}E_k(t)/\mathrm{d}t = -Av_x(t)v_y(t)$. Thus, $E_k(t)$ is a conserved quantity in the absence of the shear.

3.2.1 Linear modes

Our physical system contains acoustic wave modes and vortex modes. In general, the eigenfunctions of the modes are significantly affected by the equilibrium flow configuration. Therefore, the identification of different modes in compressible shear flows may be complicated and requires a refined procedure. In the absence of velocity shear the amplitude, frequency, wavenumbers are constant in time and solutions in the simple harmonic form $\propto \exp(\mathrm{i}\omega t)$ exist. Hence, the modes identify the dispersion equation:

$$\omega\left[\omega^2 - c_s^2(k_x^2 + k_y^2)\right] = 0. \tag{3.13}$$

Solutions of this dispersion equation describe the vortex mode with zero frequency ($\omega = 0$), and the acoustic wave mode with $\omega^2 = (k_x^2 + k_y^2)c_s^2$. The full solution is a superposition of all modal solutions and may be decomposed as follows:

$$v_x = v_x^{(\mathrm{w})} + v_x^{(\mathrm{v})}, \tag{3.14}$$

where $v_x^{(\mathrm{w})}$ and $v_x^{(\mathrm{v})}$ correspond to the oscillatory acoustic mode and aperiodic (stationary in the shearless limit) vortex mode, respectively. In the zero shear limit these solutions may be found individually from Eq. (3.7):

$$\frac{\mathrm{d}^2}{\mathrm{d}t^2}v_x^{(\mathrm{w})}(t) + c_s^2 k^2 v_x^{(\mathrm{w})}(t) = 0 \tag{3.15}$$

$$k^2 v_x^{(\mathrm{v})} = k_y I. \tag{3.16}$$

The wave mode is described by the homogeneous part of Eq. (3.7). The vortex mode is the result of a balance between the homogeneous (the second term on the left hand side) and inhomogeneous parts of the equation and is not trivial ($v_x^{(\mathrm{v})} \neq 0$) only when $I \neq 0$. In other words nonzero potential vorticity originates the vortex mode.
It is possible to classify the modes contained in Eq. (3.7) from a mathematical and a physical standpoints separately.
Mathematically, the general solution of Eq. (3.7) is a sum of the *general* solution of the corresponding homogeneous equation (oscillating, wave mode) and a *particular* solution of the inhomogeneous equation. A particular solution of the inhomogeneous equation is not uniquely determined: the sum of a particular solution of the inhomogeneous equation and any particular solution of the homogeneous equation (i.e. wave mode solution) is a particular solution of the inhomogeneous equation too, i.e. a particular solution may comprise any dose of the wave mode.
From a physical point of view, the acoustic wave mode describes the oscillations, while the vortex mode describes the aperiodic evolution of perturbations. Hence, it follows that the correspondence between the aperiodic vortex mode and a particular solution of the inhomogeneous equation is not unique – the vortex mode is only associated with the last one.
The amplitude of the vortex mode is proportional to I and goes to zero for $I = 0$. A feature which is important in our study is the loss of the non-divergent nature of the vortex mode, i.e., the aperiodic mode is compressible and has nonzero density perturbation ($D^{(\mathrm{v})} \neq 0$).
Clearly we have adhered to the physical standpoint of separation of modes/types of perturbations. Thus the wave component is determined by the oscillating behavior and the vortex component by aperiodic behavior, and we write:

$$v_x = v_x^{(\mathrm{w})} + v_x^{(\mathrm{v})}; \quad v_y = v_y^{(\mathrm{w})} + v_y^{(\mathrm{v})}; \quad \varrho = \varrho^{(\mathrm{w})} + \varrho^{(\mathrm{v})} \ . \tag{3.17}$$

In fact, the modified initial value problem is solved by using the non-modal method. Eqs. (3.3-5) describe the two modes: acoustic waves and aperiodic vortices. Clearly, the character of the dynamics depends on what mode is imposed initially in Eqs. (3.3-5): pure acoustic waves (without contribution from aperiodic vortices) or pure aperiodic vortices (without contribution from acoustic waves).

3.3 Generation of acoustic waves by SFH of the vortex mode perturbations

In this section we present a numerical study of the linear evolution of initially excited SFH of vortex mode.

The dynamics depend on the value of a time-dependent parameter:

$$R(t) \equiv \frac{A}{\omega(t)} \ . \tag{3.18}$$

Consequently, the character of the evolution changes in time. The final result is defined by the maximal value of $R(t)$ (that is achieved at $t = t^*$, when $k_x(t^*) = 0$):

$$R_{max} = \frac{A}{k_x c_s} \ . \tag{3.19}$$

Numerical calculations of Eqs. (3.3-5) are carried out for an initially pure vortex SFH (without admixes of acoustic wave) that satisfies the condition $k_y(0)/k_x > 0$. The calculations show fundamental differences between vortices at low and moderate shear rates. At high shear rates there is only a slight decrease of the wave generation. Hence we concentrate our attention on low and moderate shear rates ($R \sim 1$), where generation of waves is maximal. Results of calculations at $R_{max} = 0.05;\ 0.2;\ 0.4$ are presented on Figs. 3.1-3.

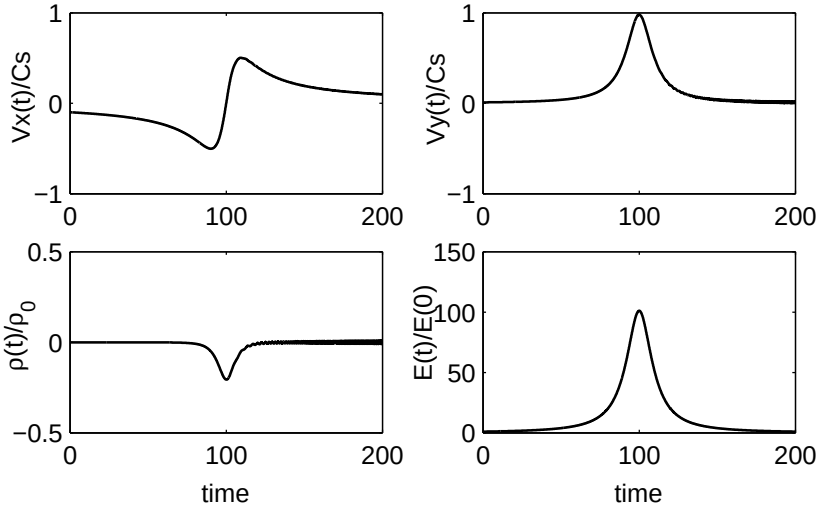

Figure 3.1: Figure shows the evolution of the normalized SFH of velocity and density perturbations ($v_x(t)/c_s$, $v_y(t)/c_s$ and $D \equiv \mathrm{i}\varrho(t)/\rho_0$) and its normalized energy ($E_{\mathbf{k}}(t)/E_{\mathbf{k}}(0)$) at $R_{max} = 0.05$. Evolving in the shear flow, the initially imposed vortex SFH (with $k_y(0)/k_x = 10$) transiently grows and retains its aperiodic nature.

At $R_{max} \ll 1$, $R(t)$ is small at all times. As one can see from Fig. 3.1, at low shear rates compressibility is negligible and there is only a

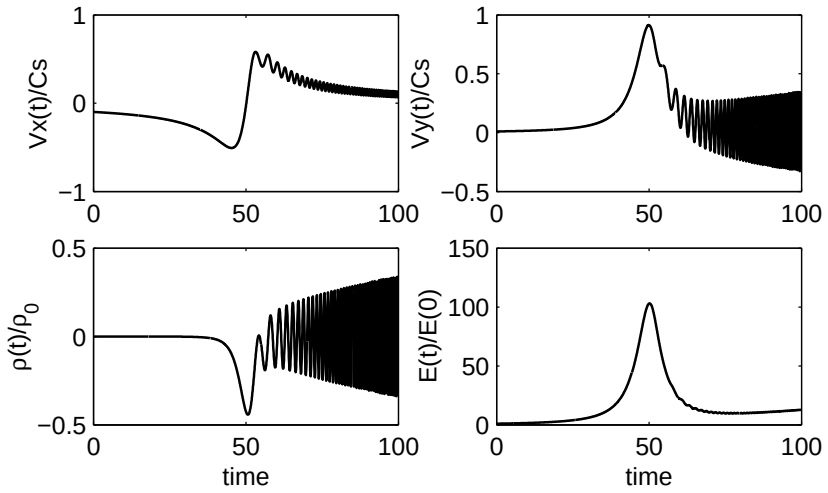

Figure 3.2: Figure shows the evolution of the normalized SFH of velocity and density perturbations ($v_x(t)$, $v_y(t)$ and $D \equiv \mathrm{i}\varrho(t)/\rho_0$) and its normalized energy ($E_{\mathbf{k}}(t)/E_{\mathbf{k}}(0)$) at $R_{max} = 0.2$. In the dynamics of the initially imposed vortex SFH (with $k_y(0)/k_x = 10$) transient growth is dominant, but the wave generation starts to be noticeable.

transient growth. It is obvious that transient growth of vortex mode exists in the exponentially stable flow system. It is a very important phenomenon that extracts shear energy and can provoke a transition to turbulence, (see Baggett et al. 1995, Gebhardt and Grossmann 1994, Grossmann 2000, Reshotko 2001, Chapman 2002, Chagelishvili et al. 1996, Rempfer 2003.) It is a well known phenomenon and has already been studied in detail in Reddy and Henningson 1993, Gustavsson 1991, Butler 1992, Moffatt 1967, Craik and Criminale 1986, Marcus and Press 1977, Lominadze et al 1988. The physics of the transient growth is described in a different manner by Landahl 1980 and Chagelishili et al. 1996.

3.3.1 Linear aerodynamic sound generation

At moderate and large R_{max} potential vorticity generates acoustic waves. The wave generation becomes noticeable at $R_{max} = 0.2$ (see Fig. 3.2) and at $R_{max} > 0.3$ it is the dominant feature in the shear flow (see Fig. 3.3).
In Fig. 3.3 we present the evolution of SFH of perturbations (v_x, v_y, D) and its normalized energy ($E_{\mathbf{k}}/E_{\mathbf{k}}(0)$) at $R_{max} = 0.4$. In this case,

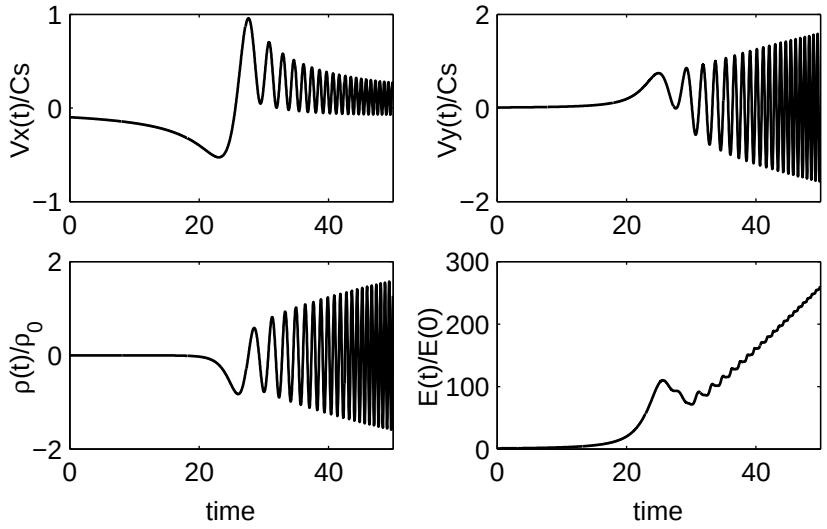

Figure 3.3: Figure shows the evolution of the normalized SFH of velocity and density perturbations ($v_x(t)/c_s$, $v_y(t)/c_s$, D) and its normalized energy ($E_{\mathbf{k}}(t)/E_{\mathbf{k}}(0)$) at $R_{max} = 0.4$. Evolving in the shear flow, the initially imposed vortex mode SFH (with $k_y(0)/k_x = 10$), gaining energy from the mean flow and amplifying, retains its aperiodic nature till $k_y(t)/kx > 0$. After time $t^* = 20$ (at which $k_y(20) = 0$), we observe the appearance of the wave SFH.

we have initially $R(t) \ll 1$ (as $k_y(0)/k_x = 10$, i. e., $(k_y(0)/k_x)^2 \gg 1$), and the initial stage is actually incompressible. The initially imposed vortex mode SFH then gains energy from the mean flow and amplifies, but retains its aperiodic nature. In due course $R(t)$ increases, becomes moderate and compressibility comes into play. As a result the oscillating part of SFH appears. Thus, the linear vortex mode is followed by the generation of a wave. Till $R(t)$ is moderate, the time scales of vortex and the wave SFH are comparable and the perturbations are not separable/distinguishable, we have a mix of SFH of aperiodic and oscillating modes. Towards the end, $R(t)$ becomes small again. The characteristic time scale of wave SFH becomes much shorter than that of vortex SFH and the modes are well distinguishable.

In spite of what we said above, we carry out a separation of the modes at time t^*, when $k_y(t^*) = 0$ and $R(t)$ is not small. The performed separation is conventional but productive, since it allows to gain more insight into the nature of the phenomenon. It establishes the initial characteristics of the generated wave SFH and determines further dynamics

of SFH even quantitatively.

3.3.2 The nature of the wave generation

As discussed at the end of previous section, we can decompose any solution v_x, v_y, D in its wave ($v_x^{(\mathrm{w})}$, $v_y^{(\mathrm{w})}$, $\varrho^{(\mathrm{w})}$) and vortex ($v_x^{(\mathrm{v})}$, $v_y^{(\mathrm{v})}$, $\varrho^{(\mathrm{v})}$) contribution for all times. In Fig. 3.4 we present this decomposition for the solution of Fig. 3.3. We can notice that, for $t < t^*$, the solution has only a vortex contribution, i.e. $v_x = v_x^{(\mathrm{v})}$, $v_y = v_y^{(\mathrm{v})}, \varrho = \varrho^{(\mathrm{v})}$ and $v_x^{(\mathrm{w})} = 0$, $v_y^{(\mathrm{w})} = 0$, $\varrho^{(\mathrm{w})} = 0$. For $t > t^*$ instead, the solution has both contributions. The two contributions are, separately, solutions of Eq. (3.7) in the interval $t > t^*$ and, in particular, the wave part is a solution of the homogeneous part of Eq. (3.7). We must also stress that the purely vortex contribution is not a solution of Eq. (3.7) for all times, because of its discontinuity at $t = t^*$. We may interpret the plots on Fig. 3.3 as an emergence of waves from vortices at $t = t^*$.
Eq. (3.7) can be solved analytically, using a series expansions and continuous solutions can be obtained (see, e.g., Rogava et al. 2001). Naturally, there is no solution that remains aperiodic during the whole time interval. Therefore, oscillations have to occur even if they are absent initially. Having in mind that the wave excitation phenomenon is a strongly non-WKB effect, we note that it can be considered as "sudden" at macroscopic scales (see Berry 1990). Hence, we assume this macroscopic approach and carry out the symmetry analysis of Eq. (3.7). The vortex mode is directly associated with the parameter of the inhomogeneity in Eq. (3.7) I and tends to the trivial solution ($v_x^{(\mathrm{v})} \to 0$) with $I \to 0$. ($v_x^{(\mathrm{v})}$) is an odd function of the argument $t - t^*$:

$$v_x^{(\mathrm{v})}(t > t^*) = -v_x^{(\mathrm{v})}(t < t^*). \tag{3.20}$$

In addition, the first term on the left hand side of Eq. (3.7), corresponds to compressibility of the flow and results in a shift of $v_x^{(\mathrm{v})}$ from zero at $t \to t^* - 0$. These two facts lead to the jump of the aperiodic/vortex mode perturbation at the point $t = t^*$, i.e.,

$$v_x^{(\mathrm{v})}(t_-^*) \neq v_x^{(\mathrm{v})}(t_+^*) \ , \tag{3.21}$$

where

$$v_x^{(\mathrm{v})}(t_-^*) \equiv \lim_{t \to t^* - 0} v_x^{(\mathrm{v})}(t) \ , \tag{3.22}$$

$$v_x^{(\mathrm{v})}(t_+^*) \equiv \lim_{t \to t^* + 0} v_x^{(\mathrm{v})}(t) \ . \tag{3.23}$$

It is from this discontinuity that the wave originates. Actually, v_x is a physical quantity and must be a continuous function of the argument

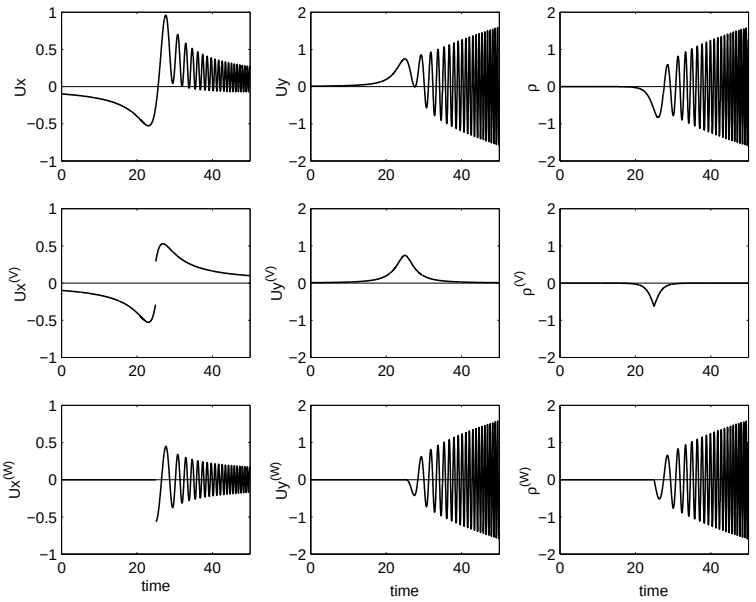

Figure 3.4: The Figure presents the dynamics of $v_x/c_s,\ v_y/c_s,\ \varrho$, their vortex $(v_x^{(\mathrm{v})}/c_s,\ v_y^{(\mathrm{v})}/c_s,\ D^{(\mathrm{v})})$ and wave parts $(\ v_x^{(\mathrm{w})}/c_s,\ v_y^{(\mathrm{w})}/c_s,\ \varrho^{(\mathrm{w})})$ for a pure vortex initial perturbation $(\ v_x^{(\mathrm{w})}(0),\ v_y^{(\mathrm{w})}(0),\ \varrho^{(\mathrm{w})}(0)=0)$ with the same parameters as in Fig. 3.3. The process may be interpreted as an abrupt emergence of wave SFH from the related vortex SFH at $t=t^*$. The amplitude of the generated wave $v_x^{(\mathrm{w})}(t^*)$ smoothes the jump in the aperiodic mode (see Eqs. 3.24-28).

t. Hence, it is necessary that at $t=t^*$ a wave arises, with the required amplitude to smooth out the discontinuity.
Thus, the initially imposed pure aperiodic/vortex mode SFH $(\ v_x(0)=v_x^{(\mathrm{v})}(0)\ )$ retains its identity until $t<t^*$. Passing the point $t=t^*$ from the left side with value $v_x^{(\mathrm{v})}(t^*_-)$, this left side aperiodic solution cannot be turned into the right side aperiodic solution of Eq. (3.7) $(\ v_x^{(\mathrm{v})}(t^*_+)\ )$ continuously. $v_x^{(\mathrm{v})}(t^*_-)$ is perceived from the right side as a sum of $v_x^{(\mathrm{v})}(t^*_+)$ and some solution of the corresponding homogeneous equation:

$$v_x^{(\mathrm{v})}(t^*_-)=v_x^{(\mathrm{v})}(t^*_+)+v_x^{(\mathrm{w})}(t^*_+)\ . \tag{3.24}$$

The amplitude of the emerging wave SFH at t^* may be calculated from Eqs. (3.22-24):

$$v_x^{(\mathrm{w})}(t^*_+)=2v_x^{(\mathrm{v})}(t^*_-)\ . \tag{3.25}$$

This is clearly seen from Figs. 3.4, where the evolution of $v_x^{(\mathrm{v})}$ and $v_x^{(\mathrm{w})}$ is given.
$v_y^{(\mathrm{v})}$ and $\varrho^{(\mathrm{v})}$ are even functions of the argument $t - t^*$ and they *do not need smoothing* when passing through the point $t = t^*$. Therefore, when the wave SFH emerges, $v_y^{(\mathrm{w})}(t_+^*), \varrho^{(\mathrm{w})}(t_+^*) = 0$ (Discontinuity of aperiodic contribution, indicating the wave excitation occurs in the first derivative of these functions).
Thus, from the above analysis and Figs. 3.4 follows:
– $v_x^{(\mathrm{v})}$ is odd function of the argument $t - t^*$;
– $v_y^{(\mathrm{v})}$ and $\varrho^{(\mathrm{v})}$ are even functions of the argument $t - t^*$;
– At $t = t^*$ the vortex mode gives rise to the corresponding SFH of the wave. We may interpret this phenomenon as the generation of a wave SFH with an amplitude needed to smooth the discontinuity in the vortex (aperiodic) mode SFH, when $k_y(t)$ changes sign;
– When the wave SFH appears (irrespective of the system parameters: A, k_x, $k_y(0)$, R_{max}) it has zero density and cross-stream velocity, and maximal streamwise velocity (see Figs. 4):

$$\varrho^{(\mathrm{w})}(t_+^*) = 0 \ , \tag{3.26}$$

$$v_y^{(\mathrm{w})}(t_+^*) = 0 \ , \tag{3.27}$$

$$|v_x^{(\mathrm{w})}(t_+^*)| = 2|v_x^{(\mathrm{v})}(t_-^*)| = 2|v_x(t^*)| \ ; \tag{3.28}$$

– The vortex and wave SFH are not coupled for $t > t^*$. The quantities $(\, v_x^{(\mathrm{v})},\ v_y^{(\mathrm{v})},\ \varrho^{(\mathrm{v})})$ and $(\, v_x^{(\mathrm{w})},\ v_y^{(\mathrm{w})},\ \varrho^{(\mathrm{w})})$ evolve in a completely independent way. For $t > t^*$, we can introduce the quadratic forms:

$$E^{(\mathrm{v})}(t > t^*) \equiv \frac{\rho_0}{2}\left(\left|v_x^{(\mathrm{v})}\right|^2 + \left|v_y^{(\mathrm{v})}\right|^2 + c_s^2\left|\frac{\mathrm{i}\varrho^{(\mathrm{v})}}{\rho_0}\right|^2\right) \ , \tag{3.29}$$

$$E^{(\mathrm{w})}(t > t^*) \equiv \frac{\rho_0}{2}\left(\left|v_x^{(\mathrm{w})}\right|^2 + \left|v_y^{(\mathrm{w})}\right|^2 + c_s^2\left|\frac{\mathrm{i}\varrho^{(\mathrm{w})}}{\rho_0}\right|^2\right) \ , \tag{3.30}$$

which also evolve independently. $E^{(\mathrm{v})}$ and $E^{(\mathrm{w})}$ have not any physical meaning in the time interval where $R(t)$ is not small and the vortex and wave SFH strongly interfere. However, can be interpreted as the vortex and wave SFH energy later, when $R(t) \ll 1$ and the interference is negligible. Consequently, introducing vortex and wave characteristics at $t \to t^* + 0$, we can determine values of physical quantities of SFH asymptotically (at $R(t) \ll 1$). Our numerical calculations show that $E^{(\mathrm{w})}(t)$ increases and $E^{(\mathrm{v})}(t)$ decreases in time. Thus, we can say, that the wave harmonic generated at $t = t^*$ (satisfying condition $k_y(t)/k_x < 0$) gains energy from the shear flow and is amplified. The vortex SFH, instead, gives energy back to the background flow and diminishes.

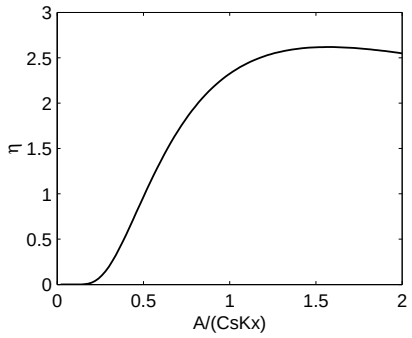

Figure 3.5: Effective parameter of the wave generation as a function of the parameter $R_{max} = A/(c_s k_x)$. η is not the efficiency of the wave generation, since it reaches values larger than 1. This indicates that the generated waves are supported energetically by the mean shear flow energy, while the vortex perturbations only trigger wave generation.

As the wave SFH energy at $(t \gg t^*)$ is uniquely determined by the value of $E^{(\mathrm{w})}(t^*_+)$, we can define the effective parameter of the acoustic wave SFH generation as:

$$\eta \equiv \frac{E^{(\mathrm{w})}(t^*_+)}{E^{(\mathrm{v})}(t^*_-)} = \frac{4v_x^2(t^*)}{v_x^2(t^*) + v_y^2(t^*) + c_s^2(\varrho(t^*)/\rho_0)^2} \ . \tag{3.31}$$

At time t^*_-, we have only vortex SFH, whose energy is defined by the quadratic form of Eq. (10). From this equation and from the symmetry properties of vortex SFH, we derive that

$$E_k(t^*_-) = E^{(\mathrm{v})}(t^*_+) \ , \tag{3.32}$$

i.e. the quadratic form for the vortex at time t^*_+ is equal to the energy of the vortex SFH at time t^*_-, independently from the value of the generated wave SFH amplitude. We can then conclude that the vortex SFH quadratic form defined by Eq. (3.12) does not depend on the amplitude of the generated wave SFH. This can be interpreted as follows: the newly created wave SFH does not change the vortex SFH energetics and thus its energy is supplied by the shear flow, i.e. the vortex SFH acts as a mediator between the background flow and the wave SFH.

We evaluated η as a function of R_{max}. The results of the numerical analysis is plotted in Fig. 5. It appears that the generation of acoustic waves by vortices becomes noticeable at $R_{max} = 0.2$, substantial at $R_{max} = 0.3$ and maximal around $R_{max} = 1.5$. The actual absence of the wave generation at low shear rates is not limited to a certain threshold, but is due to the fact that $|v_x(t^*)|$ is largely reduced at $R_{max} < 0.1$.

3.3.3 On the trajectory of the emitted waves

Using expression for the frequency:

$$\omega(k_x, k_y(t)) = \pm[k_x^2 + k_y^2(t)]^{\frac{1}{2}} c_s \tag{3.33}$$

we can define the trajectory of the emitted wave. (Of course trajectory and wave group velocity are only important for wave packets when the concept of ray is at work. See next sections.)
From Eq. (3.33) we can define the wave group velocity:

$$\mathbf{V}^G = \left(\frac{\partial \omega}{\partial k_x} \ , \ \frac{\partial \omega}{\partial k_y(t)} \right) = \left(\pm \frac{k_x c_s}{\sqrt{k_x^2 + k_y^2(t)}} \ , \ \pm \frac{k_y(t) c_s}{\sqrt{k_x^2 + k_y^2(t)}} \right) \ . \tag{3.34}$$

The $\pm$ signs refer to wave emission in opposite directions. The group velocity is time dependent as $k_y(t)$ depends on time:

$$k_y(t) = k_y(0) - A k_x t = -A k_x (t - t^*) \ . \tag{3.35}$$

At the moment of emission $t = t^*$, as $k_y(t^*) = 0$, the group velocity is directed along the X axis and two rays are emitted in opposite directions along this axis. For simplicity in Fig. 3.6 the rays originate from one point – the size of the emitting area is neglected. In time, these two rays propagate antisymmetrically: they turn in the Y direction as $k_y(t) \neq 0$ when $t > t^*$ (correspondingly $V_y^G(t) \neq 0$) and in addition they are carried backwards by the flow.
The total wave velocity is defined by:

$$\mathbf{V}^T = \mathbf{V}^G + \mathbf{U}_0 = \left(\pm \frac{k_x c_s}{\sqrt{k_x^2 + k_y^2(t)}} + Ay \ , \ \pm \frac{k_y(t) c_s}{\sqrt{k_x^2 + k_y^2(t)}} \right) \ . \tag{3.36}$$

The coordinates of the emitted waves are defined by:

$$x(\tau) = \int_{\tau^*}^{\tau} \mathrm{d}\tau'' [V_x^G(\tau'') \ + \ A y(\tau'')] \ , \tag{3.37}$$

$$y(\tau) = \int_{\tau^*}^{\tau} \mathrm{d}\tau' V_y^G \ . \tag{3.38}$$

Hence, using Eq (3.35-38) we obtain:

$$x(\tau) = \pm \frac{c_s k_x}{2|A k_x|} \left\{ \ln \left(\left| \frac{k(\tau)}{k_x} \right| - \frac{A k_y(\tau)}{|A k_x|} \right) + \frac{k_y(\tau)}{k_x} \left(\left| \frac{k(\tau)}{k_x} \right| - 2 \right) \right\} \ , \tag{3.39}$$

$$y(\tau) = \pm \frac{c_s k_x}{A|k_x|} \left(1 - \left| \frac{k(\tau)}{k_x} \right| \right) \ , \tag{3.40}$$

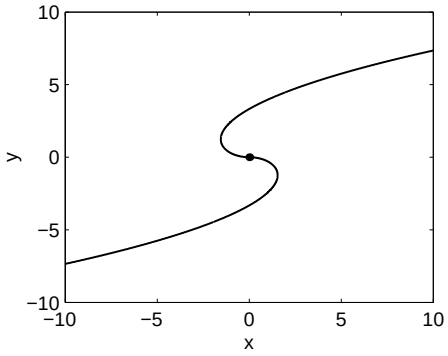

Figure 3.6: Ray trajectories of acoustic waves for $k_x = 1$, $k_y(0) = 0$ and $A/(c_s k_x) = 0.5$. Two rays of waves propagating in opposite direction from the point (0,0) are shown.

where $k(\tau)^2 = k_x^2 + k_y(\tau)^2$. In Fig. 3.6 we present the trajectories for $k_x = 1$, $A/(k_x c_s) = 0.5$ ($k_y(0) = 0$). The ray turning and directions are determined by signs of the shear parameter and wavenumbers: $A > 0$ and $k_y(\tau)/k_x < 0$ at $\tau > \tau^*$, and the asymptotic inclination is zero:

$$\lim_{\tau\to\infty} \frac{\mathrm{d}y}{\mathrm{d}x} = \lim_{\tau\to\infty} \frac{\mathrm{d}y(\tau)/\mathrm{d}\tau}{\mathrm{d}x(\tau)/\mathrm{d}\tau} = 0 \tag{3.41}$$

3.4 Emission of acoustic waves from localized packet of the vortex perturbations

In this section we present a numerical study of a localized packet of vortex perturbations embedded in a flow. We performed direct numerical simulations of Eqs. (3.3-5) in 2D.

3.4.1 Initial values of vortex mode perturbations

We choose $I(k_x, k_y)$ in such a way to obtain an initial (pure vortex/aperiodic mode perturbations) packet localized in the coordinate as well as in wave-number space. The initial values of the physical quantities may be a superposition of the background flow and perturbations:

$$\mathbf{V}(x, y, 0) = Ay\hat{x} + \mathbf{V}'(x, y, 0), \tag{3.42}$$

$$P(x, y, 0) = P_0 + P'(x, y, 0), \tag{3.43}$$

$$\rho(x, y, 0) = \rho_0 + \rho'(x, y, 0). \tag{3.44}$$

We seek the vortex mode solution of Eq. (3.7) in the following analytic form:

$$v_x(0) \equiv u_0(0) + u_1(0) + \ ... \ + u_n(0) + \ ... \ , \tag{3.45}$$

where the zero order term is deduced from the stationary form of the solution (see Eq. 3.32 at $A = 0$) and the consequent terms are derived using the iterative method:

$$u_0(t) \equiv \frac{k_y(t)}{k^2(t)} I(k_x, k_y), \qquad u_n(t) \equiv -\frac{1}{c_s^2 k^2(t)} \frac{\mathrm{d}^2}{\mathrm{d}t^2} u_{n-1}(t). \tag{3.46}$$

The principal concern with such a solution is its convergence. For instance, this solution diverges at $t = t^*$, when $k_y(t^*) = 0$ ($A \neq 0$). The interval of the divergence strongly depends on the shear parameter. In our analysis we consider moderate and relatively high shear of the velocity, when $A^2/(c_s^2(k_x^2+k_z^2)) \leq 1$. In this case the above series is convergent for times when $|k_y(t)/k_x| > 1$. Moreover, the first two term of this series appear to be an excellent approximation to the exact numerical solution for times when $|k_y(t)/k_x| \geq 2$. Therefore, we can use this analytic solution to construct the vortex mode that is localized in the wave-number space outside the $|k_y(t)/k_x| \leq 1$ area. Hence, we calculate $v_x(0)$ and its derivative for the vortex mode perturbations in explicit form:

$$v_x(0) = \left(\frac{k_y}{k_x^2 + k_y^2} + \frac{2A^2 k_x^2 k_y}{c_s^2} \frac{3k_x^2 - k_y^2}{(k_x^2 + k_y^2)^4} \right) I, \tag{3.47}$$

$$v_x'(0) = \left(A k_x \frac{k_y^2 - k_x^2}{(k_x^2 + k_y^2)^2} - \frac{2A^3 k_x^3}{c_s^2} \cdot \frac{3k_x^4 + 5k_y^4 - 24 k_x^2 k_y^2}{(k_x^2 + k_y^2)^5} \right) I, \tag{3.48}$$

where

$$v_x'(0) = \left[\frac{\mathrm{d}}{\mathrm{d}t} v_x(t) \right]_{t=0}. \tag{3.49}$$

The remaining physical variables may be computed using the following equations (cf. Eq. 3.10,11):

$$v_y(0) = \frac{1}{k_x^2 c_s^2 + A^2} \left(k_x k_y c_s^2 v_x(0) - A v_x'(0) - c_s^2 k_x I \right), \tag{3.50}$$

$$\varrho(0) = \frac{\mathrm{i}\rho_0}{k_x^2 c_s^2 + A^2} \left(-A k_y v_x(0) - k_x v_x'(0) + AI \right). \tag{3.51}$$

Hence, for an arbitrary distribution of the velocity circulation $I(k_x, k_y)$ we can use Eqs. 3.47-51 to construct vortex mode perturbations in the wave-number space.
We choose for $I(k_x, k_y)$ the form

$$I(k_x, k_y) = \frac{1}{2} \big(G_+ + |G_+| + G_- + |G_-| \big), \tag{3.52}$$

where the functions $G_+(k_x, k_y)$ and $G_-(k_x, k_y)$ define the packet geometry:

$$G_+ = \epsilon_p \arctan\left(k_R^2 - (k_x - k_{x0})^2 - (k_y - \frac{k_{y0}}{k_{x0}} k_x)^2\right), \tag{3.53}$$

$$G_- = \epsilon_p \arctan\left(k_R^2 - (k_x + k_{x0})^2 - (k_y - \frac{k_{y0}}{k_{x0}} k_x)^2\right). \tag{3.54}$$

This packet consists of two oval shaped areas in wave-number space with sizes defined by k_R and centers situated at (k_{x0}, k_{y0}) and $(-k_{x0}, -k_{y0})$, respectively (see Fig. 3.7). The amplitude of the perturbation is defined by ϵ_p . In our calculations: $A = 0.2$, $k_{x0} = 0.01$, $k_{y0} = 0.02$, $k_R = 0.005$ and $\epsilon_p = 10^{-3}$. As time passes the harmonics drift due to the velocity shear: $k_y(t) = k_y - Ak_x t$. Therefore, the shape of the oval changes due to the shearing deformation. The particular form given in Eqs. (3.53,54) is chosen to have a circular packet, when the center of the packet crosses the line $k_y = 0$. Our mechanism for acoustic wave generation by vortices is linear in nature, while Eqs. (3.3-5) used for our direct numerical simulations are nonlinear. However, embedding small amplitude initial perturbation in the equations, we minimize the action of the nonlinear terms.

We may define the perturbations in coordinate space using the numerical integration:

$$\begin{pmatrix} u_x(x,y,0) \\ u_y(x,y,0) \\ \rho'(x,y,0) \\ p'(x,y,0) \end{pmatrix} = \int\int \mathrm{d}k_x \mathrm{d}k_y \begin{pmatrix} v_x(k_x,k_y,0) \\ v_y(k_x,k_y,0) \\ \varrho(k_x,k_y,0) \\ p(k_x,k_y,0) \end{pmatrix} \exp(ik_x x + ik_y y) \ . \tag{3.55}$$

The initial vortex packet (specificially, $v_x(k_x, k_y, 0)$ and $u_x(x, y, 0)$) constructed using the above formalism is shown in Fig. 3.7. The pattern of the packet in coordinate space (**r**-space) shows a vortical velocity field parallel to wavecrests.

Results of our direct numerical simulations of the packet dynamics are shown on Figs. 3.8-11. The shearing deformation of the vortex mode packet is clearly seen in both wavenumber and in coordinate space. The packet drift in **k**-space is illustrated on Fig. 3.8: Each SFH of the packet drifts with a velocity $(0, -Ak_x)$, i.e., drifts antiparallel to the K_y axis; At $t = 10$, when the center of the packet crosses the line $k_y = 0$ and the bulk of wave generation is expected, the packet is circular in **k**-space. A weak angular scattering of the packets in **k**-space (which is a result of weak nonlinear effects) occurs at later times. This scattering becomes lower for lower amplitudes of the packet. The wave generation does not appear in this figure, as wave and vortex modes have identical dynamics/drift in **k**-space. The phenomenon of wave generation and emission is clearly

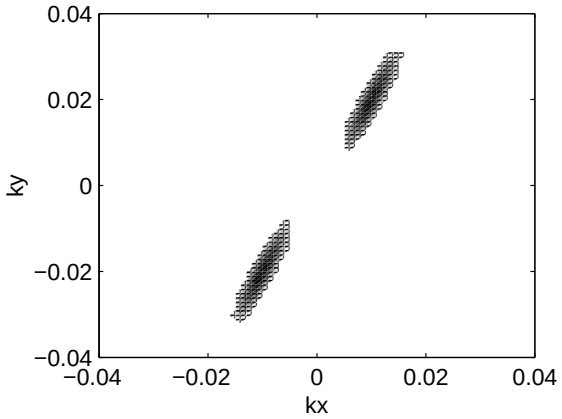

Figure 3.7: A packet of an initial vortex mode in wave-number space. The grey-scale image of the potential vorticity $I(k_x, k_y)$ is shown. The centers of the localization areas are situated at $(\pm k_{x0}, \pm k_{y0})$, where $k_{x0} = 0.01$, $k_{y0} = 0.02$ and the localization radius $k_R = 0.005$. The packet geometry is calculated in a way to obtain circular shape when the packet crosses $k_y = 0$ line.

seen in Fig. 3.9, where perturbations of the packet density in **r**-space is shown. In the beginning ($t < t^* = 10$), the vortex mode gains energy from the mean flow, is amplified and remains aperiodic in time. Wave crests turn around due to the background shear flow. The packet remains localized as the vortex mode group velocity is zero. New features appear after $t > 10$: the packet begins the crossing of $k_y = 0$ line (the central part of the packet crosses the line at $t = 10$) and starts to generate acoustic waves. This generation phenomenon may be identified by the following tracers:

(**a**) *Acoustic wave perturbations have non-zero group velocity.*
Appearance of the perturbations with non-zero group velocity is clearly seen from Fig. 3.9. The wavecrests of the initially localized vortex packet spreads after $t = 10$, when according to the generation mechanism the main part of the wave generation is expected. The vortex packet emits two packets of acoustic waves traveling in mutually antithetic directions, that results in a splitting of the wave crests (see Figs. 9, $t = 16, 20$). The phenomenon is better seen at later times, when acoustic waves leave the area of their generation (see Figs. 9, $t = 24, 28$). The wave generation is limited in time, it lasts until the packet has completely crossed the $k_y = 0$ line. Therefore in Figs. 9 at $t = 24,\ 28$ we see narrow packets

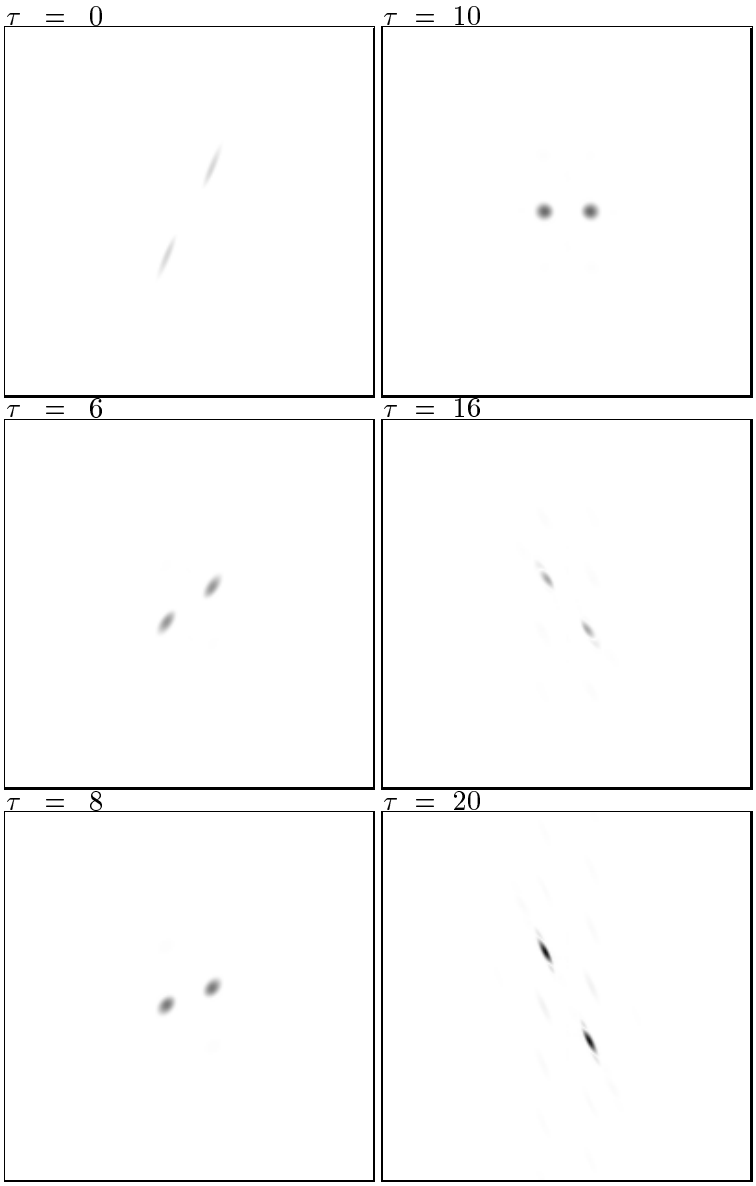

Figure 3.8: The evolution of the packet of a vortex mode in wave-numbers space. The different panels show grey-scale images of stream-wise velocity perturbations ($v_x(k_x, k_y, t)$) at different times ($t = 0,\ 6,\ 8,\ 10,\ 16,\ 20$). See text for details.

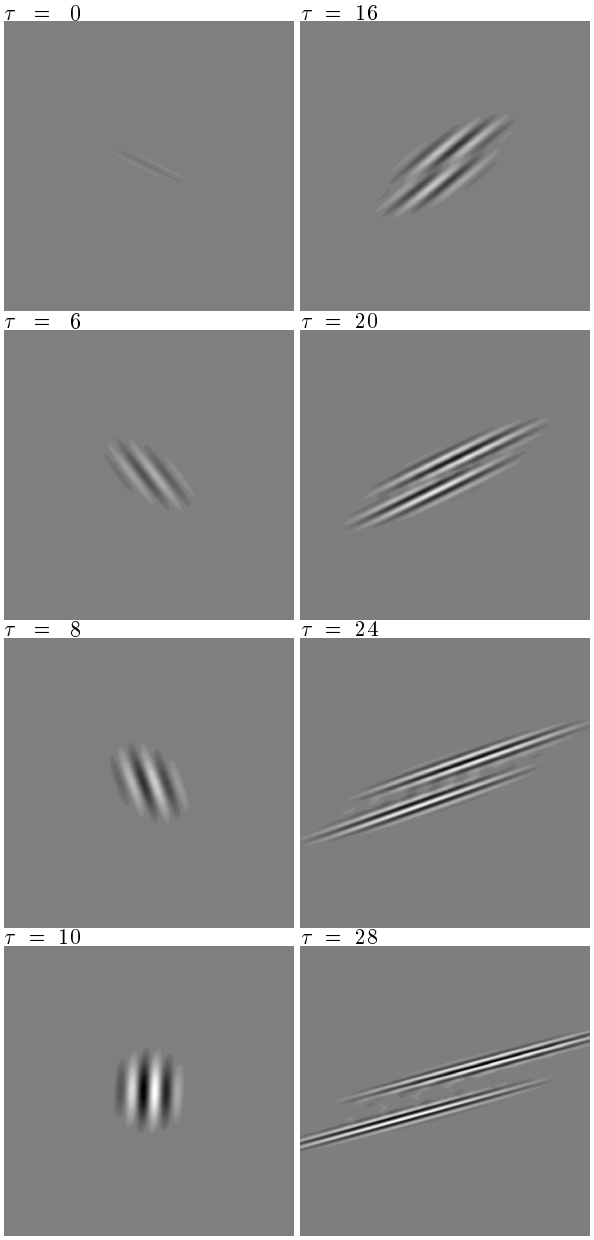

Figure 3.9: The dynamics of the packet of a vortex mode. The different panels show grey-scale images of density perturbations at different times ($t = 0$, 6, 8, 10, 16, 20, 24, 28). The figure demonstrates the generation and consequent propagation of acoustic waves from an initially localized packet of vortex perturbations. See text for details.

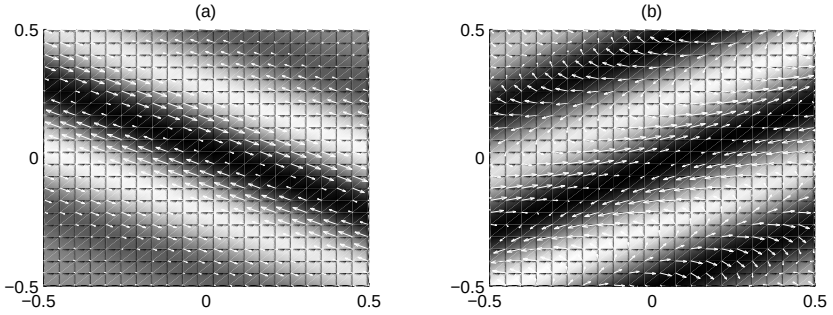

Figure 3.10: Velocity field of the perturbations on the background of the pressure (and density) of the flow, visualized by shading are presented at the initial (graphs a) and final (graph b) moments of the calculation. Initial perturbations correspond to the packet of vortex modes: velocity field is parallel to the packet wave-crests. The non-vortical characteristics are revealed on graph b, where divergent velocity field is situated outside the central area, where the vorticity of the vortex packet is localized.

receding from the center.

(**b**) *Velocity field of the acoustic waves is mainly compressible.*
The vvector plot of the velocity field of the perturbations is given on the background of the flow pressure (and density) visualized in the form of shading is presented on the Fig 3.10a and 3.10b at initial and final moments of the calculation. The mean flow velocity shear is substracted from the vector plot. The change in the kinematic characteristics of the perturbations are apparent. In Fig. 3.10a, the packet velocity field is mainly vortical and directed *parallel* to the wavecrests created by density (and pressure). While Fig. 3.10b reveals non-vortical velocity filed which is situated outside the central area, where vortex mode vorticity is localized. Indeed, waves that are generated propagate in the opposite directions thus forming the pattern of the velocity field presented on Fig. 3.10b. This in turn clearly demonstrates the generation of acoustic waves during the evolution of the vortex packet in the shear flow.

3.5 Generation of acoustic waves by a coherent ring-type vortices

In this section we report on 2D numerical simulations of Eqs. (3.3-5) for an initially coherent ring-type vortex perturbation. The selection of the

initial perturbation is somewhat intricate in contrast to the case of the localized packet. The point is that, in flows with moderate shear parameters (considered by us), compressibility effects on vortex perturbations are appreciable for $|k_y/k_x| \leq 1$. In the previous case, where all SFH fulfilled the requirement $|k_y/k_x| \geq 3/2$, this did not cause any problem. Moreover, in the present case of a ring-type coherent vortex, we have SFH for which $|k_y/k_x| < 1$ and $\ll 1$. Therefore, we can not use a purely kinematic, and perfectly ring shaped initial perturbation

$$v_x(x, y, 0) = \pm\epsilon_r y(x^2 + y^2)^n \exp[-(x^2 + y^2)] \ , \tag{3.56}$$

$$v_y(x, y, 0) = \mp\epsilon_r x(x^2 + y^2)^n \exp[-(x^2 + y^2)] \ , \tag{3.57}$$

$$\rho(x, y, 0) = 0 \ , \tag{3.58}$$

which is used in shearless cases. Eqs. (3.56-58) do not correspond to a pure vortex mode, but describe a mixture of acoustic wave and vortex mode perturbations with the density perturbations fully compensating each other. Nevertheless we use it as "pre-initial", in the sense that through Eqs. (3.56-58) we defined the distribution of $I(k_x, k_y)$ in wavenumber space. Then, using the procedure described in the previous section we construct an actual initial condition, that is an almost pure (with minimal contribution of acoustic waves) ring-type vortex with its corresponding density field. The velocity field of our initial perturbation has also somewhat changed with respect to the "pre-initial" one. In Eqs. (3.56-58) ϵ_r defines the amplitude of the perturbation and the signs define the direction of rotation of the perturbation. The upper signs corresponds to prograde vorticity of the perturbation and the mean flow, while for lower signs perturbation and the flow are adverse.

The initial perturbations of density and velocity (arrows) fields in **r**-space are presented in Fig. 3.11a. In order to have a smooth variation of voticity we use the upper sign in Eqs. (3.56-58) and $n = 0$. We present also some results of a numerical simulation with $n = 2$ for comparison. Equicontours of the initial perturbation energy density in **k**-space are presented in Fig. 3.11b. The values of the physical variables and parameters in this numerical simulations are: $\rho_0 = 1$, $P_0 = 1/\gamma = 3/5$, $c_s = 1$, $A = 0.5$ and $\epsilon_r = 10^{-3}$. The use of a small amplitude for the initial perturbation minimizes the action of nonlinear terms in Eqs. (3.3-5). Computations were made on $(2000, 750)$ point grids.

The density perturbation in **r**-space is presented on Fig. 3.12. The figure describes acoustic wave emission by a coherent vortex and the subsequent wave propagation.

The main characteristics of these phenomena are the following:

(i) The waves are emitted as mutually opposite bidirectional rays along the X axis. When time prograde these two rays are turned in diametrically opposite directions: initially towards the y direction, and then

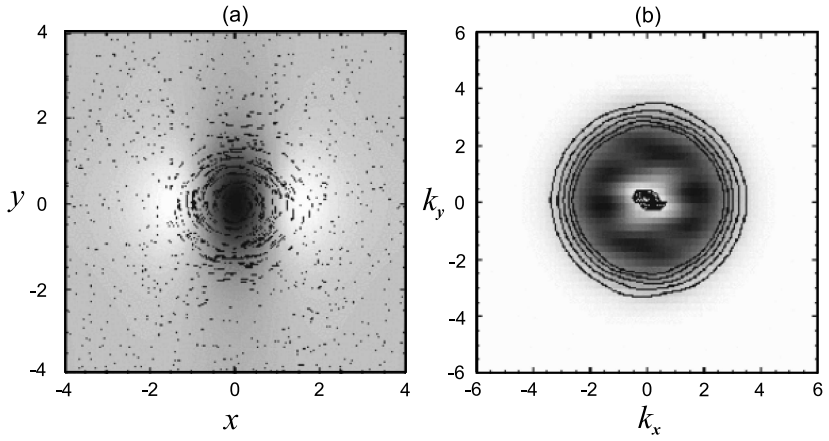

Figure 3.11: Panel (a) shows a grey-scale image of the initial distribution of perturbation density which we have superimposed a vector representation of the initial velocity perturbation. Panel (b) shows a grey scale with superimposed equicontours of the initial perturbation of the energy density in wave-number space.

backwards;
(ii) Gradual growth of the length-scales of the emitted waves;
(iii) High effectiveness of the wave emission;
(iv) Permanent character of the wave emission;
(v) Highly regular spatial structure of the propagating waves. At first sight the structure is similar to a shock wave, rather then to a regular wave. In Fig. 3.9 we present an enlarged view of density and velocity (arrows) fields of a segment of the propagating wave, in the region $8 < x < 16$ at time $t = 10$. Calculations performed for $n = 2$ show highly similar spatial regularity of the emitted wave. For comparison, in Fig. 3.5, we present cuts of the density field of the propagating wave for both cases ($n = 0$ solid curve, $n = 2$ dashed curve) for $x = 12$ at time $t = 10$.

The characteristics of the emission and propagation of the waves are well explained by the aerodynamic sound generation mechanism discussed in Sec. 3.

The trajectories of the emitted wave rays (see Fig. 3.6), calculated in Sec. 3, are in a full agreement with the simulated trajectories in all stages of the wave emission and propagation.

According to the described mechanism, wave generation takes place when a vortex SFH crosses the line $k_y = 0$. Each vortex SFH generates a corresponding wave SFH. Recall that in the vicinity of this

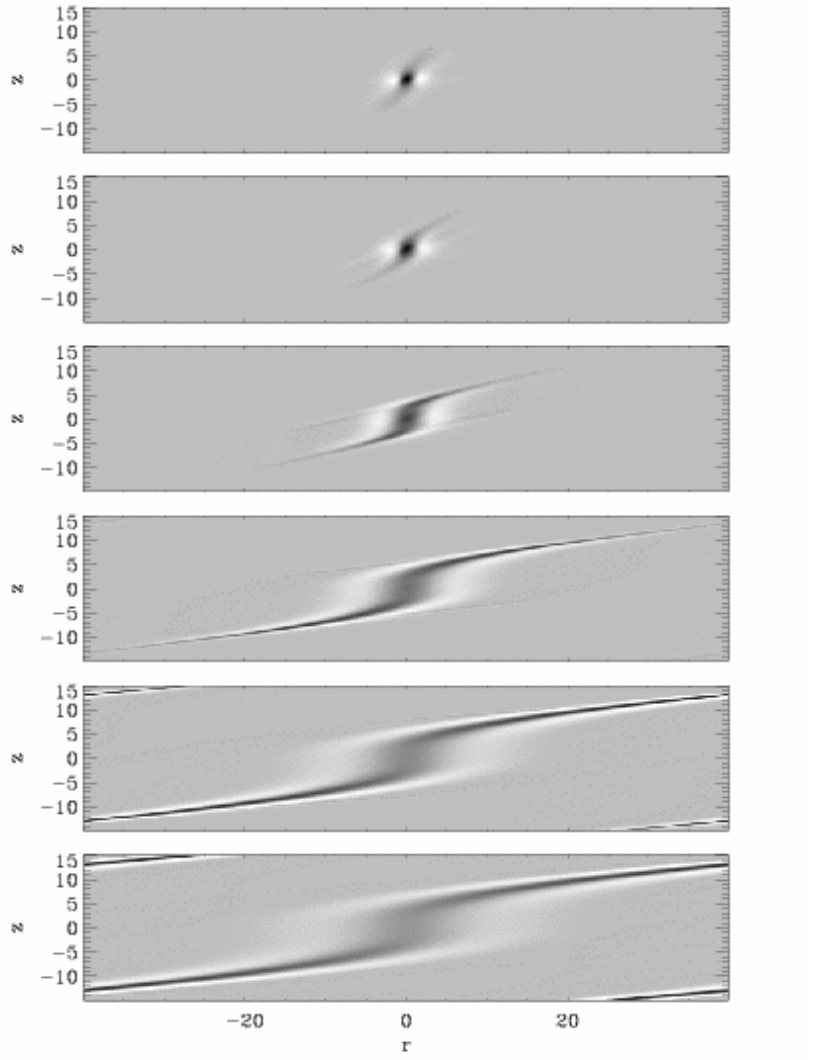

Figure 3.12: Ring-type vortex perturbations. The different panels show grey-scale images of the density distribution at different times ($t = 1, 2, 5, 10, 15, 20$).

line (where value of $R(t)$ is moderate) the vortex and the wave SFH

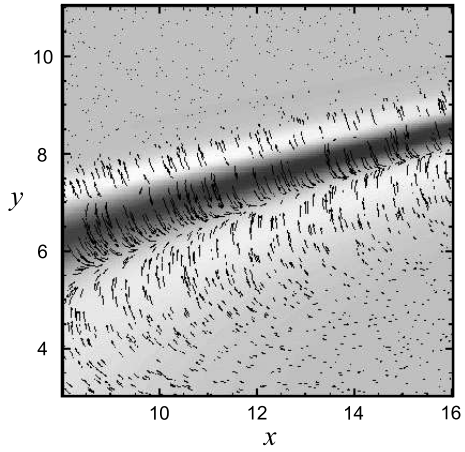

Figure 3.13: Perturbed velocity field superimposed on the grey scale image of the density distribution for a portion of the wave region at $t = 10$

are not separable and we have a contribution of SFH of aperiodic and oscillating modes with comparable time scales. At the moment of crossing it is not possible to define energies of vortex and wave SFH separately. Nonetheless, for wave SFH we introduce the quadratic form $e^{(\mathrm{w})}(k_x, t) \equiv 1/2 \cdot \rho_0 |v_x^{(\mathrm{w})}(k_x, k_y = 0, t)|^2$ that (according to our calculation) defines the energetics of the wave SFH.

The intensity of the wave SFH generation is proportional to $e^{(\mathrm{w})}(k_x, t)$ and to the velocity (of drift in wavenumber space) of vortex SFH at the crossing of the $k_y = 0$ line. From the relation $k_y(t) = k_y(0) - Ak_x t$, it follows that each SFH drifts in $\mathbf{k}$-space with a velocity $(0, -Ak_x)$. Consequently, we can estimate the intensity of the generated wave SFH by $|Ak_x| e^{(\mathrm{w})}(k_x, t)$. Finally, using Eq. (3.11), for the intensity we write:

$$I(k_x, t) = 2\rho_0 |Ak_x| v_x^2(k_x, k_y = 0, t) \ . \tag{3.59}$$

In Fig. 3.15 we plot $I(k_x, t)$ vs k_x at $t = 0; 5; 10$. As time proceeds the maximum of the curve shifts to small values of k_x. Initially, the wave SFH, that are generated with maximal intensity, has a characteristic wavenumber $k_x \approx 1$. At $t = 5$ the maximum is shifted to $k_x \approx 0.6$ and, finally, at $t = 10$ to $k_x \approx 0.3$. Hence, as time proceeds the wave number of the generated wave SFH decreases and the characteristic length scale increases.

What is the explanation of the high effectiveness of the wave emission? Initially, when the intensity is maximal in neighborhood of $k_x = 1$, the

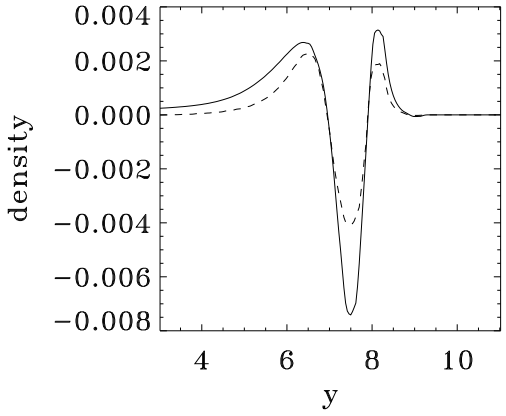

Figure 3.14: Cuts of the density field of the propagating wave at $x = 12$ and $t = 10$. The solid line is for an initial vortex with $n + 0$ and the dashed line for an initial vortex with $n = 2$.

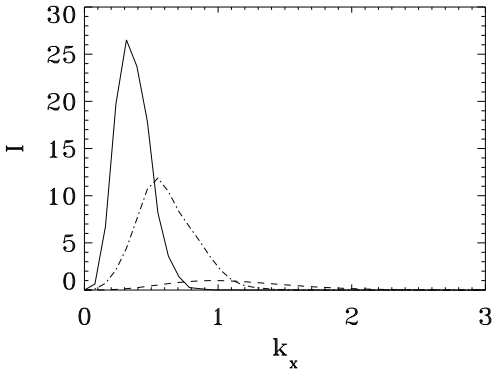

Figure 3.15: Intensity of the generation of wave SFH $I(k_x, t)$ as a function of wavenumber k_x at three different times. The dashed line is for $t = 0$, the dash-dotted line is for $t = 5$ and the solid line is for $t = 10$.

maximal shear rate can be estimated as:

$$R_{max} = \frac{A}{k_x c_s} \approx \frac{0.5}{1 \cdot 1} = 0.5. \tag{3.60}$$

When the wave number decreases, the value of shearrate increases and attains a value $R_{max} \approx 1.5$ at $t = 10$. Fig. 3.5 denotes high effectiveness of the wave generation for this range of values of R_{max}.
The total intensity of the wave generation may be estimated by:

$$I_{tot}(t) = \int_0^\infty dk_x I(k_x, t) = \int_0^\infty dk_x \cdot 2\rho_0 |2Ak_x| v_x^2(k_x, k_y = 0, t) \ . \tag{3.61}$$

In Fig. 3.16 we plot $I_{tot}(t)$ vs time. This figure shows an initial increase and then a slow decrease in time. These facts explain the permanent character of the wave generation/emission.
What about the highly regular structure of emitted waves?

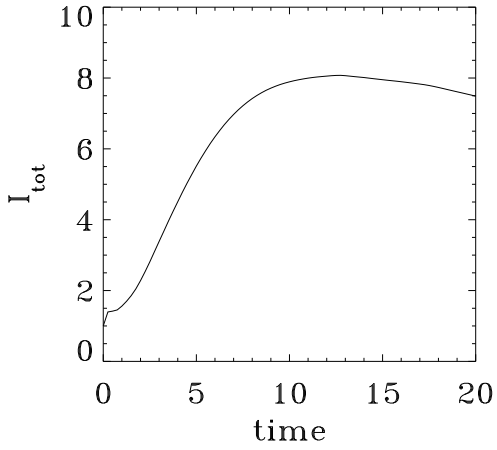

Figure 3.16: Total intensity of wave generation as a function of time.

A wide spectrum of wave SFH is generated at each moment since $I(k_x, t)$ differs from zero in a wide range of k_x. Fig. 3.14 represents an integral picture of the generated and propagating wave interference. According to Figs. 3.4 the wave harmonics, at the moment of generation, have highly regular phases that are similar to each other (specifically, all density perturbation SFH are excited with zero phase). These phase regularity and similarity are the reasons for the regular interference picture that are seen on Figs. 3.9-12.

3.6 Conclusions

In this chapter we have presented the linear, non-resonant generation of acoustic waves by vortices. We have analyzed this phenomenon in the wave-number space for a single SFH as well as in real space using direct numerical simulation.
Let us summarize the *linear* dynamics of 2D vortex mode SFH with an initial wave vector $\mathbf{k} = (k_x, k_y(0))$ in the flow $\mathbf{U_0} = (Ay, 0)$. The main properties are:

- A necessary condition for wave generation is $k_y(0)/k_x > 0$. The generation takes place at moderate to high shear rates. It becomes noticeable at $R_{max} \equiv A/(k_x c_s) = 0.2$ and is substantial at $R_{max} > 0.3$.

- The vortex SFH remains aperiodic by nature and its energy increases until $k_y(t)/k_x > 0$. SFH exhibits well known transient growth. When $k_y(t^*) = 0$, the vortex mode SFH gives rise to a

corresponding acoustic wave SFH. The generation of wave is sudden (see Fig. 3.4c). Of course this statement is arbitrary, as in the vicinity of t^*, the time scales of the vortex and the wave SFH are comparable: the perturbations are not separable and we have some contribution of SFH of aperiodic and oscillating modes. However our arbitrary separation of modes at time t^* is productive. It allows us to gain more insight into the nature of the wave generation, establish the initial characteristics of the wave SFH, determine further dynamics of SFH even quantitatively.

- When the wave SFH shows up (irrespective of the system parameters: A, k_x, $k_y(0)$, R_{max}) it has zero density and cross-stream velocity, and maximal streamwise velocity. This fact is at the basis of the highly regular picture of the wave propagation.
- The energy of the emerged wave SFH is supplied by the shear flow. The vortex SFH act as the mediator between the background flow and the wave SFH.
- After the wave emerged $(t > t^*)$, the subsequent dynamics of the vortex and wave SFH are not coupled. Generated acoustic waves extract shear flow energy and grow.

We have shown that the velocity shear induced conversion of vortices into waves becomes noticable at moderate to high shear rates. This is precisely the configuration where the non-normality of the shear flow dynamics is most profound and the modal description is invalid. For instance we emphasize the choice of the aerodynamic variable. Led by the simplicity of the homogeneous part of the wave-equation (see Eq. 3.7) we have chosen $v_x(t)$ in order to analyze the process of wave excitation for single SFH. This equation will have the similar simple form in real space as well, where the spatial derivatives stand in place of the wave-numbers. In contrast to the Eq. (3.7), consider the conventional variables used in aerodynamic research, such as density or pressure. In this case, in order to reach correct results, the analysis should be based on Eq. (3.7), or its replicated form in the **r**-space which has a quite complicated form. Otherwise, employing the acoustic analogy equation in the incorrect form, will lead to the pseudo effect of wave excitation. The linear source terms will not be zero when $I = 0$ and there should be no acoustic excitation. This circumstance, together with the non-normality of shear flow dynamics, indicate that aerodynamic sound sources evaluated through the modal approach to the acoustic analogy equation are incorrect. That is why results of the presented study fill this gap in aeroacoustic theory.

Acoustic waves generated from vortices due to the velocity shear have spatial characteristics that are similar to their sources. The excited

waves have the same *wave-numbers* as the vortex mode perturbations that generated the waves. In this respect shear flow noise intrinsically differs from the aerodynamic sound produced stochastically by turbulent fluctuations. In the latter process generated sound frequency is similar to the temporal variation scales of the source flow. Temporal variation of vortex mode perturbations is due to the velocity shear of the flow (otherwise they are stationary) and may be defined by the shear parameter A. The wave excitation occurs at $t = t^*$, where $R(t^*) = R_{max}$. Hence at $R_{max} = A/\omega(t^*) < 1$ waves with *higher frequencies* than the temporal variations in the source shear flow will be generated.

Chapter 4

Mode conversion in MHD shear flows: excitation of magnetosonic waves

In the present chapter we study the influence of a magnetic field on mode conversion studied in the previous chapters.

For the sake of direct comparison we consider the simplest example of the MHD shear flow which may support only one wave mode. For this purpose we analyze the dynamics of the planar perturbations in a 3D MHD flow with a simple geometry.

The equilibrium flow and the equations governing the linear perturbations are summarized in Sec. 1. Sec. 2 describes the linear spectrum in the absence of velocity shear. Dynamics individual modes in the flows with non-zero velocity shear are analyzed in Sec. 3. The sources of magnetosonic waves due to the velocity shear induced mode conversion mechanism are also identified their. The numerical analysis of the wave excitation phenomenon is given in Sec. 4. The chapter is summarized in Sec. 5.

4.1 Linear perturbations

Let us consider a horizontal shear flow $\mathbf{V}_0 = (Ay, 0, 0)$ in a vertical uniform magnetic filed: $\mathbf{B}_0 = (0, 0, B_0)$, $B_0 = const.$ (see Fig. 4.1). As usual we expand the physical quantities into the equilibrium and

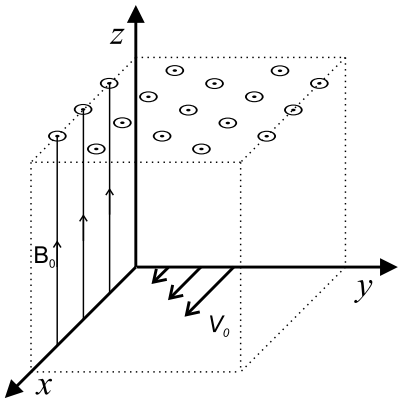

Figure 4.1: A horizontal shear flow $\mathbf{V}_0 = (Ay, 0, 0)$ in a vertical uniform magnetic field $\mathbf{B}_0 = (0, 0, B_0)$.

perturbed parts as:

$$P = P_0 + P', \quad \rho = \rho_0 + \rho', \quad \mathbf{V} = \mathbf{V}_0 + \mathbf{V}', \quad \mathbf{B} = \mathbf{B}_0 + \mathbf{B}'. \tag{4.1}$$

For simplicity we restrict ourselves to 2D perturbations, i.e., perturbations that are uniform in the vertical direction:

$$\mathcal{W} \equiv (\rho', P', V_x', V_y', V_z', B_x', B_y', B_z'), \quad \frac{\partial}{\partial z}\mathcal{W} \equiv 0. \tag{4.2}$$

Linearization of Eqs. (2.1-5) for the perturbations leads to the following system of linear differential equations:

$$\left(\frac{\partial}{\partial t} + Ay\frac{\partial}{\partial x}\right)\rho' = -\rho_0\left(\frac{\partial V_x'}{\partial x} + \frac{\partial V_y'}{\partial y}\right) = 0, \tag{4.3}$$

$$\left(\frac{\partial}{\partial t} + Ay\frac{\partial}{\partial x}\right)V_x' + AV_y' = -\frac{1}{\rho_0}\frac{\partial P'}{\partial x} - \frac{B_0}{4\pi\rho_0}\frac{\partial B_z'}{\partial x}, \tag{4.4}$$

$$\left(\frac{\partial}{\partial t} + Ay\frac{\partial}{\partial x}\right)V_y' = -\frac{1}{\rho_0}\frac{\partial P'}{\partial y} - \frac{B_0}{4\pi\rho_0}\frac{\partial B_z'}{\partial y}, \tag{4.5}$$

$$\left(\frac{\partial}{\partial t} + Ay\frac{\partial}{\partial x}\right)V_z' = 0, \tag{4.6}$$

$$\left(\frac{\partial}{\partial t} + Ay\frac{\partial}{\partial x}\right)B_x' = AB_y', \tag{4.7}$$

$$\left(\frac{\partial}{\partial t} + Ay\frac{\partial}{\partial x}\right)B_y' = 0, \tag{4.8}$$

$$\left(\frac{\partial}{\partial t} + Ay\frac{\partial}{\partial x}\right)B_z' = -B_0\frac{\partial V_x'}{\partial x} - B_0\frac{\partial V_y'}{\partial y}. \tag{4.9}$$

Let us consider adiabatically compressible perturbations:

$$P' = c_s^2 \rho'. \tag{4.10}$$

Eqs. (4.7) and (4.8) describe the stretching of the fieldlines of the perturbed magnetic field in the shearing plane. This effect is not coupled to the evolution of the perturbations of the density (ρ'), velocity ($\mathbf{V}'$) and vertical magnetic field (B_z'). In addition the magnetic field has no effect on the vertical velocity fluctuations that are convected with the background flow (see Eq. 4.6). Hence, Eqs. (4.3-4.5) and (4.9-10) are two uncoupled sets of equations that compose the closed system of the differential equations that may be solved independently. Following the standard method of the non-modal approach we expand the perturbations into the spatial Fourier harmonics with shearing wave-numbers:

$$\left\{ \begin{array}{c} \rho'(\mathbf{r},t) \\ \mathbf{V}'(\mathbf{r},t) \\ \mathbf{B}'(\mathbf{r},t) \end{array} \right\} = \left\{ \begin{array}{c} \rho(\mathbf{k},t) \\ \mathbf{v}(\mathbf{k},t) \\ \mathbf{b}(\mathbf{k},t) \end{array} \right\} \exp(\mathrm{i}k_x x + \mathrm{i}k_y(t) y), \tag{4.11}$$

$$k_y(t) = k_y(0) - A k_x t. \tag{4.12}$$

Hence, perturbation SFH is described by the following linear system:

$$\frac{\mathrm{d}}{\mathrm{d}t}\frac{\mathrm{i}\rho(t)}{\rho_0} - k_x v_x(t) - k_y(t) v_y(t) = 0, \tag{4.13}$$

$$\frac{\mathrm{d}}{\mathrm{d}t} v_x(t) + A v_y(t) + c_s^2 k_x \frac{\mathrm{i}\rho(t)}{\rho_0} + V_A^2 k_x \frac{\mathrm{i}b_z(t)}{B_0} = 0, \tag{4.14}$$

$$\frac{\mathrm{d}}{\mathrm{d}t} v_y(t) + c_s^2 k_y(t) \frac{\mathrm{i}\rho(t)}{\rho_0} + V_A^2 k_y(t) \frac{\mathrm{i}b_z(t)}{B_0} = 0, \tag{4.15}$$

$$\frac{\mathrm{d}}{\mathrm{d}t}\frac{\mathrm{i}b_z(t)}{B_0} - k_x v_x(t) - k_y(t) v_y(t) = 0, \tag{4.16}$$

where $V_A^2 = B_0^2/4\pi\rho_0$ is the Alfvén velocity.

4.2 Linear spectrum

In order to identify the linear spectrum we use a full spectral expansion of the physical variables in Eqs. (4.13-4.16) which becomes possible in the shearless limit ($A = 0$):

$$\rho(t), \mathbf{v}(t), \mathbf{b}(t) \propto \exp(\mathrm{i}\omega t) \tag{4.17}$$

This yields the following dispersion equation:

$$\omega^2(\omega^2 - (c_s^2 + V_A^2)k^2) = 0, \tag{4.18}$$

where $k^2 = k_x^2 + k_y^2$. The solutions of this dispersion equation are:

$$\omega^2 = 0, \tag{4.19}$$

$$\omega_{\rm ms}^2 = (c_s^2 + V_A^2)k^2. \tag{4.20}$$

The first solution is a stationary mode with zero frequency. The second solution (see Eq. 4.20) are the magnetosonic waves ($\omega_{\rm ms}$). For the aperiodic modes we can use $\mathrm{d}/\mathrm{d}t = 0$ and $A = 0$ in Eqs. (4.13-16) and obtain the following two stationary solutions:

$$k_x v_x + k_y v_y = 0, \tag{4.21}$$

or

$$c_s^2 \frac{\rho}{\rho_0} + V_A^2 \frac{b_z}{B_0} = 0. \tag{4.22}$$

Hence, Eq. (4.19) describes the two branches of stationary (aperiodic) solutions with intrinsically different physical nature. The first branch is similar to the hydrodynamic case and corresponds to the vortex modes with nonzero vorticity. The second branch does not involve the velocity perturbations (in zero shear limit), but describes the deviation of the system from vertical magneto-mechanic balance. The latter will be referred as an aperiodic magneto-mechanic brunch.

4.3 Dynamics of perturbation modes

The perturbations of the sheared medium are described by Eqs. (4.13-16). Obviously Eqs. (4.21,22) do not hold any longer and the corresponding modes are not stationary. However, the following quantities associated with these modes are generally time invariant:

$$I_1 = k_x v_y(t) - k_y(t) v_x(t) - A\frac{\mathrm{i}\rho(t)}{\rho_0}, \tag{4.23}$$

$$I_2 = \frac{\mathrm{i}\rho(t)}{\rho_0} - \frac{\mathrm{i}b_z(t)}{B_0}. \tag{4.24}$$

I_1 is the contribution of the vortex mode perturbations topotential vorticity of the flow which is conserved even in this magnetized case (for the given flow configuration). I_2 is the deviation from the vertical magneto-mechanical balance which is also conserved. Note, that in shear flows this aperiodic mode involves a perturbation of velocity. With the help of Eqs. (4.23,24) we may rewrite Eqs. (4.13-16) in the form of a dynamical equations for the individual modes:

$$\frac{\mathrm{d}^2 v_x(t)}{\mathrm{d}t^2} + (c_s^2 + V_A^2)k^2(t)v_x(t) = -(c_s^2 + V_A^2)k_y(t)I_1 - AV_A^2 k_y(t)I_2, \tag{4.25}$$

$$\frac{\mathrm{d}I_1}{\mathrm{d}t} = 0, \tag{4.26}$$

$$\frac{\mathrm{d}I_2}{\mathrm{d}t} = 0. \tag{4.27}$$

The homogeneous part of Eq. (4.25) describes the magnetosonic wave SFH in the absence of the aperiodic modes: $I_1 = I_2 = 0$. Eq. (4.25) is analogous to the equation for the acoustic waves in the hydrodynamic medium (see Eq. 3.7). As we have already seen, the inhomogeneous terms in this wave equation may lead to a non-resonant excitation of the system oscillations. Since we have multiple sources of oscillations that are different in nature we analyze the perturbations in more details.
The solutions of Eq. (4.25-27) describe the system completely. Using the solutions for $v_x(t)$, $\mathrm{d}/\mathrm{d}tv_x(t)$ and the conserved quantities I_1 and I_2 we can calculate the remaining physical quantities as follows:

$$v_y(t) = \frac{1}{A^2 + (c_s^2 + V_A^2)k_x^2} \times$$

$$\times \left(-A\frac{\mathrm{d}v_x(t)}{\mathrm{d}t} + (c_s^2 + V_A^2)k_x k_y(t) v_x(t) + (c_s^2 + V_A^2)k_x I_1 + AV_A^2 k_x I_2 \right), \tag{4.28}$$

$$\frac{\mathrm{i}\rho(t)}{\rho_0} = \frac{1}{A^2 + (c_s^2 + V_A^2)k_x^2} \times$$

$$\times \left(-k_x\frac{\mathrm{d}v_x(t)}{\mathrm{d}t} - Ak_y(t)v_x(t) - AI_1 + V_A^2 k_x^2 I_2 \right), \tag{4.29}$$

$$\frac{\mathrm{i}b_z(t)}{B_0} = \frac{\mathrm{i}\rho(t)}{\rho_0} - I_2. \tag{4.30}$$

Naturally, Eqs. (4.31-37) are reduced to the stationary solutions described by Eqs. (4.21), (4.22) in the zero shear limit ($A = 0$).
The homogeneous part of Eq. (4.25) describes the magnetosonic wave SFH in the absence of the aperiodic modes: $I_1 = I_2 = 0$. The inhomogeneity in this equations is due to the sources of magnetosonic waves in the system. Solutions of the vortex and magneto-mechanical modes may be found in the low shear rate approximation ($R \ll 1$). In this approximation Eqs. (4.23-25) lead to: the solution for the vortex mode perturbations SFH, when $I_1 \neq 0$, $I_2 = 0$:

$$v_x(t) = -\frac{k_y(t)}{k^2(t)} I_1, \tag{4.31}$$

$$v_y(t) = \frac{k_x}{k^2(t)} I_1 - \frac{2A^2 k_x^3}{\left[A^2 + (c_s^2 + V_A^2)k_x^2\right] k^4(t)} I_1, \tag{4.32}$$

$$\frac{\mathrm{i}b_z(t)}{B_0} = \frac{\mathrm{i}\rho(t)}{\rho_0} = -\frac{2A^2k_x^3 I_1}{[A^2 + (c_s^2 + V_A^2)k_x^2]\, k^4(t)}, \tag{4.33}$$

and for the magneto-mechanical mode, when $I_1 = 0$, $I_2 \neq 0$:

$$v_x(t) = -\frac{AV_A^2 k_y(t)}{(c_s^2 + V_A^2)k^2(t)} I_2, \tag{4.34}$$

$$v_y(t) = \frac{AV_A^2 k_x}{(c_s^2 + V_A^2)k^2(t)} I_2 - \frac{2A^3 V_A^2 k_x^4 I_2}{[A^2 + (c_s^2 + V_A^2)k_x^2]\,(c_s^2 + V_A^2)k^4(t)}, \tag{4.35}$$

$$\frac{\mathrm{i}\rho(t)}{\rho_0} = \frac{V_A^2}{c_s^2 + V_A^2} I_2 + \frac{2A^2 V_A^2 k_x^4 I_2}{[A^2 + (c_s^2 + V_A^2)k_x^2]\,(c_s^2 + V_A^2)k^4(t)}, \tag{4.36}$$

$$\frac{\mathrm{i}b_z(t)}{B_0} = \frac{c_s^2}{c_s^2 + V_A^2} I_2 + \frac{2A^2 V_A^2 k_x^4 I_2}{[A^2 + (c_s^2 + V_A^2)k_x^2]\,(c_s^2 + V_A^2)k^4(t)}, \tag{4.37}$$

Eqs. (4.34), (4.35) show that the intrinsically magneto-mechanical mode has a transient vortical field with amplitudes proportional to the flow shear rate. This creates the necessary condition for the interaction and energy transfer between the magneto-mechanic and magnetosonic waves in shear flows. Hence, similarly to the analysis of the mode conversion given in the Chap. 3 we may conclude that SFH of the vortex modes, as well as aperiodic magneto-mechanical modes may excite the magnetosonic waves with similar wave-numbers.

The main contribution to the inhomogeneity in Eq. (4.25) and hence to the sources of the magnetosonic waves at moderate shear rates ($R < 1$) comes from the vortex modes. The relative weight of the transient vortical field of the magneto-mechanical solution increases at high shear rates. For a more detailed study we employ numerical analysis.

4.4 Mode conversion

To study mode conversion we perform a numerical study of Eqs. (4.13-16) with appropriately chosen initial conditions. We calculate vortex modes by setting $I_1 = 1$, $I_2 = 0$ and by using the numerical iterative method to eliminate the magnetosonic perturbations initially. We use $I_1 = 0$ and $I_2 = 1$ as the initial conditions for the aperiodic magneto-mechanical mode. While the initial conditions for the magnetosonic waves may be chosen rigorously by setting $I_1, I_2 = 0$. To demonstrate the phenomenon of the mode conversion we study the vortex and aperiodic magneto-mechanical mode separately at moderate shear rate $R = A/(c_s k_x) = 0.4$. Fig. 4.2 illustrates the conversion of a vortex mode SFH into a magnetosonic wave. Fig. 4.3 shows the analogous effect for the magneto-mechanical mode.

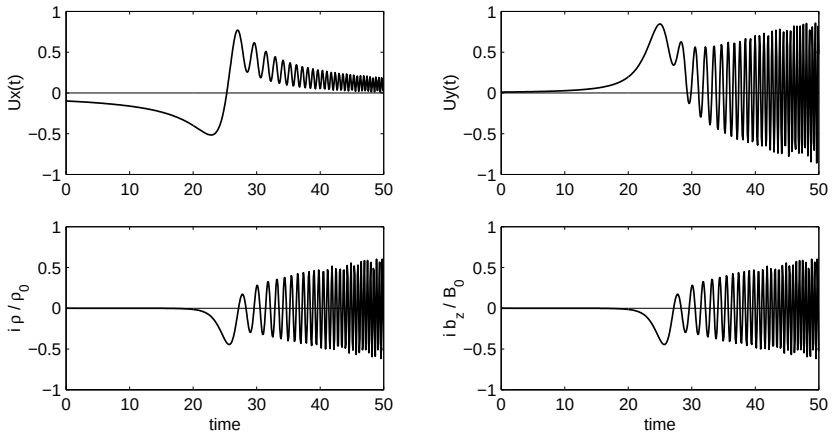

Figure 4.2: Evolution of $v_x(t)$, $v_y(t)$, $\mathrm{i}\rho(t)/\rho_0$ and $\mathrm{i}b_z(t)/B_0$ for $k_y(0)/k_x = 10$, $A/(c_s k_x) = 0.4$, $\beta = 1$, $I_1 = 1$ and $I_2 = 0$ when only the vortex modes are present initially. Generation of magnetosonic wave is clearly seen at $t > t^* = 25$ ($k_y(t^*) = 0$).

The amplitude of the excited magnetosonic waves grows with the increase of the velocity shear rate in general. Fig. 4.3 shows the total energy and the ratio of the vortical and magnetosonic energies to the total SFH energy for different parameters of the velocity shear. Here we have used the standard definitions of the perturbation SFH energy density:

$$E_{ms}(t) = \frac{\rho_0}{k^2(t)}|k_x v_x(t) + k_y(t)v_y(t)|^2 + c_s^2\rho_0\left|\frac{\rho(t)}{\rho_0}\right|^2 + V_A^2\rho_0\left|\frac{b_z(t)}{B_0}\right|^2, \tag{4.38}$$

$$E_v(t) = \frac{\rho_0}{k^2(t)}|k_x v_y(t) - k_y(t)v_x(t)|^2, \tag{4.39}$$

$$E(t) = E_v(t) + E_{ms}(t). \tag{4.40}$$

Figure 4.4 also shows the general tendency in the shear flow. Even when the mode conversion efficiency is not significant, the growing magnetosonic waves eventually become the dominant contribution to the perturbations in the flow. This fact is better seen on the graph B.2 (Fig. 4.4) where the total energy tends to accumulate into the magnetosonic wave eventually. At higher shear rates this process proceeds much faster (see graph C.2).

We can examine the amplitude of the generated wave in analytical form by using the numerical extrapolation of the excited wave amplitude by Chagelishvili et al. 2000:

$$\frac{v_x(t^*)}{I} \approx \frac{1}{1.2R}\exp\left(-\frac{1}{1.2R}\right) \tag{4.41}$$

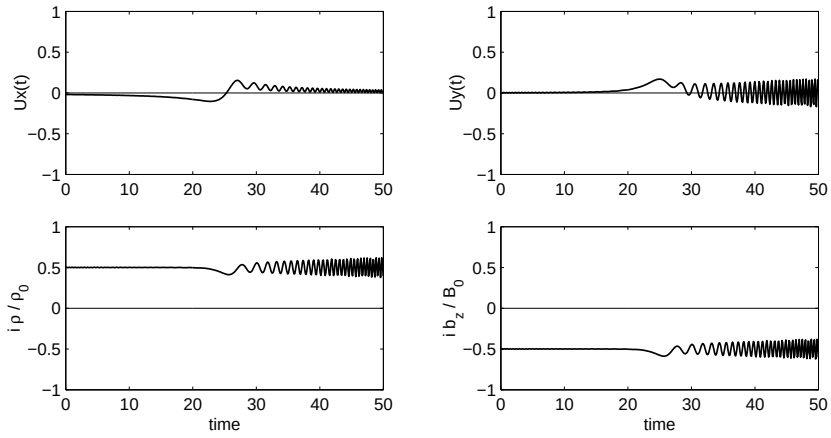

Figure 4.3: Evolution of $v_x(t)$, $v_y(t)$, $\mathrm{i}\rho(t)/\rho_0$ and $\mathrm{i}b_z(t)/B_0$ for $k_y(0)/k_x = 10$, $A/(c_s k_x) = 0.4$, $\beta = 1$, $I_1 = 0$ and $I_2 = 1$ when only the aperiodic magneto-mechanic perturbations are present initially. generation of magnetosonic wave is clearly seen at $t > t^* = 25$ ($k_y(t^*) = 0$).

When we compare Eqs. (3.7) with (4.25) and use the extrapolated analytical form we can conclude that the amplitude of the excited magnetosonic wave SFH depends on the sources of vorticity and vertical aperiodic magneto-mechanical perturbations. Hence we may derive the amplitudes of the wave SFH separately for these two cases as follows:

$$I_2 = 0 \quad : \quad V_x^{ms} = \frac{\sqrt{c_s^2 + V_A^2}}{1.2A} \exp\left(-\frac{k_x\sqrt{c_s^2 + V_A^2}}{1.2A}\right) I_1, \tag{4.42}$$

$$I_1 = 0 \quad : \quad V_x^{ms} = \frac{c_s V_A^2}{1.2\sqrt{c_s^2 + V_A^2}} \exp\left(-\frac{k_x\sqrt{c_s^2 + V_A^2}}{1.2A}\right) I_2. \tag{4.43}$$

V_x^{ms} defines the perturbations SFH of the excited magnetosonic wave at $t = t^*$, when $k_y(t^*) = 0$. For $t = t^*$: $\rho^{ms}(t^*) = b_z^{ms}(t^*) = 0$ and we can use Eqs. (4.28)-(4.30) and (4.38) to derive the estimated energy of the generated magnetosonic wave as:

$$E_{ms}(t^*) = \rho_0 |v_x^2(t^*)|. \tag{4.44}$$

Hence the ratio of the efficiencies of the excitation of magnetosonic waves by vortex and magneto-mechanical perturbations is:

$$\frac{E_{ms}^{(1)}(t^*)}{E_{ms}^{(2)}(t^*)} = \frac{(c_s^2 + V_A^2)^2}{c_s^2 V_A^4 A^2} \frac{I_1^2}{I_2^2} = \frac{(1+\beta)^2}{\beta^2 R^2} \frac{I_1^2}{c_s^2 k_x^2 I_2^2}, \tag{4.45}$$

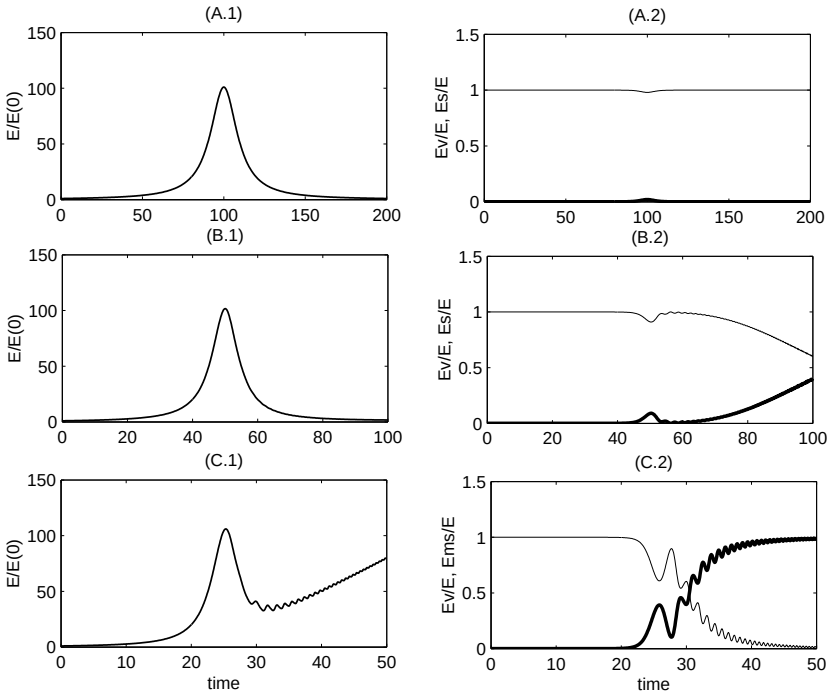

Figure 4.4: Partial values of vortical ($E_V(t)/E(t)$) and magnetosonic ($E_{ms}(t)/E(t)$, heavy graph) energies and normalized total energy ($E(t)/E(0)$) vs time are presented at the following parameters: $\beta = 1$, $k_y(0)/k_x = 10$, $I_1 = I_2 = 1$ and (A.1,2): $R = 0.1$, (B.1,2): $R = 0.2$, (C.1,2): $R = 0.4$.

where $\beta = c_s^2/V_A^2$. Eq. (4.45) shows that in case when both aperiodic modes are equally strongly present in a shear flow (i.e., $|I_1/(c_s k_x I_2)| \simeq 1$), at moderate shear rates $R \leq 1$ and weak or moderate magnetic fields $V_A^2 < c_s^2$, the vortex modes are the main contributors to the magnetosonic wave sources. At higher shear rates $R > 1$ or in strongly magnetized medium $V_A^2 \gg c_s^2$ the waves excited by magneto-mechanical wave source energetically dominate the waves produced by the vortex mode perturbations.

4.5 Summary

We have studied 2D linear perturbations in a 3D unbounded ideal MHD shear flow. The spectrum consist of magnetosonic waves and two aperiodic modes with zero frequencies: a vortex mode with an intrinsic vortical perturbation field and a magneto-mechanical mode which obtains

transient vortical characteristics in the sheared medium.

Both aperiodic modes are able to excite magnetosonic waves with similar wave-numbers when the wave-number in the direction of the velocity shear becomes zero.

The vortex modes are the main source of the waves in flows with weak or moderate magnetic fields. The magneto-mechanical mode can be the dominant generator of waves in a strongly magnetized medium at higher values of the velocity shear.

Chapter 5

Excitation of waves in the convectively unstable shear flow

5.1 Introduction

The investigation carried out in the previous chapters shows the necessity to study non-modal processes in spectrally stable shear flows, i.e., in flows where no exponentially growing solutions are present. Indeed, we have seen that non-modal analysis reveals novel channels of energy exchange between the background flow and different perturbations modes. This poses a natural question: how important are non-modal processes in spectrally unstable shear flows, i.e., in the flows where perturbations of a particular mode grow exponentially? We shall see in the present chapter, that even in this case, non-modal phenomena may play an important role. They can both modify the dynamics of exponentially unstable perturbations as well as introduce additional channels of energy exchange between the spectrally stable and unstable modes of perturbations.

In the present chapter we focus on the spectrally unstable buoyancy mode in a convectively unstable shear flow and study the linear phenomenon of the acoustic wave excitation.

It is well known that thermally unstable flows are not necessarily chaotic but often exhibit regular patterns. The Bénard cells are an example of a regular convective flow, which can be used to demonstrate typical features of the convection. The properties of thermal convection depend on various parameters. Qualitatively this process may be described as a superposition of vertical hot upflows and cold downflows, that carry and exchange the thermal energy of the lower hotter layers with the higher

cooler ones, when the equilibrium of such state is not possible. Convection in an astrophysical environment is more complicated and turbulent. However, in many cases, such as the convection zone of the Sun and presumably in other stars, convection is by no means a fully developed turbulence in the classical sense, but is rather organized, anisotropic and exhibits characteristic scales. This fact enables us to study some processes that occur in these flows using non-chaotic models of the convectively unstable medium. Hence, we employ a regular background of a thermally unstable shear flow and study the linear stage of evolution of the perturbations.

We outline the model of the convectively unstable shear flow in Sec. 2, where we also derive the equations governing the linear perturbations. We classify the linear modes and give the corresponding characteristic physical variables in Sec. 3. Effects of the velocity shear on the perturbation modes individually are investigated in Sec. 4. In this section we give a qualitative analysis of the mode conversion phenomenon, which is numerically analyzed in Sec. 5. In Sec. 6 we discuss the possible consequences of the described phenomenon with an emphasis on the solar convection zone. Finally, we shortly summarize our findings in Sec. 8.

5.2 Physical model and equations

We consider a parallel shear flow $\mathbf{V}_0 = (Ay, 0, 0)$ in the presence of a constant vertical gravity acceleration: $\mathbf{g} = (0, 0, -g)$ with $g = constant$. This geometry is often used in astrophysical applications and is employed to demonstrate novelties in the dynamics of thermally unstable shear flows. The equation of motion:

$$\left\{ \frac{\partial}{\partial t} + (\mathbf{V} \cdot \nabla) \right\} \mathbf{V} = -\frac{\nabla P}{\rho} + \mathbf{g}. \tag{5.1}$$

Together with the equation of continuity (2.1) and energy conservation (2.8) completes the system of differential equations that govern the dynamics of inviscid hydrodynamic shear flow under constant gravity. The physical system described by Eqs. (2.1), (2.8) and (5.1) has the following equilibrium solution:

$$\frac{P_0(z)}{P_0(0)} = \frac{\rho_0(z)}{\rho_0(0)} = \exp(-k_H z). \tag{5.2}$$

$k_H \equiv \gamma g / c_s^2$ is the vertical stratification scale inverse of a length scale and $c_s^2 \equiv \gamma P_0 / \rho_0$ is the sound speed. The equilibrium may be thermally stable or unstable depending on the thermodynamic parameters of the system (in the present model – depending on the parameter γ).

The linear perturbations may be introduced in the following way:

$$\mathbf{V} = \mathbf{V}_0 + \frac{\rho_0(0)}{\rho_0(z)}\mathbf{V}', \quad P = P_0 + P', \quad \rho = \rho_0 + \rho'. \tag{5.3}$$

Here the velocity perturbations are normalized to eliminate the exponential height dependence due to the vertical stratification of the background flow. We use the Cowling approximation and neglect the perturbation of the gravitational acceleration (see Cowling 1941).
Following the standard method of the non-modal analysis we introduce the spatial Fourier harmonics (SFH) of perturbations with time dependent phases:

$$\left\{ \begin{array}{c} p'(\mathbf{r},t) \\ \rho'(\mathbf{r},t) \\ \mathbf{V}'(\mathbf{r},t) \end{array} \right\} = \left\{ \begin{array}{c} p(\mathbf{k},t) \\ \rho(\mathbf{k},t) \\ \mathbf{u}'(\mathbf{k},t) \end{array} \right\} \exp(\mathrm{i}k_x x + \mathrm{i}k_y(t) y + \mathrm{i}\tilde{k}_z z), \tag{5.4}$$

$$k_y(t) = k_y(0) - A k_x t, \tag{5.5}$$

where $\tilde{k}_z \equiv k_z + \mathrm{i}k_H/2$. This complex wave-number is employed to re-scale the vertical axis in the stratified medium (see Lerche & Parker 1967). To avoid complex coefficients in the dynamical equations, we construct the normalized entropy and vertical velocity perturbation SFHs in the following way:

$$s \equiv \left(\mathrm{i}c_s^2 \tilde{k}_z^* - g\right) \frac{p - c_s^2 \rho}{(\gamma - 1) g}, \tag{5.6}$$

$$v \equiv (c_s^2 \tilde{k}_z^* + \mathrm{i}g) u_z, \tag{5.7}$$

where $\tilde{k}_z^* = k_z - \mathrm{i}k_H/2$. Using straightforward manipulations of Eqs. (5.1-7) we obtain the following set of differential equations that govern the SFH of the linear perturbations in stratified shear flows:

$$\frac{\mathrm{d}}{\mathrm{d}t} p(t) = c_s^2 (k_x u_x + k_y(t) u_y) + v, \tag{5.8}$$

$$\frac{\mathrm{d}}{\mathrm{d}t} u_x(t) = -A u_y - k_x p, \tag{5.9}$$

$$\frac{\mathrm{d}}{\mathrm{d}t} u_y(t) = -k_y(t) p, \tag{5.10}$$

$$\frac{\mathrm{d}}{\mathrm{d}t} v(t) = (N_\mathrm{B}^2 - c_s^2 \bar{k}_z^2) p - N_\mathrm{B}^2 s, \tag{5.11}$$

$$\frac{\mathrm{d}}{\mathrm{d}t} s(t) = v. \tag{5.12}$$

N_B^2 is the square of the Brunt-Väisälä frequency: $N_\mathrm{B}^2 \equiv g k_H (\gamma - 1)/\gamma$ and $\bar{k}_z^2 = |\tilde{k}_z|^2 = k_z^2 + k_H^2/4$. In order to model convective instability we

adopt an effective γ model introduced in Ryu & Goodman 1992. The essence of this approximation is that we can use an artificial gamma value instead of the adiabatic factor when the flow is heated uniformly and cooled according to a certain thermodynamic law. In this case the effective $\gamma < 1$, while the adiabatic index $\Gamma = 5/3$. Note, that in Eqs. (5.8-12) we retain $N_{\rm B}^2$ and argue that these equations are more general than the underling γ prescription.
The spectral energy density of the perturbations can be defined as follows:

$$e = e_{\rm k} + e_{\rm p} + e_{\rm t}, \tag{5.13}$$

$$e_{\rm k} = \frac{1}{2}\rho_0(0)\left(u_x^2 + u_y^2 + \frac{v^2}{c_s^2(c_s^2\bar{k}_z^2 - N_{\rm B}^2)}\right), \tag{5.14}$$

$$e_{\rm p} = \frac{1}{2c_s^2\rho_0}p^2, \tag{5.15}$$

$$e_{\rm t} = \frac{N_{\rm B}^2 s^2}{2c_s^2(c_s^2\bar{k}_z^2 - N_{\rm B}^2)\rho_0}. \tag{5.16}$$

where $e_{\rm k}$, $e_{\rm p}$ and $e_{\rm t}$ are the kinetic, elastic and thermobaric energy densities, respectively. Formally the perturbation energy is conserved in the shearless limit: $\mathrm{d}e/\mathrm{d}t = Ac_s^2u_xu_y$ and $e = const$ when $A = 0$. Here we should note, that the thermobaric energy may not be defined separately in the classical sense, due to its negative sign. It reveals the instability of convective eddies and gives a correct contribution to the total energy of the perturbations. For the description of the energy accumulated in the convective (thermal) eddies itself we should take the absolute value of Eq. (5.16).

5.3 Perturbation modes

The linear modes can be classified explicitly in the shearless limit ($A = 0$). In this case the full Fourier expansion of the linear perturbations

$$\left\{\begin{array}{c} p(\mathbf{k},t) \\ \rho(\mathbf{k},t) \\ \mathbf{u}'(\mathbf{k},t) \end{array}\right\} = \left\{\begin{array}{c} \tilde{p}(\mathbf{k},\omega) \\ \tilde{\rho}(\mathbf{k},\omega) \\ \tilde{\mathbf{u}}'(\mathbf{k},\omega) \end{array}\right\} \exp(-\mathrm{i}\omega t), \tag{5.17}$$

yields the dispersion equation:

$$\omega(\omega^4 - c_s^2k^2\omega^2 + N_{\rm B}^2c_s^2k_\perp^2) = 0, \tag{5.18}$$

where $k_\perp^2 \equiv k_x^2 + k_y^2$ and $k^2 = k_\perp^2 + \bar{k}_z^2$. This fifth order equation describes three different modes and five branches of perturbations. Hence, we identify the perturbation modes as solutions of Eq. (5.18):

$$\omega_{\rm v} = 0, \tag{5.19}$$

$$\omega_s^2 = \frac{1}{2}c_s^2 k^2 \left\{ 1 + \left(1 - \frac{4N_{\rm B}^2 k_\perp^2}{c_s^2 \bar{k}^4} \right)^{1/2} \right\}, \tag{5.20}$$

$$\omega_c^2 = \frac{1}{2}c_s^2 k^2 \left\{ 1 - \left(1 - \frac{4N_{\rm B}^2 k_\perp^2}{c_s^2 \bar{k}^4} \right)^{1/2} \right\}, \tag{5.21}$$

where the $\omega_{\rm v}$, ω_s and ω_c correspond to the vortex, acoustic and convective modes, respectively. The vortex mode is described by the stationary zero frequency solution. The acoustic mode frequency is given by Eq. (5.20). The convective mode corresponds to buoyancy perturbations. In stratified flow, when $N_B^2 < 0$, the square of the convective frequency is negative: $\omega_c^2 < 0$. Therefore ω_c is imaginary. Hence this convective mode is unstable and grows exponentially with a growth rate $|{\rm i}\omega_c| = \sqrt{-\omega_c^2}$ (see Eq. 5.17).

5.3.1 Dynamics of perturbation modes

The fact that separate solutions for individual modes exist in the shearless limit imply that Eqs. (5.8-12) may be decoupled in this limit. Indeed, introducing notations:

$$\psi(t) \equiv \left(s(t) - \frac{\bar{k}_z^2}{k^2} p(t) \right), \tag{5.22}$$

and

$$\Omega_s^2 = c_s^2 k^2 - N_B^2 \frac{k_\perp^2}{k^2}, \tag{5.23}$$

$$\Omega_c^2 = N_B^2 \frac{k_\perp^2}{k^2}, \tag{5.24}$$

we may derive physical variables:

$$\Phi_s(t) \equiv \frac{\Omega_c^4}{(\Omega_s^2 - \omega_s^2)(\Omega_c^2 - \omega_c^2) + \Omega_c^4} \left[p(t) + N_B^2 \frac{\Omega_s^2 - \omega_s^2}{\Omega_c^4} \psi(t) \right] \tag{5.25}$$

$$\Phi_c(t) \equiv \frac{\Omega_c^4}{(\Omega_s^2 - \omega_s^2)(\Omega_c^2 - \omega_c^2) + \Omega_c^4} \left[\psi(t) - \frac{(\Omega_c^2 - \omega_c^2)}{N_B^2} p(t) \right] \tag{5.26}$$

that transform Eqs. (5.8-12) into decoupled equations. The radical factors in Eqs. (5.25,26) are arbitrary and are chosen to simplify the further analysis for $A \neq 0$. Hence the decoupled equations that govern the different modes are:

$$\frac{{\rm d}^2}{{\rm d}t^2}\Phi_s(t) + \omega_s^2 \Phi_s(t) = 0, \tag{5.27}$$

$$\frac{{\rm d}^2}{{\rm d}t^2}\Phi_c(t) + \omega_c^2 \Phi_c(t) = 0, \tag{5.28}$$

$$\frac{\mathrm{d}}{\mathrm{d}t}(k_x u_y - k_y u_x) = 0. \tag{5.29}$$

The last equation describes the vortex mode with conservation of vorticity in the zero shear limit. Since we have identified the characteristic physical variables and the equations for the modes separately we may define their energies as follows:

$$e_{con} = \frac{\left((\Omega_s^2 - \omega_s^2)(\Omega_c^2 - \omega_c^2) + \Omega_c^4\right)^2}{2c_s^2\rho_0\Omega_c^8}\left[\Phi_c^2 + \frac{1}{\omega_c^2}\left(\frac{\mathrm{d}\Phi_c}{\mathrm{d}t}\right)^2\right], \tag{5.30}$$

$$e_{vib} = \frac{N_\mathrm{B}^2\left((\Omega_s^2 - \omega_s^2)(\Omega_c^2 - \omega_c^2) + \Omega_c^4\right)^2}{2c_s^2(c_s^2\bar{k}_z^2 - N_\mathrm{B}^2)\rho_0\Omega_c^8}\left[\Phi_s^2 + \frac{1}{\omega_s^2}\left(\frac{\mathrm{d}\Phi_s}{\mathrm{d}t}\right)^2\right], \tag{5.31}$$

where e_{con} and e_{vib} correspond to the energy density of the convective modes and vibrational energy density of the acoustic oscillations, respectively. Starting from this simple situation we study the velocity shear effects on the perturbation modes.

5.4 Velocity shear effects

We rewrite Eqs. (5.8-12) for the characteristic physical variables in order to analyze the effects of the velocity shear of the flow on the individual modes:

$$\frac{\mathrm{d}^2\Phi_s}{\mathrm{d}t^2} + \alpha_1(t)\frac{\mathrm{d}\Phi_s}{\mathrm{d}t} + \alpha_2(t)\Phi_s + \alpha_3(t)\frac{\mathrm{d}\Phi_c}{\mathrm{d}t} + \alpha_4(t)\Phi_c + \xi_1(t)I = 0, \tag{5.32}$$

$$\frac{\mathrm{d}^2\Phi_c}{\mathrm{d}t^2} + \beta_1(t)\frac{\mathrm{d}\Phi_c}{\mathrm{d}t} + \beta_2(t)\Phi_c + \beta_3(t)\frac{\mathrm{d}\Phi_s}{\mathrm{d}t} + \beta_4(t)\Phi_s + \xi_2(t)I = 0, \tag{5.33}$$

$$\frac{\mathrm{d}I}{\mathrm{d}t} = \frac{\mathrm{d}}{\mathrm{d}t}\left(k_x u_y - k_y(t)u_x - \frac{A}{c_s^2}(p - s)\right) = 0. \tag{5.34}$$

The coefficients of these equations are given in the appendix A. Starting from Eqs. (5.32) and (5.33) we use several approximations that simplify farther analysis.
First of all we adopt the small scale approximation:

$$k_z^2 \gg k_H^2, \tag{5.35}$$

or in other words we study perturbations with characteristic vertical length-scales much shorter than the vertical stratification scale of the convection. This approximation strongly simplifies the mathematical analysis and is valid for the following two reasons. Firstly, our analysis needs constant vertical gravity, an assumption that may be adopted for perturbations with vertical height scales shorter than the stratification

scale. Secondly, this approximation is necessary for our assumption of a constant linear shear of the flow velocity, especially in the turbulent flows. This approximation yield the following inequality

$$c_s^2 k_z^2 \gg N_{\mathrm{B}}^2 \tag{5.36}$$

and conditions:

$$\Omega_s^2 \approx \omega_s^2, \tag{5.37}$$

$$\Omega_c^2 \approx \omega_c^2. \tag{5.38}$$

The characteristic physical quantities of the modes are also strongly simplified:

$$\Phi_s(t) \approx p(t), \tag{5.39}$$

$$\Phi_c(t) \approx s(t) - \frac{\bar{k}_z^2}{k^2(t)} p(t) \equiv \psi(t). \tag{5.40}$$

Equations (5.32,33) govern the dynamics of the three modes that are obviously coupled due to the velocity shear of the flow (compare with Eqs. 5.27,28).

In case of convective instability, when exponentially growing aperiodic unstable g-modes are present, vortex modes may not give any noticeable contribution to the global dynamics of the shear flow system. Therefore we neglect the effect of the vortex modes on the unstable g-modes. Coupling of the vortex modes with acoustic modes have been studied in Chap. 3. Therefore we also exclude this effect at the present moment. Hence, for simplicity we exclude the vortex modes by setting the condition of zero initial circulation: $I = 0$.

We may also exclude the effect of the acoustic waves on the spectrally unstable convective modes, by neglecting the effect of the pressure perturbations on the evolution (exponential amplification) of the unstable g-mode perturbations and adopt that $\beta_3(t)\mathrm{d}/\mathrm{d}t\Psi_s \approx 0$ and $\beta_4(t)\Psi_s \approx 0$ in Eq. (5.33).

Hence, with these approximations we can rewrite Eqs. (5.32,33) as follows:

$$\frac{\mathrm{d}^2}{\mathrm{d}t^2} p(t) + \alpha_1(t) \frac{\mathrm{d}}{\mathrm{d}t} p(t) + \alpha_2(t) p(t) = -\alpha_3(t) \frac{\mathrm{d}}{\mathrm{d}t} \psi(t) - \alpha_4(t) \psi(t), \tag{5.41}$$

$$\frac{\mathrm{d}^2}{\mathrm{d}t^2} \psi(t) + \beta_1(t) \frac{\mathrm{d}}{\mathrm{d}t} \psi(t) + \beta_2(t) \psi(t) = 0. \tag{5.42}$$

From the physical point of view we consider free convection in shear flows, which exponentially dominates and affects the acoustic wave mode perturbations.

5.4.1 Dynamics of the convection

The unstable g-mode is described by the Eq. (5.42). The effect of the velocity shear may be understood when Eq. (5.42) is compared with Eq. (5.28) which describes exponentially growing solutions for negative buoyancy $N_B^2 < 0$, when $\omega_c^2 < 0$. To analyze the instability in the sheared case we rewrite Eq. (5.42) in the formally more conventional form:

$$\frac{\mathrm{d}^2}{\mathrm{d}t^2} y(t) + \Lambda(t) y(t) = 0, \tag{5.43}$$

where

$$y(t) = \psi(t) \exp\left(\frac{1}{2} \int \beta_1(t) \mathrm{d}t\right), \tag{5.44}$$

and

$$\Lambda(t) = \beta_2(t) - \frac{1}{2}\left(\beta_1^2(t) + \frac{\mathrm{d}}{\mathrm{d}t}\beta_1(t)\right). \tag{5.45}$$

The stability of the buoyancy perturbations can be determined by the function $\Lambda(t)$. To illustrate the velocity shear effect on the SFH of the convective perturbations we plot $\Lambda(t)$ for different velocity shear rates R as well as for different wave-numbers on Fig. 5.1.
It appears that velocity shear has a stabilizing effect on the convectively unstable modes. Indeed, it turns out that the velocity effect may even change the sign of $\Lambda(t)$ and hence change the character of the evolution of the perturbations from exponential growth to a stable evolution. As illustrated in graph 5.1.a the stabilization increases proportional to the shear parameter and is strongest in the vicinity of the point where $k_y(t) = 0$. The transient character of this phenomenon is evident from the fact that the velocity shear results in a time dependence of the $k_y(t)$: the modes ultimately leave the stability area in wave-number space and become unstable. This effect occurs differently at different wave-numbers. It seems that the stabilization is most profound for SFH with $k_z/k_x > 1$ and is almost suppressed for SFH with $k_z \ll k_x$ (see graph 5.1.b). In short, the velocity shear of the background flow exerts a stabilization effect on the convection depending on the velocity shear rate at particular wave-numbers.

5.4.2 The acoustic waves

The acoustic perturbations are determined by Eq. (5.41) that is the equation of a forced oscillator with inhomogeneous terms that are associated with the velocity shear and the convective modes. The acoustic waves in the absence of the buoyancy perturbations are described by the homogeneous part of this equation. The acoustic wave frequency and amplitude variations are described by the parameters $\alpha_1(t)$ and $\alpha_2(t)$ and were studied previously (see Chapters 2 and 3 for details).

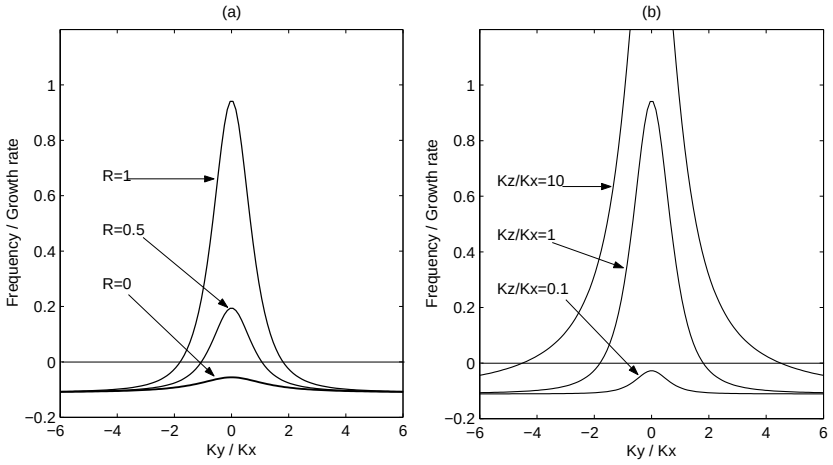

Figure 5.1: Stability parameter of the buoyancy perturbations $\Lambda(\mathbf{k})$ vs. ratio $k_y(t)/k_x$ in the case of thermodynamically unstable flow $\gamma = 0.9$. Graph (a) illustrates the stability parameter for different rates of velocity shear $R = 0,\ 0.5$ and 10 when $k_x = 10$ and $k_z = 10$. Graph (b) illustrates the stability characteristics at different wave-numbers $k_z/k_x = 0.1,\ 1$ and 10 when R=1.

The most interesting aspect here are terms in the rhs (right hand side) of Eq. (5.41) that describe the coupling between the convective and acoustic modes. This coupling implies that acoustic waves can be excited by the buoyancy perturbations. As we have already seen in chapter 3 the excitation of oscillations in such a system may occur even when the source function is regular if the coefficients of the equation are time dependent leading to the existence of non-adiabatic interval. Indeed, the condition for the existence of non-adiabatic interval is fulfilled at times $t = t^*$, when $k_y(t^*) = 0$. Hence this is the point in time when we should expect the excitation of acoustic oscillations by the velocity shear induced coupling to the convective mode.
As we will verify numerically, the convective modes are able to excite acoustic waves at a particular point in time, or in other words at particular wave-numbers depending on the initial wave-numbers of the SFH and the velocity shear parameter.
For a quantitative description of this mode conversion we employ the numerical analysis. Our analytic arguments may still provide us with general qualitative results. The amplitude of the excited wave depends on the values of the parameters of the source terms $\alpha_3(t)$ and $\alpha_4(t)$. Using the approximation (5.39) we may rewrite these coefficients as follows:

$$\alpha_3(t) \approx -2A\frac{k_x k_y(t)}{k_\perp(t)k(t)}, \tag{5.46}$$

$$\alpha_4(t) \approx -2A^2 \frac{k_x^2 k_\perp(t)}{k^3(t)} \left(1 - \frac{k_y^2(t)\bar{k}_z^2}{k_\perp^4(t)}\right). \tag{5.47}$$

So, convective modes with zero streamwise wavenumbers ($k_x = 0$) are not be able to generate acoustic waves at all ($\alpha_3 = \alpha_4 = 0$ when $k_x = 0$). The maximal efficiency of mode conversion occurs at $k_z = 0$, or in a realistic physical approximation (see Eq. 5.35) at $k_z^2 \geq N_{\rm B}^2/c_s^2$. Naturally, acoustic wave emission from convection generally increases when the mean flow shear parameter A increases.
A schematic outline of g-modes in an unstably stratified shear flow is as follows: The SFH of the convective modes with initial wave-numbers that satisfy the condition $k_y(0)/(Ak_x) > 0$ grow exponentially in time before it reaches a transiently stable state and excites the SFH with similar wave-numbers at $k_y(t) = 0$ through mode conversion. As a result the acoustic radiation of convection is fed by the thermal and kinematic energy of the velocity inhomogeneity of the flow. In order to study the conversion of convective modes into the acoustic waves in detail we employ the numerical analysis.

5.5 Numerical analysis

For the purpose of the presentation of the numerical results we introduce dimensionless notations:

$$U_{x,y}(\tau) = c_s u_{x,y}(t), \quad V(\tau) = \frac{v(t)}{c_s k_H}, \tag{5.48}$$

$$P(\tau) \equiv \frac{p(t)}{P_0(0)}, \quad S(\tau) \equiv \frac{s(t)}{P_0(0)}. \tag{5.49}$$

With the use of the non-dimensional time and shear scales:

$$\tau \equiv c_s k_H t, \quad R \equiv \frac{A}{c_s k_H}, \tag{5.50}$$

we normalize the wave-numbers:

$$K_x \equiv \frac{k_x}{k_H}, \; K_y(\tau) \equiv \frac{k_y(t)}{k_H}, \; K_z \equiv \sqrt{\frac{k_z^2}{k_H^2} + \frac{1}{4}}. \tag{5.51}$$

The condition that the perturbations are small scale ($k_z \gg k_H$) is $K_z \gg 1$. Finally, we introduce the normalized buoyancy parameter:

$$\sigma \equiv \frac{N_{\rm B}^2}{c_s^2 k_H^2} = \frac{\gamma - 1}{\gamma^2} \tag{5.52}$$

that describes the stratification of the equilibrium. For a neutral fluid $\sigma = 0$, while positive and negative values of this parameter correspond to a stably and unstably stratified medium, respectively.
We introduce the energy density scale:

$$e = \frac{1}{2}\rho_0(0)c_s^2 E \tag{5.53}$$

and using Eqs. (5.13-16) derive the non-dimensional energy densities of the perturbation SFH:

$$E(\tau) = U_x^2(\tau) + U_y^2(\tau) + \frac{V^2(\tau)}{K_z^2 - \sigma} + P^2(\tau) + \frac{\sigma}{K_z^2 - \sigma}S^2(\tau), \tag{5.54}$$

We also define the compression $\Sigma(\tau)$ as follows:

$$\Sigma(\tau) \equiv \frac{1}{\sqrt{K^2(\tau)}}\left(K_x U_x(\tau) + K_y(\tau)U_y(\tau) + V(\tau)\right). \tag{5.55}$$

where $K^2(\tau) = K_x^2 + K_y^2(\tau) + K_z^2$. For the definition of the vibrational and convective energies of the perturbation we use Eqs. (5.30,31) in the local approximation (using Eqs. 5.35 and 5.36):

$$E_{vib}(\tau) = P^2 + \frac{K^2(\tau)}{\Omega_S^2(\tau)}\Sigma^2 \tag{5.56}$$

$$E_{con}(\tau) = \frac{\sigma}{K_z^2 - \sigma}\left(\Psi^2(\tau) + \frac{1}{\Omega_C^2(\tau)}\frac{\mathrm{d}}{\mathrm{d}\tau}\Psi(\tau)\right). \tag{5.57}$$

where

$$\Psi = S - \frac{K_z^2}{K^2(\tau)}P \tag{5.58}$$

and

$$\Omega_S^2(\tau) = K^2(\tau) - \sigma\frac{K_x^2 + K_y^2(\tau)}{K^2(\tau)}, \tag{5.59}$$

$$\Omega_C^2(\tau) = \sigma\frac{K_x^2 + K_y^2(\tau)}{K^2(\tau)}. \tag{5.60}$$

To illustrate the generation of acoustic waves by convection we present numerical solutions of Eqs. (5.8-12) without any additional assumptions. We choose the initial values of perturbation SFH so that only the convective modes are excited. Vortex modes are excluded rigorously, by choosing perturbations with $I(\mathbf{k}) = 0$, since velocity circulation is a conserved quantity in the shear flow. The acoustic wave modes are filtered in two steps. Firstly, we satisfy $\Psi_s(0) = 0$ condition at initial point of time and secondly, we use a numerical iterative method to reduce acoustic noise level which is due to the deviation of the acoustic variable from

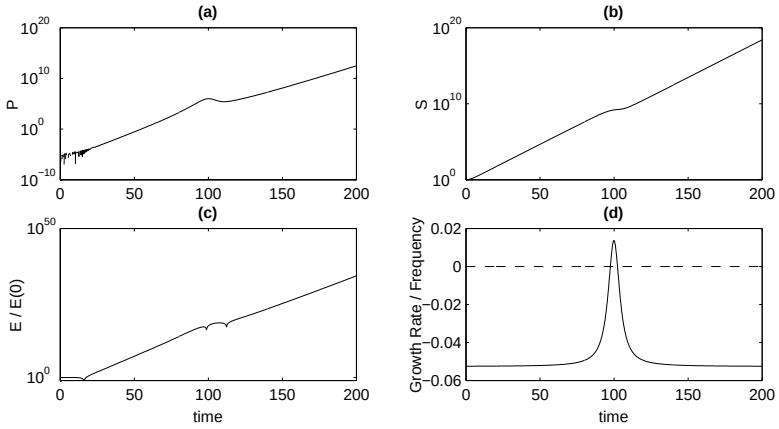

Figure 5.2: Evolution of a buoyancy perturbation in a convectively unstable medium: $\sigma = -0.055$ ($\gamma = 0.95$), $K_x = K_z = 10$, $K_y(0) = 200$ and $R = 0.2$. Pressure $P(\tau)$, Entropy $S(\tau)$ normalized total energy density $E(\tau)/E(0)$ and convective stability parameter $\Lambda(\tau)$ are shown on the a, b, c and d graphs, respectively. Purely buoyancy perturbations are excited initially.

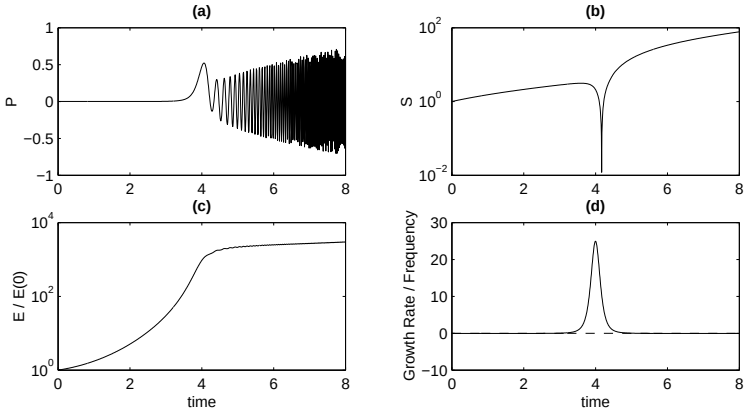

Figure 5.3: Evolution of a buoyancy perturbation in a convectively unstable medium: $\sigma = -0.055$ ($\gamma = 0.95$), $K_x = K_z = 10$, $K_y(0) = 200$ and $R = 5$. Pressure $P(\tau)$, Entropy $S(\tau)$ normalized total energy density $E(\tau)/E(0)$ and convective stability parameter $\Lambda(\tau)$ are are shown on panels a, b, c and d, respectively. Purely buoyancy perturbations are excited initially. Evolution of the pressure perturbations reveal the acoustic wave generation phenomenon. Oscillations are generated at $\tau = 4$, when wave-number along the flow shear is zero $K_y(4) = 0$.

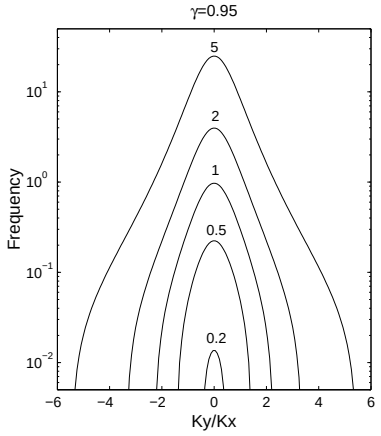

Figure 5.4: Transient stability characteristics of the convective perturbations at different shear rates. Here $\gamma = 0.95$, $K_x = K_z = 10$. Graphs are shown for different shear rates: from the bottom to the top: $R = 0.2,\ 0.5,\ 1,\ 2$ and 5.

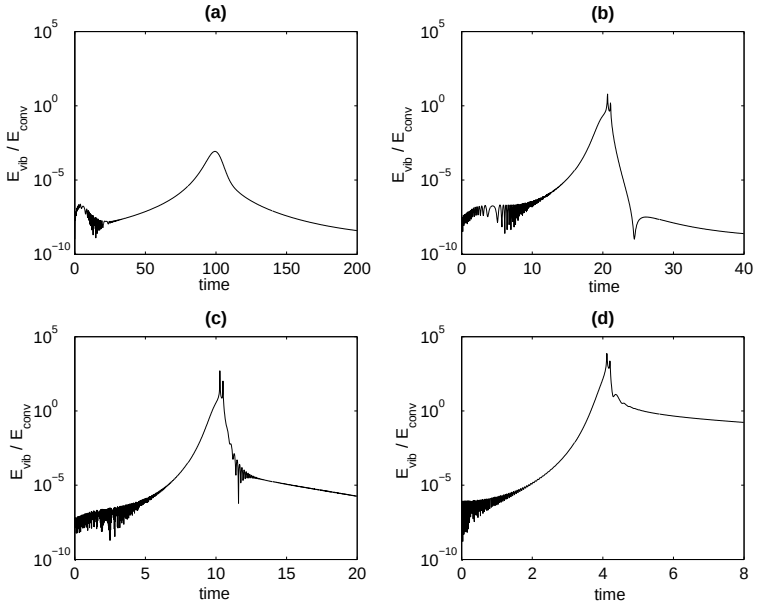

Figure 5.5: The ratio of the vibrational to the thermal energy of the SFH of perturbations (E_{vib}/E_{con}) vs time is shown at different velocity shear rates. Here $K_x = K_z = 10$, $K_y(0) = 200$ and $\sigma = -0.055$ ($\gamma = 0.95$). $R = 0.2, 1, 2, 5$ on the a, b, c and d graphs respectively. The time interval is chosen to show symmetric values of $K_y(\tau)$: $|K_y(0)| = |K_y(2\tau^*)|$ and $K_y(\tau^*) = 0$, where $\tau^* = 100, 20, 10, 4$ on the a, b, c and d graphs, respectively.

its shearless value (Ψ_s). The second step becomes necessary at higher shear rates ($R > 1$).

Fig. 5.2 shows the dynamics of the g-modes in a convectively unstable medium at low mean flow shear. In this case we study weakly unstable medium: $\sigma = -0.055$. The initial perturbations have no contribution from the vortex and acoustic wave modes and the numerical results illustrate the dynamics of the pure buoyancy perturbations. As expected the dynamics of the total energy reveals the transient stabilization effect of the shear flow on the convective instability in the vicinity of $|K_y(\tau)/K_x| < 1$. Pressure and compression perturbations are influenced by the minor variations of the convective mode in the same time interval due to the shear flow.

The dynamics of the buoyancy modes at high values of the shear parameter is shown in Fig. 5.3. The transient stabilization effect is stronger at this shear rate. Fig. 5.3 clearly shows that initially aperiodic pressure perturbations acquire an oscillatory behavior after a certain point in time $\tau = \tau^*$, when the wave-number along the shear axis is zero: $K_y(\tau^*) = 0$. Hence the convective mode is converted into an acoustic wave mode. This fact is also revealed in the evolution of the total energy density of perturbations (see Fig. 5.3).

We plot the frequency of the convective mode perturbations on the Fig. 5.4. The region where the stable state is occurred are plotted at different values of the velocity shear. In this region the definition of the vibrational and thermal energies may not be valid. Obviously, the deviation from the shearless definitions will be maximal for $R = 5$ in the interval $K_y(\tau)/K_x \approx \pm 5.5$, which correspond to the time interval $(\tau^* - 1.1), (\tau^* + 1.1)$ during the evolution of the perturbation SFH. The figure reveals the wave-numbers and corresponding time intervals when the velocity shear effect is most profound, shear induced temporal variation of the system parameters reach its non-adiabatic values and wave-generation phenomena occur. This is the region where the separation of the perturbation mode energies is not valid due to the shear effects.

Fig. 5.5 shows the ratio of the vibrational to the thermal energy densities of modes at different velocity shear rates. Initial values of perturbations are chosen to satisfy the condition: $E_{vib}(0)/E_{con}(0) \simeq 10^{-8}$. The ratio transiently picks and sometimes reaches values higher than 1 at $\tau = \tau^*$, where our definition of the mode energies is not accurate (see Fig. 5.3). Figure reveals the remarkable growth of the vibrational energy compared to the convective one at $\tau = 2\tau^*$, where $K_y(2\tau^*)/K_x = -20$ and the separation of energies of acoustic oscillations and buoyancy perturbations is highly accurate. The excitation of oscillations is evident at higher shear rates when a significant increase of the vibrational energy is revealed. The figure clearly shows that efficiency of the wave excitation increases with the velocity shear rate R. It seems that at $R = 5$ the ratio of the vibrational to the thermal energy saturates ultimately at values as high as 0.2.

It seems that excitation of the acoustic waves by unstable convection becomes profound already at $R = 5$. At $R = 10$ the energy of the excited oscillations becomes equal to the energy of the source – the buoyancy perturbations. At lower shear rates the energy of the excited oscillations may be several orders of magnitude smaller than the energy of the source perturbations. However having in mind amount of energy carried by g-modes in the convection excited acoustic waves may still lead to an important physical consequences.
We have also tested the excitation phenomenon at different wave-numbers of the convective modes. As expected from analytic arguments (see Eqs. 5.46 - 5.47) the process of wave excitation proceeds quite differently at different wave-numbers: wave emission from buoyancy perturbations with mainly vertical wave-numbers ($K_z \gg K_x$) is nearly suppressed even at high shear parameters.

5.6 Discussion

We have found that velocity shear introduces a novel channel of energy exchange between the acoustic waves and the g-modes. Obviously, the process will be an important ingredient for convectively unstable shear flows, where energy accumulated in the buoyancy perturbations and hence the potential sources of acoustic waves are significant. This linear phenomenon indicates that the convection in general is intrinsically "noisy" due to its persistent velocity inhomogeneities that are supported by thermo-mechanic forces. This phenomenon should occur not only in astrophysical flows (high opacity thermally unstable regions of the accretion disks of compact objects, stellar and solar convective envelopes, etc.), but in terrestrial (atmospheric), engineering and other types of the compressible convection. We will concentrate on the solar convection zone that is probably the best studied example of the convection in the astrophysical context.

5.7 Oscillations in the solar convection zone

The subject of solar oscillations is an important problem in solar physics. Several different mechanisms have been suggested to explain the excitation of the solar p-mode oscillations in the convection zone. Lighthill's (1952) classical theory of turbulent sound production has been extended to the convective turbulence by Stein (1967) who has also estimated the acoustic energy flux from the solar convection zone due to the stochastic excitation of oscillations (Stein 1968). Several authors have studied this approach later (see e.g. Goldreich and Kumar 1990, Goldreich and Keele 1997, etc.) which employs the acoustic sources of the stochastic

nature resulting from the turbulent fluctuations of the Reynolds stress in the upper layers of the convection zone. The thermal overstability of the acoustic oscillations in the convection zone that has been proposed by Balmforth (1992a, 1992b) as a major source of acoustic oscillations. Excitation of waves due to the localized cooling events have been described by Rast (1999), who proposed a thermal plume as an acoustic wave source. Other thermodynamic mechanisms include "kappa" and "gamma" mechanisms that operate in the regions where opacity is proportional to a positive power of temperature (κ-mechanism, see Eddington 1941) or where compression increases ionization degree of the gas, rather than the temperature (γ-mechanism, see Cox et al. 1996).

Zhughzda (1998) and Stix et al. (1998) have investigated the dynamics of acoustic waves in a spatially structured medium. They have found that non-radial solar p-modes may be excited as a result of the coupling between vibrations of the cellular convective structures and acoustic waves.

The outer solar envelope is an acoustical cavity that possesses its own characteristic oscillation frequencies. It is not necessary and also highly improbable that acoustic emission sources produce oscillations that exactly match eigenmodes of the Sun. Acoustic oscillations should be excited with different frequencies and wave-numbers depending on the origin of their excitation. Subsequently the nonlinear and dissipative forces cascade energy between the different time and spatial scales to result in 5-minute oscillations on the solar surface.

Here we concentrate on sources rather than the observed frequencies and the global characteristics of the solar oscillations. As we have seen from the linear analysis convection is able to excite acoustic waves due to the velocity shear induced mode conversion phenomenon. Hence we introduce the novel channel of the wave excitation in the solar convection zone. Interplay of the kinematic inhomogeneities and the unstable stratification in the top of the solar convection zone may produce a significant level of acoustic noise due to this linear mechanism. An important motivation for the non-modal study of this phenomenon is that the amplitudes of the solar oscillations are sufficiently small for linear oscillation theory to an excellent approximation (see Hill et al. 1996).

We focus on buoyancy perturbations with characteristic length-scales shorter than the pressure stratification scale: $1/k_H$. Unfortunately we do not have the observational data about the kinematic structure, or any possible velocity gradients with enough spatial resolution to make the direct estimates. The pressure stratification scale at the top of the convection zone is about 130km. Hence, the task is to observe the structure of the solar surface with < 0.1 arcsec spatial resolution, which is not yet achieved. Hence, waves and their convective sources will contribute to the cumulative blurred picture of the unresolved velocities in the present observational data. However, we may still draw a qualitative conclusions

based on properties of the proposed excitation mechanism.

Specific to this phenomenon is that perturbations of buoyancy are able to excite acoustic waves with similar wave-numbers. This property makes it clearly distinct from stochastic excitation, where the generated frequencies are similar to the life-times of the source perturbations. In contrast, the frequencies of the oscillations generated by the mean flow velocity shear induced mode conversion may be qualitatively higher than the temporal variation scales of perturbations in the source flow of a compressible convection. The frequency spectrum of the excited acoustic waves should be intrinsically correlated to the velocity field of the turbulent source flow. Shear flow induced wave excitation in stratified flows offers a natural explanation for the fact, that the solar acoustic oscillation are mainly excited in the high shear regions of the convection, intergranular dark lanes (see Rimmele et al. 1995). It also explains the puzzling wave-number dependence of the observed mode energies at fixed frequencies (see Goldreich et al. 1994 and references therein).

In the investigation of the observable acoustic sources of the sun Strous et al. (2000) have found that the excited acoustic power in the seismic events is linearly proportional to the convective velocity. This should indicate that the acoustic waves are produced by a linear mechanism such as mode conversion and not the stochastic mechanism, where the dependence of the convective velocity and the acoustic power is highly nonlinear.

Finally we note that in the present formalism we have focused on the waves with frequencies higher than the characteristic cut-off frequency for the acoustic waves in the convection zone. Shear flow initiates the qualitative change of the temporal variation scales of perturbations and the excitation of waves that are not trapped in the convective envelope. Hence, this mode conversion presents a new significant contribution into the channel of energy transfer from the dynamically active interior to the atmosphere of the Sun.

5.8 Summary

We have presented a study of compressible convection in shear flows. In particular we have focused on linear small-scale perturbations in unstably stratified flows with constant shear of velocity. The linear character of the system enables us to identify the modes and to study their dynamics individually. We find a mode conversion that originates from the velocity shear of the flow. Exponentially growing perturbations of convection are able to excite acoustic waves. In particular thermal perturbations (perturbations of buoyancy) feed the acoustic radiation with similar wave-numbers. The generated oscillations are spatially corre-

lated with the source flow. This process offers a novel approach to the hydrodynamic problem of the acoustic wave generation.
This process may be an important ingredient of the dynamics of convection in astrophysical context. A particular example is the solar convective envelope. Being responsible for the wave generation in high shear regions of a stratified turbulent flow, this non-resonant phenomenon can contribute to the production of sound in the solar convection zone.

Chapter 6

Dynamics of vortices in differentially rotating flows

6.1 Introduction

In this chapter we present a non-modal analysis of non-axisymmetric perturbations in differentially rotating hydrodynamic flows in a gravitational field. The interest in this problem is twofold. Firstly, flows of this type are common in many astrophysical situations and their analysis might be a key for understanding phenomena in accretion disks. Secondly, it gives us an opportunity to study vortex-wave mode conversion in a medium, where two intrinsically different wave modes are present: sound waves as well as internal gravity-spiral waves.

The physical model, the equilibrium configuration, the equations governing the linear perturbations in local frame and the linear spectrum are outlined in Sec. 1. The conversion of the vortex mode into the gravity-spiral wave mode is analyzed in Sec. 2. Here we also analyze a multiple mode conversion process - the simultaneous excitation of acoustic and gravity-spiral waves. In Sec. 4 we concentrate on the accretion disk dynamics. Here we describe problems in the theory of accretion disks and their stability and present a bypass concept of the transition to turbulence. We analyze 2D and 3D vortex modes and discuss their role in the flow transition scenario. The chapter is summarized in Sec. 5, where the main findings are shortly outlined.

6.2 Physical model and equations

The object under study is a rotating disk flow under gravity. Due to the axial symmetry of the basic flow it is useful to study the problem in cylindrical coordinates. In this coordinates Eqs. (2.1), (2.2) and (2.8) read as follows:

$$\frac{\partial \rho}{\partial t} + \frac{\partial}{\partial r}(\rho V_r) + \frac{1}{r}\frac{\partial}{\partial \phi}(\rho V_\phi) + \frac{\partial}{\partial z}(\rho V_z) = 0, \tag{6.1}$$

$$\frac{\partial V_r}{\partial t} + (\mathbf{V}\cdot\nabla)V_r - \frac{V_\phi^2}{r} = -\frac{1}{\rho}\frac{\partial P}{\partial r} - \frac{\partial \Phi}{\partial r}, \tag{6.2}$$

$$\frac{\partial V_\phi}{\partial t} + (\mathbf{V}\cdot\nabla)V_\phi + \frac{V_r V_\phi}{r} = -\frac{1}{\rho r}\frac{\partial P}{\partial \phi}, \tag{6.3}$$

$$\frac{\partial V_z}{\partial t} + (\mathbf{V}\cdot\nabla)V_z = -\frac{1}{\rho}\frac{\partial P}{\partial z} - \frac{\partial \Phi}{\partial z}, \tag{6.4}$$

$$\left(\frac{\partial}{\partial t} + (\mathbf{V}\cdot\nabla)\right) P = \gamma \frac{P}{\rho}\left(\frac{\partial}{\partial t} + (\mathbf{V}\cdot\nabla)\right)\rho, \tag{6.5}$$

where

$$(\mathbf{V}\cdot\nabla) \equiv V_r\frac{\partial}{\partial r} + \frac{V_\phi}{r}\frac{\partial}{\partial \phi} + V_z\frac{\partial}{\partial z}. \tag{6.6}$$

6.2.1 Equilibrium flow

We consider a differentially rotating flow around a central gravitating object located at $r = z = 0$ with the rotation axis parallel to the z axis: $\mathbf{V_0} = (0, V_{0\phi}, 0)$, with $\mathbf{\Omega} = (0, 0, \Omega(\mathbf{r}))$ and $V_{0\phi} = r\Omega(\mathbf{r})$. In this equilibrium the balances are described by the Eqs. (6.3) and (6.4):

$$r\Omega^2(r) = \frac{1}{\rho_0}\frac{\partial P_0}{\partial r} + \frac{\partial \Phi(\mathbf{r})}{\partial r}, \tag{6.7}$$

$$\frac{1}{\rho_0}\frac{\partial P_0}{\partial z} + \frac{\partial \Phi(\mathbf{r})}{\partial z} = 0. \tag{6.8}$$

We neglect self-gravity and assume that the total gravitational field is equal to that produced by the central object:

$$\Phi(\mathbf{r}) = -\frac{GM}{\sqrt{r^2+z^2}}\ . \tag{6.9}$$

The rotation of the matter follows a Keplerian orbit:

$$\Omega^2(\mathbf{r}) = \frac{GM}{(r^2+z^2)^{3/2}}, \tag{6.10}$$

where G is the gravitational constant and M is the mass of the central object. Substitution of Eqs. (6.9) and (6.10) into Eq. (6.7) yields that

$$\frac{\partial P_0}{\partial r} = 0. \tag{6.11}$$

The centrifugal acceleration is fully compensated by the gravitation in the radial direction and pressure does not depend on the radial coordinate.
For simplicity we consider a locally isothermal equilibrium flow with a constant adiabatic sound speed:

$$c_s^2 = \frac{\gamma P_0}{\rho_0} = \text{const}. \tag{6.12}$$

Here $\gamma \geq 1$, i.e., the flow is convectively stable. Hence, using Eq. (6.12) in (6.8) we derive:

$$\frac{\partial}{\partial z}\ln\rho_0 = -\frac{\gamma}{c_s^2}\frac{\partial \Phi(\mathrm{r})}{\partial z}. \tag{6.13}$$

Further we use the thin disk approximation under constant gravity (see e.g., Ryu and Goodman 1992) and state that the vertical gravitational acceleration is constant, apart from the variation in sign at the $z = 0$ horizontal plane. In this approximation we take the average value of the vertical gravitational acceleration as a constant parameter as follows:

$$\frac{\partial \Phi(\mathbf{r})}{\partial z} = \Omega^2(\mathbf{r})z \approx \mathrm{sgn}(z)g \tag{6.14}$$

and derive the following well known equilibrium state:

$$\frac{P_0(z)}{P_0(0)} = \frac{\rho_0(z)}{\rho_0(0)} = \exp\left(-\frac{|z|}{H}\right). \tag{6.15}$$

$$H = \frac{c_\mathrm{s}^2}{\gamma g}, \tag{6.16}$$

is the vertical stratification scale of the disk flow. Hence, using Eqs. (6.14-16) we may connect the vertical gravitational constant with the rotation rate in the middle plane of the disk:

$$\Omega^2(r,0) = \frac{\gamma g^2}{c_s^2}. \tag{6.17}$$

6.2.2 Linear perturbations in local frame

We use a local non-axisymmetric frame in order to analyze the differentially rotating system. For this purpose we transform the coordinates to the co-rotating frame at the radius $\mathbf{r} = (r_0, 0, 0)$:

$$x \equiv r - r_0, \qquad y \equiv r_0(\phi - \Omega_0 t), \qquad z = z\ . \tag{6.18}$$

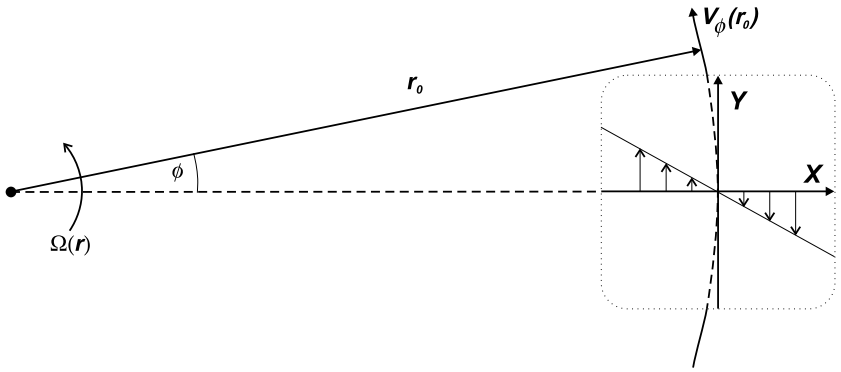

Figure 6.1: Local Cartesian coordinate system with respect to the global cylindrical disk flow shown in the (r, ϕ) plane. The local (X, Y) frame co-rotates with the disk matter at the distance $r = r_0$ with velocity $V_\phi = r_0\Omega(r_0, 0, 0)$. In this frame we neglect the curvature of the flow but retain the effect of the radial differential rotations that is projected in this framework into the plane shear flow.

$\Omega_0 = \Omega(r_0, 0, 0)$ is the rotation rate of the co-rotating frame. We study perturbations with characteristic length-scales shorter than the distance to the central object:

$$\frac{x}{r_0}, \frac{y}{r_0}, \frac{z}{r_0} \ll 1. \tag{6.19}$$

In this limit we neglect the curvature of the flow streamlines, but retain the effect of the radial velocity shear of the background velocity (see Fig. 6.1). We introduce normalized linear quantities so that the vertical height dependence due to the gravity is removed:

$$\mathbf{V} = \mathbf{V}_0 + \frac{\rho(0)}{\rho(z)}\mathbf{V}', \quad P = P_0 + P', \quad \rho = \rho_0 + \rho'. \tag{6.20}$$

Hence, using Eqs. (6.18-20) in Eqs. (6.1-6) we can derive the equations governing the linear perturbations in the local Cartesian frame:

$$\left(\frac{\partial}{\partial t} + 2Ax\frac{\partial}{\partial y}\right) V_x' - 2\Omega_0 V_y' + \frac{\partial P'}{\partial x} = 0, \tag{6.21}$$

$$\left(\frac{\partial}{\partial t} + 2Ax\frac{\partial}{\partial y}\right) V_y' + 2(\Omega_0 + A)V_x' + \frac{\partial P'}{\partial y} = 0, \tag{6.22}$$

$$\left(\frac{\partial}{\partial t} + 2Ax\frac{\partial}{\partial y}\right) V_z' + \frac{\partial P'}{\partial z} + g\rho' = 0, \tag{6.23}$$

$$\left(\frac{\partial}{\partial t} + 2Ax\frac{\partial}{\partial y}\right) \rho' + \frac{\partial V_x'}{\partial x} + \frac{\partial V_y'}{\partial y} + \frac{\partial V_z'}{\partial z} = 0, \tag{6.24}$$

$$\left(\frac{\partial}{\partial t}+2Ax\frac{\partial}{\partial y}\right)P'+c_{\rm s}^2\left(\frac{\partial V_x'}{\partial x}+\frac{\partial V_y'}{\partial y}+\frac{\partial V_z'}{\partial z}\right)+(\gamma-1)gV_z'=0\ . \quad (6.25)$$

$$A\equiv-\frac{1}{2}\left[r\frac{\partial\Omega}{\partial r}\right]_{r=r_0} \quad (6.26)$$

is the Oort's constant which describes the background velocity shear parameter in the local frame. In the case of a Keplerian law of rotation:

$$A=-\frac{3}{4}\Omega_0<0 \quad (6.27)$$

We follow the standard non-modal analysis and we introduce the spatial Fourier harmonics (SFH) of the perturbations with time dependent wavenumbers:

$$\left\{\begin{array}{c}p'(\mathbf{r},t)\\ \rho'(\mathbf{r},t)\\ \mathbf{V}'(\mathbf{r},t)\end{array}\right\}=\left\{\begin{array}{c}p(\mathbf{k},t)\\ \varrho(\mathbf{k},t)\\ \mathbf{u}'(\mathbf{k},t)\end{array}\right\}\exp(\mathrm{i}k_x(t)x+\mathrm{i}k_y y+\mathrm{i}\tilde{k}_z z), \quad (6.28)$$

$$k_x(t)=k_x(0)-2Ak_y t, \quad (6.29)$$

where $\tilde{k}_z\equiv k_z+\mathrm{i}k_H/2$. To avoid complex coefficients in the dynamical equations, we construct the normalized entropy and vertical velocity perturbation SFHs as follows:

$$s\equiv\left(\mathrm{i}c_s^2\tilde{k}_z^*-g\right)\frac{p-c_s^2\varrho}{(\gamma-1)g}, \quad (6.30)$$

$$v\equiv(c_s^2\tilde{k}_z^*+\mathrm{i}g)u_z, \quad (6.31)$$

where $\tilde{k}_z^*=k_z-\mathrm{i}k_H/2$. Substitution of Eqs. (6.28-31) into the (6.21-25) yields the system of ordinary differential equations that governs the SFH of linear perturbations:

$$\frac{\mathrm{d}}{\mathrm{d}t}p(t)=c_{\rm s}^2\left(k_x(t)u_x(t)+k_y u_y(t)\right)+v(t), \quad (6.32)$$

$$\frac{\mathrm{d}}{\mathrm{d}t}u_x(t)=2\Omega_0 u_y(t)-k_x(t)p(t), \quad (6.33)$$

$$\frac{\mathrm{d}}{\mathrm{d}t}u_y(t)=-2(\Omega_0+A)u_x(t)-k_y p(t), \quad (6.34)$$

$$\frac{\mathrm{d}}{\mathrm{d}t}v(t)=\left(N_{\rm B}^2-c_s^2\bar{k}_z^2\right)p(t)-N_{\rm B}^2 s(t), \quad (6.35)$$

$$\frac{\mathrm{d}}{\mathrm{d}t}s(t)=v(t). \quad (6.36)$$

The local approximation is valid for small-scale perturbations, which meet the condition $k_z \gg k_{\rm H}$ in respect to the disk thickness. The conservation of the potential vorticity is described by the following time invariant solution of Eqs. (6.33-37):

$$\mathcal{I} = k_y u_x(t) - k_x(t) u_y(t) - \frac{2(\Omega_0 + A)}{c_s^2} \left[p(t) - s(t) \right]. \qquad (6.37)$$

This in turn indicates that there is a stationary mode in the linear spectrum.

6.2.3 The linear spectrum

The dispersion equation in absence of velocity shear ($A = 0$, using the full Fourier expansion of the variables ($\Psi \propto \exp(i\omega t)$)) is:

$$\omega \left\{ \omega^4 - \left(c_{\rm s}^2 k^2 + 4\Omega_0^2 \right) \omega^2 + c_{\rm s}^2 \left(N_{\rm B}^2 k_\perp^2 + 4\Omega_0^2 \bar{k}_z^2 \right) \right\} = 0 \qquad (6.38)$$

where $4\Omega_0^2$ is a local epicyclic frequency square, $\bar{k}_z^2 = k_z^2 + k_H^2$, $k_\perp^2 = k_x^2 + k_y^2$, $k^2 = k_\perp^2 + \bar{k}_z^2$ and $N_{\rm B}$ is the frequency of Brunt-Väisälä:

$$N_{\rm B}^2 \equiv (\gamma - 1) g^2 / c_{\rm s}^2 > 0. \qquad (6.39)$$

This dispersion equation has three different solutions corresponding to the following modes:

1. a high frequency acoustic wave with

$$\omega_s^2 = \frac{c_s^2 k^2 + 4\Omega_0^2}{2} \left[1 + \left(1 - \frac{4 c_s^2 (N_B^2 k_\perp^2 + 4\Omega_0^2 \bar{k}_z^2)}{(c_s^2 k^2 + 4\Omega_0^2)^2} \right)^{\frac{1}{2}} \right], \qquad (6.40)$$

   or in $k_z \gg k_H$ approximation $\omega^2 \simeq c_{\rm s}^2 k^2$;

2. a low frequency density-spiral wave with

$$\omega_{g\Omega}^2 = \frac{c_s^2 k^2 + 4\Omega_0^2}{2} \left[1 - \left(1 - \frac{4 c_s^2 (N_B^2 k_\perp^2 + 4\Omega_0^2 \bar{k}_z^2)}{(c_s^2 k^2 + 4\Omega_0^2)^2} \right)^{\frac{1}{2}} \right], \qquad (6.41)$$

   or in $k_z \gg k_H$ approximation $\omega^2 \simeq N_{\rm B}^2 \frac{k_\perp^2}{k^2} + 4\Omega_0^2 \frac{\bar{k}_z^2}{k^2}$;

3. a vortex perturbations with

   $\omega = 0$.

The eigenfunction of the vortex mode may be found from Eqs. (6.32-36). Indeed, the stationary solution of this system ($\partial_t \Psi \equiv 0$) is:

$$u_x = -\frac{k_y}{2\Omega_0} p, \quad u_y = \frac{k_x}{2\Omega_0} p, \quad u_z = 0, \quad \rho = \frac{N_{\rm B}^2 - c_s^2 k_z^2}{N_{\rm B}^2} p. \qquad (6.42)$$

Notwithstanding the formal similarity, this vortex mode is different from the vortex mode occurring in a simple not-stratified compressible hydrodynamic flow. The difference is in the topological properties, as well as in the origin of the mode. The perturbations of the present vortex mode are polarized in the flow rotation plane; they are 2-dimensional in the shearless limit ($u_z \to 0$ when $A \to 0$). This mode originates from the combined action of the vertical gravity force and the Coriolis force. In absence of any one of these forces this mode degenerates into a trivial solution of the system. When both forces are absent, the density-spiral wave mode ($g\Omega$ mode) degenerates into the vortex mode that is a key ingredient of turbulence in the simple (plane and non-stratified) hydrodynamic shear flow.

In previous works, the role of this vortex mode has been often underestimated (cf. Dwarkadas & Balbus 1996; Ryu & Goodman 1992, Goodman & Balbus 2001), or it has been confused with fictitious displacements that arise in Lagrangian formalism (see Friedman & Schutz 1978). This mode has also been ignored in the recent paper by Goodman and Balbus (2001), which retains only the wave modes.

Using the solutions of the dispersion equations (6.40) and (6.41) in the system (6.32-36) we may derive the characteristic variables of the perturbation modes in the shearless limit:

$$\Psi_s(t) \equiv p(t) + \frac{\omega_s^2 + N_{\rm B}^2 - 4\Omega_0^2 - c_s^2 k^2}{\omega_s^2 \frac{k_\perp^2}{k^2} - 4\Omega_0^2 \frac{\bar{k}_z^2}{k^2} - N_{\rm B}^2 \frac{k_\perp^2}{k^2}} \left(s(t) - \frac{\bar{k}_z^2}{k^2} p(t) \right) \tag{6.43}$$

$$\Psi_{g\Omega}(t) \equiv (N_{\rm B}^2 - 4\Omega_0^2) \left(s(t) - \frac{\bar{k}_z^2}{k^2} p(t) \right) + \left(\omega_{g\Omega}^2 - N_{\rm B}^2 \frac{k_\perp^2}{k^2} - 4\Omega_0^2 \frac{\bar{k}_z^2}{k^2} \right) p(t) \tag{6.44}$$

Hence, the modes can be studied individually by the following equations:

$$\frac{\mathrm{d}^2}{\mathrm{d}t^2} \Psi_s(t) + \omega_s^2 \Psi_s(t) = 0, \tag{6.45}$$

$$\frac{\mathrm{d}^2}{\mathrm{d}t^2} \Psi_{g\Omega}(t) + \omega_{g\Omega}^2 \Psi_c(t) = 0, \tag{6.46}$$

$$\frac{\mathrm{d}}{\mathrm{d}t} \mathcal{I} = 0, \tag{6.47}$$

Naturally, the velocity shear modifies these modes introducing novel channels of energy exchange between the modes and the background flow, as well as between the modes themselves.

6.3 Dynamics of mode conversion

A flow with a given kinematic shear parameter A results in different shear rates for waves with different wave-lengths. Waves with longer

wave-lengths are more effectively influenced by the velocity shear of the background flow. In Keplerian accretion disks the differential rotation sets a certain shear parameter – in terms of the local frame: $2A = -3\Omega_0/2$. (Here note, that the real shear parameter is $2A$ when A is defined to be Oort's constant.) We may define the effective shear rate for an individual wave mode as follows:

$$R \equiv |2A|/\omega(t^*), \tag{6.48}$$

with the wave frequency taken at time $t = t^*$ when $k_x(t^*) = 0$, and the frequency is minimal and the mode coupling is strongest. We can estimate this efficiency factor by taking the wave frequencies obtained in the shearless limit (Eqs. 6.40,41). For the production of density-spiral waves its value is:

$$\begin{aligned} R_{g\Omega} &= \frac{2|A|}{\sqrt{4\Omega_0^2\frac{k_z^2}{k^2} + N_B^2\frac{k_y^2}{k^2}}} \\ &= \frac{2|A|}{\sqrt{4\Omega_0^2\frac{k_z^2}{k^2} + \frac{\gamma-1}{\gamma}4\Omega_0^2\frac{k_y^2}{k^2}}} \approx \frac{|A|}{\Omega_0} = \frac{3}{4}. \end{aligned} \tag{6.49}$$

For the production of rotational-acoustic waves it is:

$$R_s = \frac{2|A|}{\sqrt{c_s^2(k_y^2+k_z^2) + 4\Omega_0^2}} \simeq \frac{3k_H}{2\sqrt{\gamma(k_y^2+k_z^2)}}. \tag{6.50}$$

The ratio of $R_{g\Omega}$ to R_s is

$$\frac{R_{g\Omega}}{R_s} \simeq \left(\frac{\gamma(k_y^2+k_z^2)}{4k_H^2}\right)^{1/2}. \tag{6.51}$$

In the present problem $k_H/k_z \ll 1$ and hence $R_s \ll R_{g\Omega}$. Hence we can anticipate that mainly density-spiral waves are excited. Our calculations confirm this expectation.

6.3.1 Excitation of the density spiral waves

In order to study the excitation of density-spiral waves due to the vortex-wave mode conversion we numerically analyze Eqs. (6.32-36) with initial values of the perturbations corresponding to purely vortex-modes. The purpose of this analysis is twofold. Firstly, we confirm results obtained in the Boussinesq analysis and secondly, we study the excitation of density-spiral waves in more detail.

Figs. 6.2 show the results of the numerical calculations that demonstrate that vortex mode harmonics are able to excite the density-spiral waves in

the Keplerian shear flow. Transient phenomena occur in both eigenfunctions, acoustic as well as density-spiral waves. However, wave excitation phenomenon is clearly seen at longer times, when established oscillations of the lower wave mode is revealed in the characteristic perturbations of density-spiral waves.
We investigate this process for different initial wave-numbers – different polarizations of the source mode. On Fig. 6.3 we see the interplay of the two non-modal phenomena: the transient amplification of aperiodic perturbations and the wave excitation due to the vortex-wave mode conversion phenomenon. the process of the mode conversion is strongest for the waves with small vertical wave-numbers and is much reduced for high k_z. For higher values of the vertical wave-numbers transient amplification of the vortex mode perturbations is highly reduced, while the mode conversion phenomenon is completely depressed.

6.3.2 Double excitation of acoustic and density-spiral waves

The velocity shear rate allocated with the Keplerian differential rotation is not large enough to significantly affect the acoustic wave modes. Interaction of the acoustic waves with the vortex modes becomes significant on energetic scales at much higher velocity gradients. Here we simulate flows with higher velocity shears than the standard Keplerian gradient having in mind that these situations may occur in particular regions of the disk flows, where high kinematic gradients may be created due to various local effects.
For this purpose we numerically analyze Eqs. (6.32-36) for different shear parameters. The results of the numerical calculations are shown on Fig. 6.4 The initial values of the perturbations are chosen in order to excite only the vortex modes initially. The amplitudes of the excited wave harmonics are significantly different. Obviously, in the considered case the shear rate for the density spiral waves is much higher than that for the acoustic waves at the given shear parameter A. Numerical calculations show that the ratio of the generated wave energies is proportional to the ratio of the effective shear rates, i.e., to the ratio of their frequencies.

6.4 Dynamics of astrophysical disks

Accretion is important for many astrophysical systems, e.g. binary stars, quasars and active galactic nuclei. Possible mechanisms that govern accretion have been schematically understood during the very first years of investigations (Shakura & Sunyaev 1973; Pringle 1981): the inward transport of matter and the outward transport of angular momentum in

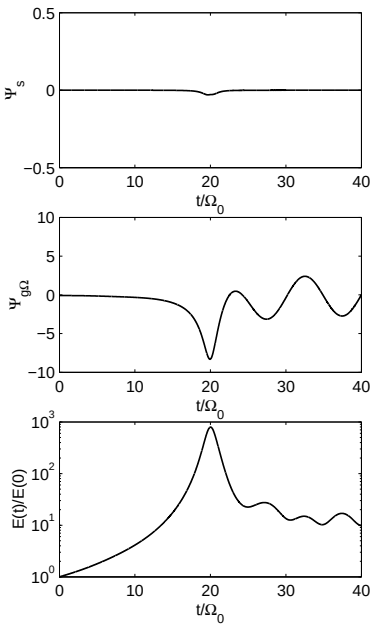

Figure 6.2: Evolution of perturbations in the Keplerian shear flow. Initial values of perturbations correspond to the purely vortex mode perturbations. Here $k_x/k_H = -300$, $k_y/k_H = 10$, $k_z/k_H = 10$, $\gamma = 5/3$ and $R = 3/4$. Figure shows the eigenfunctions of the acoustic $\Psi_s(t)$ and density-spiral $\Psi_{g\Omega}(t)$ waves and total spectral energy of perturbations $E_k(t)/E(0)$ vs the normalized time scale t/Ω_0. Excitation of the density-spiral waves clearly occurs at $t = 10$, when $k_x(10) = 0$.

accretion disks was ascribed to a turbulent (anomalous) viscosity. Substantial progress has been achieved in the nineties with the discovery of a linear instability in magnetized disks (Balbus & Hawley 1991, 1992, 1998; Hawley & Balbus 1991, 1992; Hawley et al. 1995; Stone et al. 1996). In contrast, the investigations of the accretion problem in the non-magnetized case has not yet reached sufficient maturity. Moreover, the very occurrence of turbulence in non-magnetized disks has been questioned by Balbus et al. (1996) and Balbus & Hawley (1998). The reason is that cylindrical flows with a Keplerian profile are smooth shear flows, *i.e.* without any inflection point. It is well known that these flows are spectrally stable, although they may become turbulent in the laboratory. The situation has changed in recent years, with the emergence of the *bypass concept* for the onset of turbulence in spectrally stable flows.

Our approach parallels that of Longaretti (2002), who analyzed the existing experimental and numerical results, and who also insisted, as we shall do here, on the similarity of subcritical shear turbulence in plane and rotating flows.

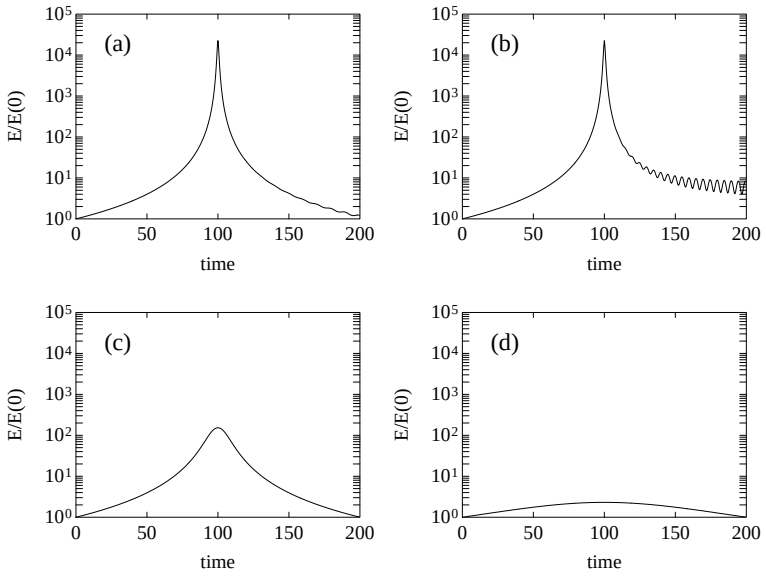

Figure 6.3: Dynamics of the spectral energy densities of the perturbations in the Keplerian shear flows. Initial values of perturbations in all cases correspond to the purely vortex mode perturbations. Here $k_x(0)/k_H = -150$, $K_z = 10$ and $k_z/k_y = 0.01$ on graph a; $k_z/k_y = 0.1$ on graph b; $k_z/k_y = 10$ on graph c and $k_z/k_y = 100$ on graph d.

6.4.1 From spectral decay to transient growth and bypass transition

On the onset of turbulence in spectrally stable shear flows

Some flows are spectrally stable at all Reynolds numbers (e.g. plane Couette or pipe Hagen-Poiseuille flows), while others become spectrally unstable at high enough Reynolds numbers (e.g. plane Poiseuille or Blasius flows). In the latter case the flow is characterized by a critical Reynolds number, such that above this threshold value spectral instability occurs. In this sense the critical Reynolds number of a spectrally stable flow is infinite.

Here we shall consider smooth shear flows (without inflection point in the velocity profile), like in Keplerian disks. These are linearly stable according to classical fluid mechanics. As shown by Rayleigh (1880), the existence of an inflection point (more precisely of a vorticity extremum, as pointed out by Fjørtøft 1950) in the equilibrium velocity profile is a necessary condition for linear (spectral) instability in hydrodynamic flows. Hence, smooth shear flows (flows without a vorticity extremum)

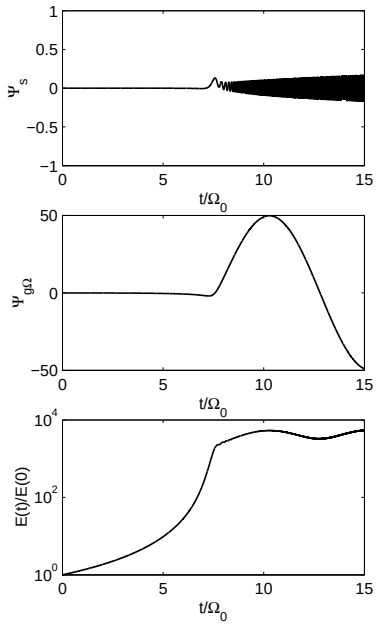

Figure 6.4: Evolution of perturbations in the high shear flow. Initial values of perturbations correspond to the purely vortex mode perturbations. Here $k_x/k_H = -300$, $k_y/k_H = 10$, $k_z/k_H = 10$, $\gamma = 5/3$ and $R = 2$. Figure shows the eigenfunctions of the acoustic $\Psi_s(t)$ and density-spiral $\Psi_{g\Omega}(t)$ waves and total spectral energy of perturbations $E_k(t)/E(0)$ vs the normalized time scale t/Ω_0. The simultaneous excitation of the both wave modes is clearly seen in the evolution of the eigenfunctions of perturbation modes. Note, that the amplitude of the generated density-spiral wave harmonic is much higher than the amplitude of the acoustic wave harmonics.

are "relaxed" in this context. They are spectrally stable and exponentially growing solutions are absent. However, it is well known from laboratory experiments and from numerical simulations that finite amplitude perturbations may cause a transition from laminar to turbulent state at moderate, less than critical Reynolds number.

This has led to the concept of *nonlinear instability* in hydrodynamics (cf. Bayly 1986; Bayly et al. 1988; Herbert 1988; Orszag & Kells 1980; Orszag & Patera 1980, 1983). Until about ten years ago, the predominant view of this laminar-turbulent transition was centered around the slow linear amplification of exponentially growing perturbations (the familiar T-S waves), which modify the flow profile and thereby allow a secondary instability, further nonlinearity and finally a breakdown to turbulent flow. According to this concept of nonlinear instability, the perturbations (and the turbulent state itself) are energetically sustained by nonlinear processes. This concept of nonlinear instability has been borrowed by astrophysicists, who still use it to explain turbulent processes in smooth astrophysical flows, where no spectrally unstable solution is known, and in particular in Keplerian disks flows (see Balbus & Hawley 1998). However, there are subcritical transition phenomena that cannot be attributed to a nonlinear instability.

During the last decade of the 20th century, another viewpoint has emerged in the hydrodynamic community for explaining the onset of turbulence in spectrally stable shear flows, labeled as *bypass transition* (cf. Boberg

& Brosa 1988; Butler & Farrell 1992; Reddy & Henningson 1993; Trefethen et al. 1993; Morkovin 1993; Gebhardt & Grossmann 1994; Henningson & Reddy 1994; Baggett et al. 1995; Waleffe 1997; Grossmann 2000; Reshotko 2001; Chagelishvili et al. 2002; Chapman 2002; Rempfer 2003). Although the bypass transition scenario involves nonlinear interactions – which intervene once the perturbations have reached a finite amplitude – the dominant mechanism leading to these large amplitudes appears to be linear. This concept of onset of turbulence is based on the *linear transient growth of vortex (aperiodic) modes*. The potential for the transient growth has been recognized for more than a century (see Kelvin 1887, Orr 1907a,b). However only recently has the importance of this phenomenon been better understood (cf. Moffatt 1967; Marcus & Press 1977; Gustavsson & Hultgren 1980; Craik & Criminale 1986; Farrell & Ioannou 1993; Reddy & Henningson 1993; Chagelishvili et al. 1997).

The bypass concept implies that the energy extracted by linear transient mechanisms from the basic flow causes an increase of the total perturbation energy during the transition process. The nonlinear terms are conservative and only redistribute the energy produced by the linear mechanisms.

Thus, according to this concept, the transient growth of perturbations (*i.e.* the linear process) is the key element in the transition to turbulence in spectrally stable flows. The importance of this linear process has been stressed in the titles of several seminal papers: Henningson & Reddy (1994) (*"On the role of linear mechanisms in transition to turbulence"*); Baggett et al. (1995) (*"A mostly linear model of transition to turbulence"*) and Reshotko (2001) (*"Transient growth: A factor in bypass transition"*).

On the mechanism of perturbation amplification in spectrally stable shear flows

An investigation of the dynamics of shear flows can be carried out as follows. First introduce perturbations into a mean flow, then linearize of the governing equations, and finally study the dynamics of flow by use of the solutions of the initial value problem (*i.e.* following temporal balances in the flow). In principle this can be done, but in practice it is a formidable task. Instead, the assumptions was adopted that the solution is separable in eigenmodes. The point is then to find the one unstable eigensolution. This method focused attention on the asymptotic stability of the flow and *no attention* was paid to the eigenfunction in a the finite time interval. Indeed, this phase of the evolution was not thought to have any significance. Recently, the early transient phase for the perturbations has been shown to contain "rich" and complicated

behavior leading to different consequences.
It was found in 1990s that smooth shear flows are crowded by processes of mean flow energy extraction by perturbations, energy exchange between perturbations, etc. even in the linear approximation, while according to the classical theory they are spectrally stable and consequently "relaxed." Especially it has been shown that a superposition of decaying normal modes may grow initially, but will eventually decay as time goes on – a new *linear* transient channel of energy exchange between the mean flow and perturbations has appeared. Moreover, it has been shown that transient growth can be significant even for subcritical values of the Reynolds number and that its interplay with nonlinear processes can result in a transition to turbulence without any "nonlinear instability" of the flows.

On the nonorthogonality of linear operators

An exact resonance is not necessary to obtain transient growth. This is the consequence of the non-normal character of the operators that determine the linear perturbations in flows (see, *e. g.* Reddy et al. 1993). The fact that the eigenfunctions of the linearized Navier-Stokes equations are not orthogonal (*i.e.* the operator is non-normal) is sufficient to allow for solutions that exhibit transient growth, depending on the initial conditions, before finally decaying (see Criminale & Drazin 1990; Trefethen et al. 1993). The mechanism of the transient growth is essentially inviscid. The operators are highly non-normal for large Reynolds numbers and the transient growth is asymptotically large in Re. This fact is extremely important in the case of Keplerian accretion disks, where the Reynolds number is literally astronomical: $Re > 10^{10}$!

6.4.2 The similarity between Keplerian flow and plane parallel shear flow

Since our aim is to elucidate the basic similarity of the dynamics of plane shear flows and of Keplerian disks, we approximate the Keplerian flow in the two dimensional (2D) limit by its tangent plane parallel flow, while retaining the effect of rotation through the Coriolis force.
For the present purpose, we consider only 2D perturbations, independent of the axial coordinate z. The resulting linear equations for the perturbations of the radial velocity (u_r), the azimuthal velocity (u_ϕ) and the pressure (p) take the form:

$$\frac{\partial u_r}{\partial t} + Ax\frac{\partial u_r}{\partial y} - 2\Omega_0 u_\phi = -\frac{\partial p}{\partial x} + \nu\Delta u_r, \tag{6.52}$$

$$\frac{\partial u_\phi}{\partial t} + Ax\frac{\partial u_\phi}{\partial y} + 2\Omega_0 u_r + Au_r = -\frac{\partial p}{\partial y} + \nu\Delta u_\phi, \tag{6.53}$$

$$\frac{\partial u_r}{\partial x} + \frac{\partial u_\phi}{\partial y} = 0. \tag{6.54}$$

We have adopted the incompressible limit to leave out the acoustic wave modes and to keep only the vortex modes, which are the basic ingredient of the bypass scenario. In this case the energy density of the perturbation depends only on its kinematic characteristics and not on the thermodynamics, such as pressure.

Pressure terms are also absent when the dynamical equations are written in vorticity form (for $\omega = \mathrm{curl}\,\mathbf{u}$), taking the curl of eqs. (6.52, 6.53). This is probably the reason why the pressure perturbations have been often ignored when discussing the dynamics of shear flows. However they play a very important role, even in the incompressible case, because they are the mediators of momentum exchange between fluid particles, which results in the transient growth of the vortex mode. (The physics of the "mediator activity" of the pressure perturbations is described in detail in Chagelishvili et al. 1993, 1996.) The importance of the pressure terms is clearly seen in the following analysis.

We multiply Eqs. (6.52) and (6.53) respectively by u_r and u_ϕ, in order to put them in kinetic energy form, and average them over a domain which is symmetrical in x. This procedure is similar to that performed by Balbus et al. (1996) and Balbus & Hawley (1998).

$$\frac{\partial}{\partial t}\left\langle \frac{u_r^2}{2} \right\rangle = 2\Omega_0 \langle u_r u_\phi \rangle - \left\langle u_r \frac{\partial p}{\partial x} \right\rangle - \nu \big\langle |\nabla u_r|^2 \big\rangle, \tag{6.55}$$

$$\frac{\partial}{\partial t}\left\langle \frac{u_\phi^2}{2} \right\rangle = -[2\Omega_0 + A]\langle u_r u_\phi \rangle - \left\langle u_\phi \frac{\partial p}{\partial y} \right\rangle - \nu \left\langle |\nabla u_\phi|^2 \right\rangle. \tag{6.56}$$

The source of the instability is the shear term $A\langle u_r u_\phi \rangle$. However, the Coriolis term $2\Omega_0 \langle u_r u_\phi \rangle$ is explicitly present too, and in eq. (6.56) it overbalances the source term, since $A = -3/2\Omega_0$ in the Keplerian disk. Hence, the impression is that the Coriolis force has a strong influence on the shear flow stability, as it has been argued by Balbus & Hawley (1996). This conclusion is contradicted by the fact that the Coriolis terms disappears when summing Eqs. (6.55) and (6.56), meaning that the growth rate of the total kinetic energy is independent of the Coriolis force.

A more detailed analysis shows that the Coriolis terms may be eliminated also on the level of the dynamical equations, by a suitable renormalization of the pressure perturbation. In this two-dimensional and incompressible case, the perturbation velocity field derives from a stream function ψ:

$$u_r \equiv -\frac{\partial \psi}{\partial y}; \qquad u_\phi \equiv \frac{\partial \psi}{\partial x}. \tag{6.57}$$

When we renormalize the pressure perturbation

$$p^R \equiv p - 2\Omega_0\psi, \tag{6.58}$$

we can rewrite Eqs. 6.52–6.54, 6.55 and 6.56 as:

$$\frac{\partial u_r}{\partial t} + Ax\frac{\partial u_r}{\partial y} = -\frac{\partial p^R}{\partial x} + \nu\Delta v_r, \tag{6.59}$$

$$\frac{\partial u_\phi}{\partial t} + Ax\frac{\partial u_\phi}{\partial y} + Au_r = -\frac{\partial p^R}{\partial y} + \nu\Delta v_\phi, \tag{6.60}$$

$$\frac{\partial u_r}{\partial x} + \frac{\partial u_\phi}{\partial y} = 0. \tag{6.61}$$

$$\frac{\partial}{\partial t}\left\langle \frac{u_r^2}{2} \right\rangle = -\left\langle u_r \frac{\partial p^R}{\partial x} \right\rangle - \nu\langle |\nabla u_r|^2 \rangle, \tag{6.62}$$

$$\frac{\partial}{\partial t}\left\langle \frac{u_\phi^2}{2} \right\rangle = -A\langle u_r u_\phi \rangle - \left\langle u_\phi \frac{\partial p^R}{\partial y} \right\rangle - \nu\left\langle |\nabla u_\phi|^2 \right\rangle. \tag{6.63}$$

We have outlined the bypass concept in Cartesian/planar shear flows. Since we wish to apply a similar scenario to differentially rotating disks, we shall write the Cartesian counterparts of the averaged equations for comparison. If y is the streamwise variable, and x is the shearwise variable as in the considered case (i.e., x is analog to r, and y to ϕ), then the equations are:

$$\frac{\partial}{\partial t}\left\langle \frac{u_x^2}{2} \right\rangle = -\left\langle u_x \frac{\partial p^c}{\partial x} \right\rangle - \nu\langle |\nabla u_x|^2 \rangle, \tag{6.64}$$

$$\frac{\partial}{\partial t}\left\langle \frac{u_y^2}{2} \right\rangle = -A^c\langle u_x u_y \rangle - \left\langle u_y \frac{\partial p^c}{\partial y} \right\rangle - \nu\left\langle |\nabla u_y|^2 \right\rangle \ . \tag{6.65}$$

A^c is the shear parameter of the Cartesian flow $U_0^c(0, A^c x)$; u_x, u_y and p^c are the perturbations of velocity and pressure, respectively. If the flow is set up with U_0^c decreasing with x (i.e. $A^c < 0$), then Eq. (6.65) shows that steady flow is marked by transport in the direction of increasing x, as in the Keplerian disk.

These equations are identical to the normalized equations derived above for the Keplerian case, which stresses the similarity of these two flows. However, these equations deal with spatially averaged quantities, and one may wish to establish that the similarity is even more profound, namely that the local kinematics and energy of 2D vortex perturbations of plane and disk flows are the same in time and space, starting from identical initial conditions.

6.4.3 Transient growth in 2D

Mainly for the purpose of illustrating the bypass mechanism, we shall describe now the temporal evolution of an initial perturbation, in two dimensions. We perform a spatial Fourier transform of all relevant variables, as shown here for the pressure fluctuation:

$$p(x,y,t) = \hat{p}(k_x(t),k_y,t)\exp\left[\mathrm{i}k_x(t)x + \mathrm{i}k_y y\right]. \tag{6.66}$$

In a shearing flow, the perturbations cannot keep the form of a simple wave, since the wave-number of each spatial Fourier harmonics (SFH) depends on time (see Criminale & Drazin 1990 for a rigorous mathematical interpretation). In our geometry

$$k_x(t) = k_x(0) - Ak_y t, \tag{6.67}$$

thus the wave-number of each SFH varies in time along the flow shear: it "drifts" in **k**-space. Therefore p in Eq. (6.66) depends on time through $k_x(t)$.
Equations (6.54), (6.55) and (6.56) take the following form in Fourier space:

$$\frac{\mathrm{d}}{\mathrm{d}t}\hat{u}_r(k_x(t),k_y,t) - 2\Omega\hat{u}_\phi(k_x(t),k_y,t) = -\mathrm{i}k_x(t)\hat{p}(k_x(t),k_y,t), \tag{6.68}$$

$$\frac{\mathrm{d}}{\mathrm{d}t}\hat{u}_\phi(k_x(t),k_y,t) + (2\Omega + A)\hat{u}_r(k_x(t),k_y,t) = -\mathrm{i}k_y\hat{p}(k_x(t),k_y,t), \tag{6.69}$$

$$k_x(t)\hat{u}_r(k_x(t),k_y,t) + k_y\hat{u}_\phi(k_x(t),k_y,t) = 0. \tag{6.70}$$

For simplicity, we have ignored the viscous forces. They can be easily incorporated in the analysis later, as we shall see below.
One readily shows that these equations possess a time invariant

$$\mathcal{I} = k_y\hat{u}_r(t) - k_x(t)\hat{u}_\phi(t), \tag{6.71}$$

which expresses the conservation of vorticity in Fourier space. Making use of this invariant, we may write the solution of the system (6.68–6.70) as follows:

$$\hat{u}_r(k_x(t),k_y,t) = \frac{k_y}{k_x^2(t)+k_y^2}\mathcal{I}, \tag{6.72}$$

$$\hat{u}_\phi(k_x(t),k_y,t) = -\frac{k_x(t)}{k_x^2(t)+k_y^2}\mathcal{I}, \tag{6.73}$$

$$\hat{p}(k_x(t),k_y,t) = \frac{\mathrm{i}\left[Ak_y^2 + 2\Omega_0(k_x^2(t)+k_y^2)\right]}{\left[k_x^2(t)+k_y^2\right]^2}\mathcal{I}. \tag{6.74}$$

The perturbed quantities vary aperiodically in time (as is natural for vortex modes), and they undergo transient amplification. Energy is exchanged between the perturbations and the background flow, and this is the basis of the bypass transition scenario. Note that the kinematic characteristics of the perturbations do not depend on the rotation rate Ω_0. They are identical to those of Cartesian shear flows. Only the pressure perturbation depends on Ω_0. Consequently, the energetics of the SFH is identical to that of the Cartesian case:

$$\hat{u}^2(k_x(t),k_y,t) \equiv \hat{u}_r^2(k_x(t),k_y,t) + \hat{u}_\phi^2(k_x(t),k_y,t) =$$

$$= \frac{1}{k_x^2(t)+k_y^2}\mathcal{I}^2 = \hat{u}^2(k_x(0),k_y,0)\frac{k_x^2(0)+k_y^2}{k_x^2(t)+k_y^2} \ . \qquad (6.75)$$

The amplitude of the kinetic energy is maximal for $k_x(t)=0$. Similarly, the renormalized pressure perturbation does not involve Ω_0:

$$\hat{p}^R(k_x(t),k_y,t) = \hat{p}(k_x(t),k_y,t) - 2\Omega_0\hat{\psi}(k_x(t),k_y,t) = \frac{\mathrm{i}Ak_y^2}{[k_x^2(t)+k_y^2]^2}\mathcal{I} \ . \qquad (6.76)$$

This expression is identical to that for the evolution of the pressure perturbation in a Cartesian flow, which proves the similarity of transient growth in both types of flows, in two dimensions.

The above analysis is for an inviscid flow. Accounting for viscosity is a straightforward procedure (see Fridman 1989). It may be done by multiplying the equations by the factor $\exp\left[-\nu\int_0^t \mathrm{d}t'(k_x^2(t')+k_y^2)\right]$. For instance, eq. (6.68) and (6.75) will read as follows:

$$\hat{u}_r(k_x(t),k_y,t) = \frac{k_y\mathcal{I}}{k_x^2(t)+k_y^2}\ e^{-\nu\int_0^t \mathrm{d}t'[k_x^2(t')+k_y^2]} \ , \qquad (6.77)$$

$$\hat{u}^2(k_x(t),k_y,t) = \frac{\mathcal{I}^2}{k_x^2(t)+k_y^2}\ e^{-2\nu\int_0^t \mathrm{d}t'[k_x^2(t')+k_y^2]} \ . \qquad (6.78)$$

To estimate the maximum amplification in this transient growth at $k_y^2 \ll k_x^2(0)$, we assume that the largest perturbation wave-number corresponds to the Kolmogorov dissipation scale: $|k_x(0)|\,r_0 \approx Re^{3/4}$, where the Reynolds number is defined as $Re = \Omega_0 r_0^2/\nu$. Then

$$\frac{\hat{u}^2_{\max}}{\hat{u}^2(k_x(0),k_y,0)} \approx \frac{k_x^2(0)}{k_y^2} \approx \left(\frac{Re}{(k_y\,r_0)^2}\right)^{3/2} , \qquad (6.79)$$

which can reach a huge value in astrophysical disks.

6.4.4 Dynamics of 3D perturbations

We are primarily interested in the transient growth of vortex perturbations in AD and its comparison with a similar process in plane shear flow. Hence we analyze plane shear flow in the same manner. For this purpose we set $g = 0,\ k_H = 0,\ N_B^2 = 0,\ \Omega_0 = 0$ and $A < 0$ in Eqs. (6.32-36). The evolution of vortex mode SFH, in disk flows and plane shear flows, is presented in Figs. 6.5-7 for different ratios of the vertical and azimuthal wave-numbers k_z/k_y: 0.1, 1, 10; in all cases $k_x(0)/k_y = -150$. All calculations for the plane case are carried out with the same kinematic shear parameter. (When comparing the figures, beware that the graphs are not on the same scale.)

The numerical results illustrate the effect of rotation and vertical stratification on the transient growth in Keplerian disks. The quasi-2D vortex modes (i.e. with $k_z \ll k_y$) are amplified by nearly the same factor as in plane shear flow (Fig. 6.5). This amplification is somewhat less in the $k_z \sim k_y$ case (Fig. 6.6), while the transient growth is strongly reduced for vortex modes with $k_z \gg k_y$ (Fig. 6.7).

The calculations also show a novel linear effect which accompanies the evolution of vortex modes in the Keplerian disk, namely the excitation of density-spiral waves ($g\Omega$ modes), which may play an important role in the onset and in the maintenance of turbulence in AD. For a physical description of this excitation we refer to Chagelishvili et al. (1997). The phenomenon is clearly visible on Figs. 6.5-7, in the graphs of u_z, Reϱ and $E(t)/E(0)$. We start with a pure vortex/aperiodic SFH at $k_x(0)/k_y < 0$, then the perturbation energy reaches a peak value at time $t = t^* \equiv k_x(0)/2Ak_y$. After that maximum, the SFH exhibit nearly periodic oscillations, meaning that the vortex mode excites a density-spiral wave corresponding to the same SFH; the result is a mixed vortex-wave SFH.

While the vortex energy steadily decreases after the maximum, as in the 2D case, the wave energy remains constant, and is responsible for the plateau in the $E(t)$ graphs. (In that respect, the disk case bears some similarity with the plane case, where the energy also settles on a plateau.) The plateau energy is more than one order of magnitude lower than the peak energy. For $k_z/k_y = 0.1$ (Fig. 6.5) the peak energy is $2.23 \cdot 10^4$ and plateau energy 10.9 in normalized units. For $k_z/k_y = 1$ (Fig. 6.6) the peak energy is somewhat lower: $2 \cdot 10^4$, whereas that of the plateau is much higher than in the preceding case: $2.95 \cdot 10^2$. This indicates that the excitation of the wave mode is much stronger when $k_z \sim k_y$.

The action of the Coriolis force reduces the rate of transient amplification and it somewhat changes its character in 3D. Consider the case $k_z = k_y$ (Fig. 6.6). In the plane flow, the SFH energy increases transiently,

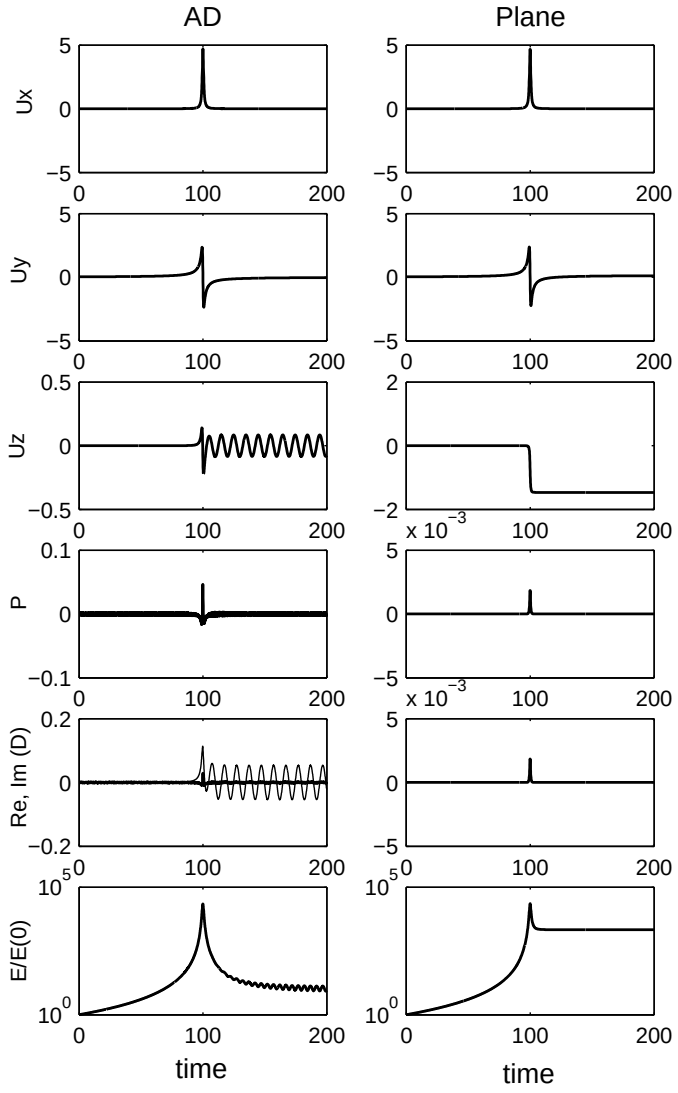

Figure 6.5: Dynamics of the perturbation SFH in the Keplerian disk (left column) and plane shear flow (right column). From the top to bottom: $u_x(t)/(\rho_0 c_s)$, $u_y(t)/(\rho_0 c_s)$, $\tilde{u}_z(t)/(\rho_0 c_s)$, $\tilde{p}(t)/P_0$, $\mathrm{Re}\varrho/\rho_0$ and $\mathrm{Im}\varrho/\rho_0$ (heavy and thin curves, respectively; same in the plane flow) and normalized energy $E(t)/E(0)$ (the latter on logarithmic scale). Here $k_x(0)/k_y = -150$, $k_z/k_y = 0.1$. In the AD case: $k_H/k_z = 0.1$ and $R_s = 0.1 \ll R_{g\Omega} = 3/4$. The initial values of perturbations correspond to the quasi-two dimensional pure vortex mode. The initial value of the spectral energy density is in both cases $E(0)/(\rho_0 c_s^2) = 10^{-3}$.

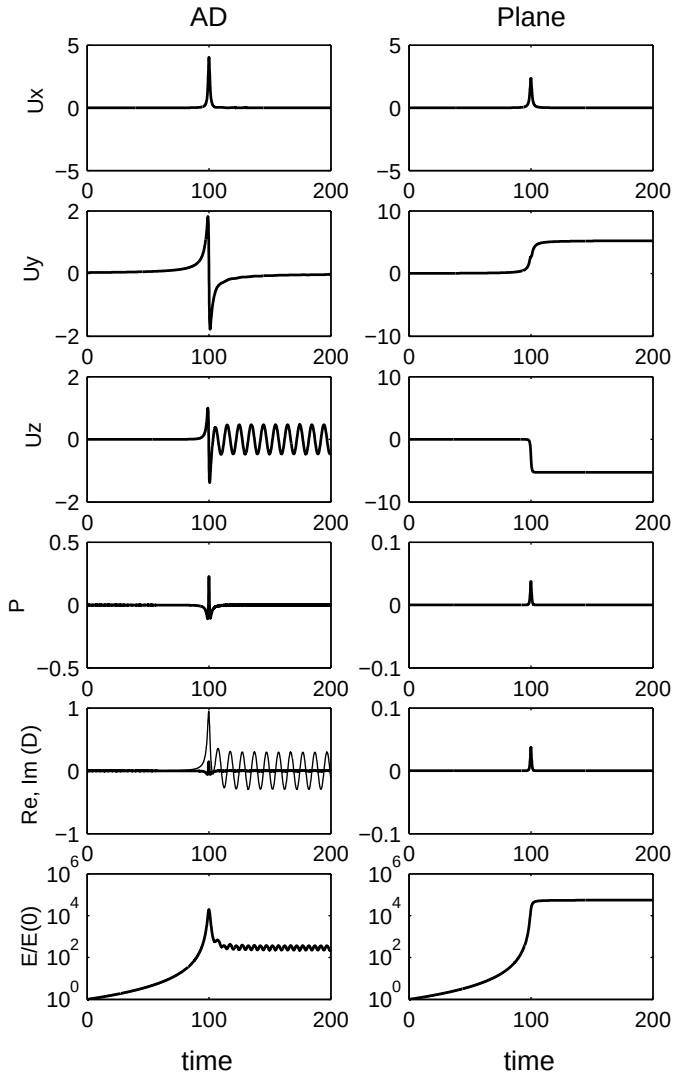

Figure 6.6: The same as in Fig. 6.5, but for $k_z/k_y = 1$. The initial perturbations correspond to the pure vortex mode with equal vertical and azimuthal length-scale.

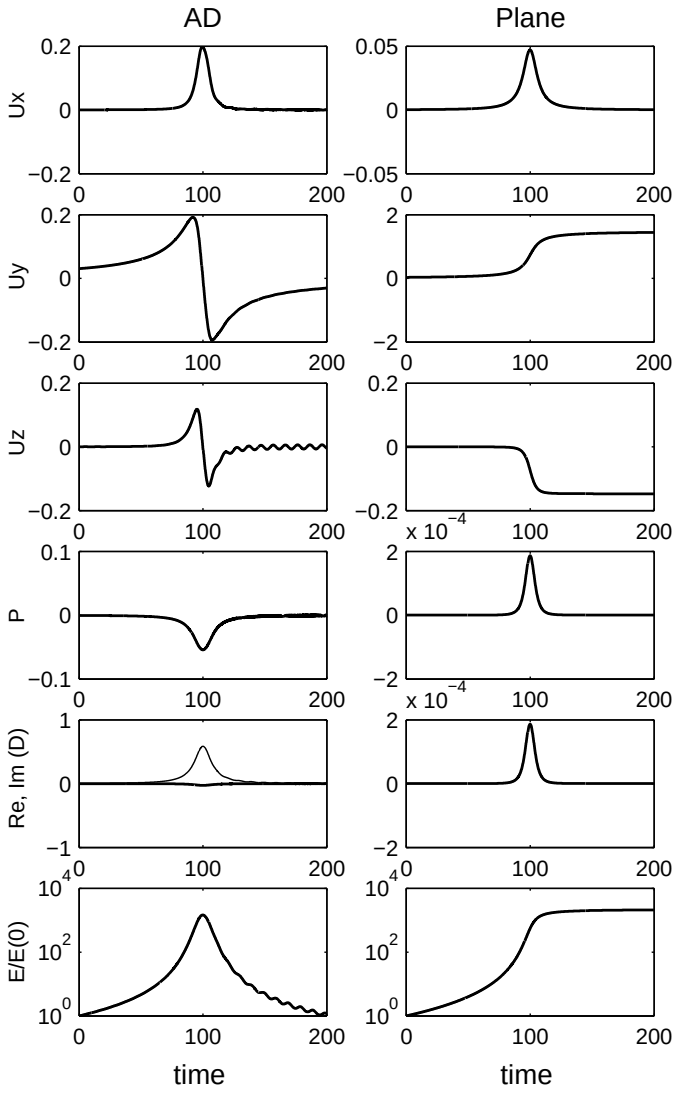

Figure 6.7: The same as in Fig. 6.6, but at $k_z/k_y = 10$. Initial perturbations correspond to the pure vortex mode with length-scales much less in the vertical than in the azimuthal direction.

but tends monotonically and smoothly to some E_{max} when $t \to \infty$ ($k_x(t)/k_y \to \infty$). In the disk case, the SFH energy reaches its peak value E_{peak} at $k_x(t) = 0$, subsequently it decreases, and settles on a plateau with energy E_{plat} after a time where $k_x(t)/k_y \approx 10$. To estimate quantitatively the effect of rotation, we have to compare E_{max} with E_{peak} or/and E_{plat}. These quantities are determined by the values of $k_x(0)/k_y$ and k_z/k_y. A substantial transient growth occurs when k_z is less or of the order of k_y. Let us introduce the parameter

$$\mu \equiv \left(\frac{k_x(0)}{k_y}\right)^2 \tag{6.80}$$

and calculate the dependence of E_{max}, E_{peak}, E_{plat} on μ , for the same $E(0)$ and $k_z = k_y$. The results of our calculations are plotted on Fig. 6.7. The variation of the maximal amplification rate in the plane and AD case is qualitatively the same, and it scales linearly with μ, as was shown in Paper I for 2D perturbations. To reach the same maximal amplification in the disk and plane flows (i.e., $E_{peak} \simeq E_{max}$), the parameter μ is one order of magnitude higher in the disk than in the plane flow. To reach $E_{plat} \simeq E_{max}$, μ ought to be more than two orders of magnitude large. For instance: $E_{max}/E(0) = 2.45 \cdot 10^3$ is reached at $\mu = 10^3$. The same value of $E_{peak}/E(0)$ is attained at $\mu = 2.89 \cdot 10^3$, when $E_{plat}/E(0) = 2.45 \cdot 10^3$ is reached at $\mu = 1.96 \cdot 10^5$ (see Fig. 6.8). Let us analyze these results in terms of the Reynolds number, which we define as

$$R_e = \frac{\Omega_0 H^2}{\nu} \ . \tag{6.81}$$

ν is the kinematic viscosity, and H is the height of the disk (or pressure scale height). The smallest perturbation scale whose transient growth can overcome viscous dissipation can be determined by a local balance between transient growth and viscous dissipation (For details see Chagelishvili et al. 2003.) Thus, it may be determined by the local balance of transient growth term ($2Au_xu_y$) and well known viscous dissipation term ($\nu k^2 u^2$):

$$\nu k^2 u^2 = -2A\, u_x u_y. \tag{6.82}$$

We have seen that optimal growth is achieved when both

$$\mu = \left(\frac{k_x(0)}{k_y}\right)^2 \gg 1 \qquad \text{and} \quad k_y \approx k_z \approx 1/H. \tag{6.83}$$

At $|k_x/k_y| \gg 1$, the vortex mode compressibility is negligible and the velocity field is mainly parallel to the disk plane ($u_z \ll u_x, u_y$). Thus, from the continuity equation it follows that

$$|k_x u_x| \approx |k_y u_y|. \tag{6.84}$$

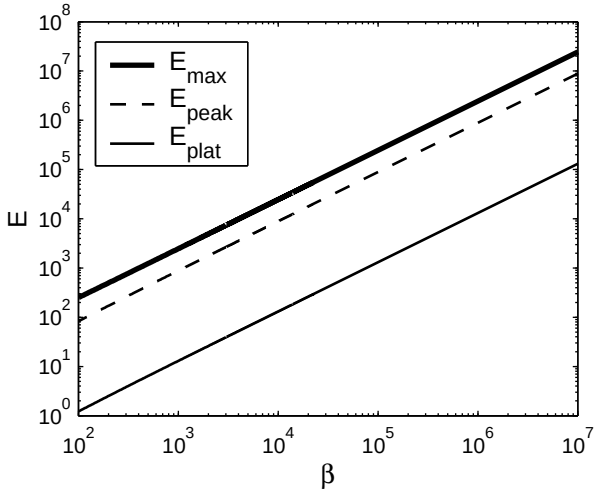

Figure 6.8: Maximum normalized energy E_{max} in the plane case, peak energy E_{peak} and plateau energy E_{plat} in the disk case, vs. $\mu \equiv (k_x(0)/k_y)^2$, for the same $E(0)$ and $k_z = k_y$.

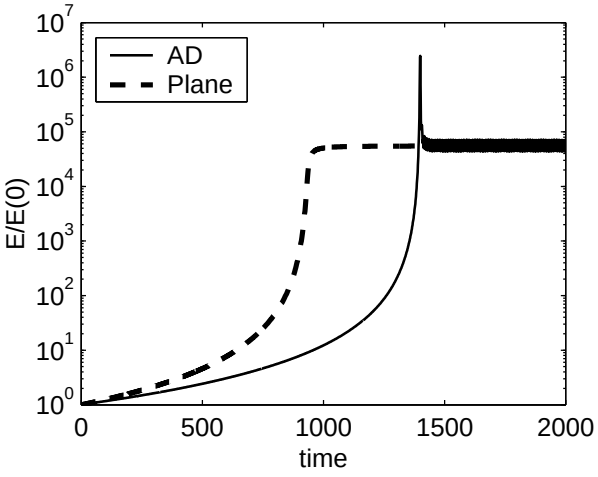

Figure 6.9: $E(t)/E(0)$ vs. t for the Keplerian disk and plane cases for values of μ ($\mu_{plane} = 2.25 \cdot 10^3$ and $\mu_{AD} = 4.41 \cdot 10^6$) at which $E_{max}/E(0) = E_{plat}/E(0) = 5 \cdot 10^4$. In the figure $k_z = k_y$.

Applying these equations to the initial value $k_x = k_x(0)$, we get the following relation between R_e and μ:

$$R_e \approx \mu^{3/2}. \tag{6.85}$$

This permits us to transpose the results given above, namely the amplification factors vs. μ given in Fig. 5, in terms of the Reynolds number Re. For instance, we see that to achieve the same amplification in plane and disk flow (i.e. $E_{max} = E_{plat}$), the Reynolds number must be about three order of magnitudes higher in the disk flow than in the plane flow.

6.4.5 Discussion

We have seen that the theory of the nonlinear stability in smooth spectrally stable shear flows has undergone substantial revision in the hydrodynamic community. Nowadays the concept of *the bypass transition to turbulence* has become popular and is under intensive development.
Let us summarize the main characteristics of this concept:
– the onset of turbulence and the turbulent state itself in smooth spectrally stable shear flows is supported energetically by *the linear transient growth of vortex modes*. The key ingredient of the turbulence are the vortex modes (eddy), and the key phenomenon is the linear transient growth of the perturbation;
– nonlinear processes *do not contribute to any energy growth*, but regenerate vortex modes that are able to extract shear flow energy. Doing so, nonlinear processes only *indirectly* favor the energy extraction by the vortex modes;
– the non-orthogonal nature of the operators in the linearized Navier-Stokes equations is the formal reason of the transient growth;
– the non-orthogonal nature increases with increasing Reynolds number; thus the operators are highly non-normal for the huge Reynolds numbers of Keplerian disks ($Re > 10^{10}$) and the transient growth is asymptotically large in Re.
We aim to contribute to the revival of hydrodynamic shear turbulence as a possible explanation for the "anomalous" viscosity in non-magnetized Keplerian accretion disks. Specifically, we focus on the bypass concept. We showed that in disk flows vortex modes exist that are similar to those which are held responsible for the onset of turbulence in Cartesian shear flow. The key point of our analysis is the important role of the pressure perturbations in the dynamical processes.
In fact, the kinematics and energetics of the vortex modes are identical in the rotating disk and the Cartesian shear flows in the 2D case. The Coriolis force only causes deviation of the pressure perturbations from the Cartesian case. By focusing on the epicyclic motions, and underestimating the action of the pressure terms, one is led to the false conclusion

that the Coriolis force suppresses hydrodynamic turbulence in Keplerian flows (Balbus et al. 1996; Balbus & Hawley 1998).

This property of the pressure perturbations has been established here in the 2D case. In the more general case of 3D perturbations, the dynamics of vortex modes is somewhat more complicated. But the role of the pressure perturbations is still to counteract the Coriolis force. In the 3D disk case, the wave-number domain where the perturbation undergoes transient growth is smaller in comparison to 3D Cartesian flows, but this is compensated by the very large Reynolds number characterizing astrophysical disks.

The promising line leading to the turbulence in hydrodynamic disks have been recently explored in Yecko (2004), Umurhan (2004), Afshordi, Mukhopadhyay and Narayan (2005). All these papers deal with transient amplification of vortical perturbations due to the Keplerian shear flow and study the possibility of the turbulence transition using the Lagrangian and numerical techniques. However, to fill the gap in the turbulence bypass scenario it is necessary to study the processes leading to the nonlinear feedback loop. In this sense the analysis of the mode coupling, the process that is not well appreciated in the above papers, becomes the subject of the primary interest. Analysis of the mode coupling is necessary for understanding of the nonlinear consequences and possible turbulence developed due to the transient growth of linear perturbations.

Other scenarios which may lead to hydrodynamic turbulence in astrophysical disks have been presented recently. They invoke a linear (spectral) instability due to the stratification perpendicular to the disk (Dubrulle et al. 2002) or due to deviations from cylindrical rotation (Urpin 2002; Klahr & Bodenheimer 2002), or due to the baroclinicity of the accretion disk (Klahr 2004, Johnson, Gammie 2005) These instabilities may well compete with the bypass mechanism, and at present it is not possible to conclude which is the best candidate for making astrophysical disks turbulent.

In laboratory experiments the field narrows, because there is no stratification in the fluid (other than imposed on purpose), and there the bypass mechanism provides an attractive explanation for the turbulence detected in flows which are linearly stable (angular momentum increasing outwards). We refer to Couette-Taylor experiments performed by Wendt (1933), Taylor (1936), Coles (1950) and Van Atta (1966). Very recently such turbulence has been observed also in rotation profiles which share the properties of Keplerian disks, namely with their angular velocity decreasing outwards (Richard 2001).

Decisive conclusions about the self-sustenance of the turbulent state need to be supported by numerical simulations. To our knowledge, the simulations reported so far have failed to detect hydrodynamic shear turbulence

in rotating flows with angular momentum increasing outwards. In a recent paper, Longaretti (2002) has discussed the possible explanations of this negative result. The main reason is probably the lack of spatial resolution, which still prevents from reaching even the Reynolds numbers at which turbulence is detected in the laboratory. At this stage, we hope that the analysis presented here will help to build a fruitful background for the nonlinear numerical stability analysis of rotating astrophysical shear flows. In any way, the definite answer will result from the convergence of theoretical, numerical and experimental work.

6.5 Conclusions

In the present chapter we have analyzed differentially rotating stably stratified hydrodynamic disks. Mode conversion is inherent for this type of shear flow. Vortices are able to excite density-spiral and acoustic waves with different amplitudes depending on the velocity shear of the flow. The main attention is on the Keplerian shear flow, which is the usual case for astrophysical disk flows. Let us recall the main results concerning this linear dynamics.

- The stratification of the disk flow (vertical gravity) is necessary for the vortex/aperiodic mode of fluid motion to exist. In the case of rigid rotation ($A = 0$) the vortex mode is characterized by a planar velocity field parallel to the disk plane. At $z \neq 0$ this mode involves vertical velocity perturbations (u_z).

- The vortex mode SFH that satisfy the condition $k_x(0)/k_y < 0$ (as $A < 0$), can transiently be amplified by several orders of magnitude by a linear mechanism. Peak energy is reached at $t = t^*(\equiv k_x(0)/2Ak_y)$. This peak value scales linearly with the parameter $\mu = (k_x(0)/k_y)^2$. It is largest for $|k_z/k_y| \approx 1$, and diminishes rapidly for $|k_z/k_y| \gg 1$;

- After reaching its peak, the vortex mode SFH gives rise to a density-spiral wave of same SFH. Subsequently, the evolution of the vortex and the excited density-spiral wave proceeds independently. Whereas the vortex energy decreases steadily, the wave energy is constant in time. The wave excitation phenomenon is most effective for vortices with nearly equal vertical and azimuthal wave-numbers: $k_z \sim k_y$. In this case, the plateau energy is about two orders of magnitude lower than the peak energy.

- The inhibiting action of the Coriolis force on the transient growth mechanism is not decisive. To reach the same level of amplification

as in parallel shear flow, the vortex mode in the disk flow requires a Reynolds number about 4,000 times higher.

The implications of the present study in the dynamics of accretion disks are discussed. In this context we present the new concept of turbulence in smooth shear flows and analyze the novelties that are introduced to this model by the Coriolis force (rotation).

The transient amplification of vortices, together with the phenomenon of wave excitation by these vortices, appears to be a promising mechanism that leads to the onset of turbulence in astrophysical disks. Namely, these vortex modes fit naturally into the recently developed concept of bypass transition to turbulence for plane smooth shear flows. The detailed description of the concept was presented in Paper 1. Here we only enumerate four basic steps of the bypass scenario:

(i) the linear "drift" of SFH of the vortex mode in the **k**-space;
(ii) the transient growth of SFH;
(iii) viscous dissipation;
(iv) nonlinear processes that close the feedback loop of the transition by mode mixing and angular redistribution of SFH in the **k**-space.

It is important to note that the nonlinear processes do not contribute to the energy growth, as in genuine nonlinear instability, but they close the loop, providing a positive feedback.

In the classical bypass concept, the main contributors to turbulence in shear flows are the vortex modes. However, according to the present study, vortex mode perturbations in Keplerian disks first undergo transient growth and then are converted into density-spiral waves. These waves become ingredients of the system. Hence, most likely, wave-wave nonlinear decay processes should contribute significantly to the nonlinear interactions of step (iv). The latter should be properly accounted for by a turbulence model.

To conclude, the linear phase of the bypass concept is now well established, and this scenario appears as a very promising route to turbulence in Keplerian disks. The positive nonlinear feedback that is required to sustain turbulence remains to be confirmed. This can only be achieved through numerical simulations, performed at high Reynolds number.

Chapter 7

Transformation of waves in MHD shear flows

In previous chapters we have learnt that velocity shear of the background flow induces coupling between the wave, vortex and the unstable modes during their linear stage of evolution. However, the scales of the temporal variation of the modes were qualitatively different for different modes, and the described coupling processes are non-resonant in nature. The intensity of the energy exchange between the coupled modes is controlled by the velocity shear parameter and generally increases with this parameter. This fact indicates that non-resonant mode conversion becomes important in flows with significant velocity inhomogeneities.

In present chapter we analyze mode coupling in shear flows when the frequencies of the coupled waves are similar and direct resonance is possible. The important novelty of the resonant interaction of the wave modes in shear flows is that the intensity of the energy exchange between the waves could depend on how the resonance conditions are realized rather than the increase of the velocity shear rate.

For this purpose we consider linear MHD waves and their resonant interactions in shear flows with a uniform magnetic field (see Chagelishvili et al. 1997). The linear MHD shear flow is described in Sec. 1, where we derive the equations that govern the dynamics of the SFH of the linear perturbations. Linear modes are identified and the corresponding physical variables are derived in Sec. 2. In Sec. 3 we study the velocity shear effects on the MHD wave modes individually, and the effects of their coupling. Here we also describe the mechanical analogy of the shear flow system, which will help us to grasp the physics of the resonant wave transformations. Transformation of the Alfvén and fast magnetosonic waves are analyzed in Sec. 4. Transformation of the Alfvén and the slow magnetosonic waves are analyzed in Sec. 5. Double transforma-

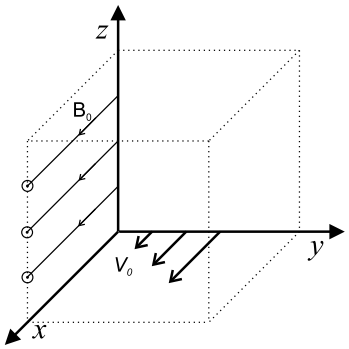

Figure 7.1: Horizontal shear flow $\mathbf{V}_0 = (Ay, 0, 0)$ in the uniform magnetic field directed along the streamlines $\mathbf{B}_0 = (B_0, 0, 0)$, $B_0 = const.$

tions in which all three MHD wave modes can be resonantly coupled are described in Sec. 7. In Sec. 8 we analyze the slow magnetosonic waves when they undergo both, a non-modal amplification and a resonant coupling with the Alfvén waves. We discuss our findings in Sec. 9, where astrophysical implications are discussed. Finally, the chapter is summarized in Sec. 10.

7.1 Mathematical formalism

Let us consider a compressible, unbounded, parallel shear flow with a uniform velocity shear $\mathbf{V}_0 = (Ay, 0, 0)$. The background density ρ_0 pressure P_0 and magnetic field $\mathbf{B_0}$ are constants. The magnetic field and equilibrium flow velocity are parallel $\mathbf{V_0} \parallel \mathbf{B_0}$ (see Fig. 7.1). The linear version of the standard MHD equations (see Eqs. 2.1-5) in this situation is:

$$\left(\frac{\partial}{\partial t} + Ay\frac{\partial}{\partial x}\right)\rho = -\rho_0\frac{\partial v_x}{\partial x} - \rho_0\frac{\partial v_y}{\partial y} - \rho_0\frac{\partial v_z}{\partial z}, \tag{7.1}$$

$$\left(\frac{\partial}{\partial t} + Ay\frac{\partial}{\partial x}\right)v_x = -Av_y - \frac{1}{\rho_0}\frac{\partial p}{\partial x} \tag{7.2}$$

$$\left(\frac{\partial}{\partial t} + Ay\frac{\partial}{\partial x}\right)v_y = -\frac{1}{\rho_0}\frac{\partial p}{\partial y} + \frac{B_0}{4\pi\rho_0}\left(\frac{\partial b_y}{\partial x} - \frac{\partial b_x}{\partial y}\right), \tag{7.3}$$

$$\left(\frac{\partial}{\partial t} + Ay\frac{\partial}{\partial x}\right)v_z = -\frac{1}{\rho_0}\frac{\partial p}{\partial z} + \frac{B_0}{4\pi\rho_0}\left(\frac{\partial b_z}{\partial x} - \frac{\partial b_x}{\partial z}\right), \tag{7.4}$$

$$\left(\frac{\partial}{\partial t} + Ay\frac{\partial}{\partial x}\right)b_y = B_0\frac{\partial v_y}{\partial x}, \tag{7.5}$$

$$\left(\frac{\partial}{\partial t} + Ay\frac{\partial}{\partial x}\right)b_z = B_0\frac{\partial v_z}{\partial x}, \tag{7.6}$$

$$\frac{\partial b_x}{\partial x} + \frac{\partial b_y}{\partial y} + \frac{\partial b_z}{\partial z} = 0. \tag{7.7}$$

We use the adiabatic energy equilibrium, so that:

$$p = c_s^2 \rho \tag{7.8}$$

In order to analyze the temporal evolution of the harmonics we employ a Fourier expansion with "shearing sheet" wave-numbers (see Eq. 2.24):

$$\begin{pmatrix} \rho(\mathbf{r},t) \\ \mathbf{v}(\mathbf{r},t) \\ \mathbf{b}(\mathbf{r},t) \end{pmatrix} = \int \begin{pmatrix} \tilde{\rho}(\mathbf{k},t) \\ \tilde{\mathbf{v}}(\mathbf{k},t) \\ \tilde{\mathbf{b}}(\mathbf{k},t) \end{pmatrix} \exp(\mathrm{i}k_x x + \mathrm{i}(k_y - Ak_x t)y + \mathrm{i}k_z z)\mathrm{d}\mathbf{k} \tag{7.9}$$

Substitution of Eq. (7.9) into Eqs. (7.1) - (7.8) yields a system of ordinary differential equations that describes the perturbation SFH:

$$\frac{\mathrm{d}}{\mathrm{d}t}\frac{\mathrm{i}\tilde{\rho}(t)}{\rho_0} = k_x\tilde{v}_x(t) + k_y(t)\tilde{v}_y(t) + k_z\tilde{v}_z(t), \tag{7.10}$$

$$\frac{\mathrm{d}\tilde{v}_x(t)}{\mathrm{d}t} = -A\tilde{v}_y(t) - c_s^2 k_x \frac{\mathrm{i}\tilde{\rho}(t)}{\rho_0}, \tag{7.11}$$

$$\frac{\mathrm{d}\tilde{v}_y(t)}{\mathrm{d}t} = -c_s^2 k_y(t)\frac{\mathrm{i}\tilde{\rho}(t)}{\rho_0} + V_A^2 \frac{k_x^2 + k_y^2(t)}{k_x}\frac{\mathrm{i}\tilde{b}_y(t)}{B_0} + V_A^2 \frac{k_y(t)k_z}{k_x}\frac{\mathrm{i}\tilde{b}_z(t)}{B_0}, \tag{7.12}$$

$$\frac{\mathrm{d}\tilde{v}_z(t)}{\mathrm{d}t} = -c_s^2 k_z \frac{\mathrm{i}\tilde{\rho}(t)}{\rho_0} + V_A^2 \frac{k_y(t)k_z}{k_x}\frac{\mathrm{i}\tilde{b}_y(t)}{B_0} + V_A^2 \frac{k_x^2 + k_z^2(t)}{k_x}\frac{\mathrm{i}\tilde{b}_z(t)}{B_0}, \tag{7.13}$$

$$\frac{\mathrm{d}}{\mathrm{d}t}\frac{\mathrm{i}\tilde{b}_y(t)}{B_0} = -k_x\tilde{v}_y(t), \tag{7.14}$$

$$\frac{\mathrm{d}}{\mathrm{d}t}\frac{\mathrm{i}\tilde{b}_z(t)}{B_0} = -k_x\tilde{v}_z(t), \tag{7.15}$$

The complex coefficients of the density and magnetic field perturbation harmonics indicate a phase shift of $\pi/2$ with respect to the velocity perturbation harmonics. The longitudinal component of the perturbed magnetic field can be found from the divergence free condition:

$$\tilde{b}_x(t) = -\frac{k_y(t)}{k_x}\tilde{b}_y(t) - \frac{k_z}{k_x}\tilde{b}_z(t). \tag{7.16}$$

The spectral energy density of perturbations may be calculated as follows:

$$E_{kin}(t) = \frac{1}{2}\rho_0 \left(|\tilde{v}_x(t)|^2 + |\tilde{v}_y(t)|^2 + |\tilde{v}_z(t)|^2\right), \tag{7.17}$$

$$E_s(t) = \frac{c_s^2}{2\rho_0}|\tilde{\rho}(t)|^2, \tag{7.18}$$

$$E_{mag}(t) = \frac{\rho_0 V_A^2}{2B_0^2}\left(|\tilde{b}_x(t)|^2 + |\tilde{b}_y(t)|^2 + |\tilde{b}_z(t)|^2\right), \tag{7.19}$$

$$E(t) = E_{kin}(t) + E_s(t) + E_{mag}(t), \tag{7.20}$$

where E_{kin}, E_s, E_{mag} and E correspond to the kinetic, compressible, magnetic and the total energy of perturbations respectively.
Eqs. (7.10) - (7.15) determine the three MHD waves in the shear flow, their individual properties and the possible interactions. However, to get more insight into the wave coupling we first consider the shearless limit.

7.2 Perturbation modes

The linear spectrum in this MHD flow may be readily described in the zero shear limit: $A = 0$. In this limit we may employ the full spectral expansion of the perturbation SFH

$$\begin{pmatrix} \tilde{\rho}(t) \\ \tilde{\mathbf{v}}(t) \\ \tilde{\mathbf{b}}(t) \end{pmatrix} \propto \exp(-\mathrm{i}\omega t) \tag{7.21}$$

and derive the following dispersion equation:

$$\left(\omega^2 - V_A^2 k_x^2\right)\left(\omega^4 - (c_s^2 + V_A^2)k^2\omega^2 + V_A^2 c_s^2 k_x^2 k^2\right) = 0. \tag{7.22}$$

The solutions of this equation are the frequencies of the well known MHD wave modes in a homogeneous medium:

$$\omega_A^2 = V_A^2 k_x^2, \tag{7.23}$$

$$\omega_f^2 = \frac{1}{2}(c_s^2 + V_A^2)k^2\left\{1 + \sqrt{1 - \frac{4V_A^2 c_s^2 k_x^2}{(c_s^2 + V_A^2)^2 k^2}}\right\}, \tag{7.24}$$

$$\omega_s^2 = \frac{1}{2}(c_s^2 + V_A^2)k^2\left\{1 - \sqrt{1 - \frac{4V_A^2 c_s^2 k_x^2}{(c_s^2 + V_A^2)^2 k^2}}\right\}. \tag{7.25}$$

In order to obtain equations for the MHD modes we define the following characteristic variables:

$$\Phi_A(t) \equiv k_y \frac{\mathrm{i}\tilde{b}_z(t)}{B_0} - k_z \frac{\mathrm{i}\tilde{b}_y(t)}{B_0}, \tag{7.26}$$

$$\Phi_f(t) \equiv \frac{\mathrm{i}\tilde{b}_x(t)}{B_0} + \frac{\omega_f^2 - V_A^2 k^2}{V_A^2 k^2}\frac{\mathrm{i}\tilde{\rho}(t)}{\rho_0} \tag{7.27}$$

$$\Phi_s(t) \equiv k_x\tilde{v}_x(t) + \frac{\omega_s^2}{V_A^2k^2}\big(k_x\tilde{v}_x(t) + k_y\tilde{v}_y(t) + k_z\tilde{v}_z(t)\big) \tag{7.28}$$

The three component equations in the shearless limit are:

$$\left\{\frac{\mathrm{d}^2}{\mathrm{d}t^2} + \omega_A^2\right\}\Phi_A(t) = 0, \tag{7.29}$$

$$\left\{\frac{\mathrm{d}^2}{\mathrm{d}t^2} + \omega_f^2\right\}\Phi_f(t) = 0, \tag{7.30}$$

$$\left\{\frac{\mathrm{d}^2}{\mathrm{d}t^2} + \omega_s^2\right\}\Phi_s(t) = 0, \tag{7.31}$$

We are not able to explicitly derive the dispersion equation in the sheared flow, but we may still use the characteristic variables for the description of the wave dynamics.

7.3 Wave transformations

The MHD waves are significantly modified by the background velocity shear. The shear of the flow velocity complicates Eqs. (7.29-31) and introduces coupling terms that describe the interaction of different MHD modes (see Chagelishvili et al. 1996). First we adopt qualitative approach and analyze novelties that may be introduced by the shear flow. As we know, SFH of perturbations drift in the wave-number space. The wave number along the velocity shear is time-dependent: $k_y = k_y(t)$. The wave-numbers determine the frequencies of the MHD waves. Therefore the wave frequencies also vary in time: $\omega = \omega(\mathbf{k}) = \omega(t)$. MHD waves have quite distinctive dispersions, which means that the difference between frequencies of the different wave modes is also time dependent. At particular wave-numbers the difference between frequencies may be sufficiently small for wave resonance to occur.

We illustrate a simple case of possible wave transformations in Fig. 7.2. Let us consider two wave branches with time dependent frequencies $\omega_1^2(t)$ and $\omega_1^2(t)$. We assume that initially we have only one wave (lower branch) in the system. The frequency of the wave SFH varies until it enters the resonance area. When it passes the resonance area it simultaneously resonates with the second wave (upper branch). As a result the initial wave SFH leaves the resonance area weakened – part of its energy is transferred into the second wave SFH. The second wave will be generated with an amplitude that depends on the details of the resonance process.

Resonant transformation of waves has to be reciprocal and symmetric, with equal transformation rates for upward and downward transformation (see Fig. 7.2) at particular parameters of the system. From the

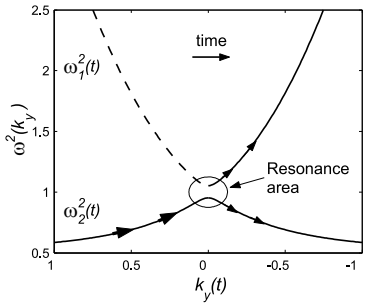

Figure 7.2: Sketch illustration of two wave resonance in the shear flow system. Difference between the wave frequencies is minimal at $k_y(t) = 0$ and the direct resonance occurs. As a result the wave which starts on the lower brunch enters the resonant area and generates the wave of the upper brunch during the limited time interval. After it leaves the resonant area its initial energy will be partially transferred into the upper wave brunch.

physical point of view the transformation of waves will occur in a limited time interval, when frequencies of the MHD waves satisfy the resonance conditions.
With the use of the MHD wave frequencies obtained in the shearless limit (Eqs. 7.19-21) we may derive the necessary conditions for the transformation of waves in unbounded homogeneous MHD shear flows. Using the well known relation between the MHD wave frequencies

$$\omega_f^2 \geq \omega_A^2 \geq \omega_s^2 \tag{7.32}$$

we should seek for mutual transformation of:
(i) Fast magnetosonic and Alfvén waves ($\omega_f^2 \approx \omega_A^2$) when $\beta < 1$ and $k_z/k_x \ll 1$;

(ii) Alfvén and slow magnetosonic waves ($\omega_A^2 \approx \omega_s^2$) when $\beta > 1$;

(iii) fast and slow magnetosonic and Alfvén waves simultaneously ($\omega_f^2 \approx \omega_A^2 \approx \omega_s^2$) when $\beta = 1$ and $k_z/k_x \ll 1$.

We anticipate a mutual transformation of waves when $k_y(t)$ becomes zero, since then the difference between the MHD wave frequencies becomesminimal (see Eqs. 7.23-25). Hence, we may anticipate transformation for the SFH with appropriate wave-numbers ($k_y(0) > 0$ when $A > 0$) to pass through the $k_y(t) = 0$ value in one of the above described cases.
For a more rigorous interpretation of the wave transformations in shear flows we analyze the resonant interaction of the fast magnetosonic and Alfvén waves.

7.3.1 Waves in cold plasmas

In what follows we use the cold plasma approximation and retain only two wave modes. Indeed, for a strongly magnetized plasma $V_A^2 \gg c_s^2$ we

may consider the $\beta = 0$ limit. In this case the linear spectrum and the corresponding physical quantities are:

$$\omega_f^2 \simeq V_A^2 k^2, \quad \Phi_f(t) \simeq \frac{\mathrm{i}\tilde{b}_x(t)}{B_0}, \tag{7.33}$$

$$\omega_A^2 \simeq V_A^2 k_x^2, \quad \Phi_A(t) = k_y \frac{\mathrm{i}\tilde{b}_z(t)}{B_0} - k_z \frac{\mathrm{i}\tilde{b}_y(t)}{B_0}, \tag{7.34}$$

$$\omega_s^2 \simeq 0, \quad \Phi_s(t) \simeq k_x \tilde{v}_x(t). \tag{7.35}$$

To eliminate the aperiodic slow magnetosonic mode we study perturbations with zero longitudinal velocity component: $\tilde{v}_x(t) = 0$. Hence, in this approximation $\Psi_s(t) = 0$ and the dynamics of the fast magnetosonic and the Alfvén waves are described by the following equations:

$$\left\{ \frac{\mathrm{d}^2}{\mathrm{d}t^2} + 2A \frac{k_x k_y(t)}{k_y^2(t) + k_z^2} \frac{\mathrm{d}}{\mathrm{d}t} + \left(V_A^2 k^2(t) + 2A^2 k_x^2 \frac{k_y^2(t) - k_z^2}{(k_y^2(t) + k_z^2)^2} \right) \right\} \Psi_f(t) =$$

$$= -2A \frac{k_z}{k_y^2(t) + k_z^2} \frac{\mathrm{d}\Psi_A(t)}{\mathrm{d}t} - 4A^2 \frac{k_x k_y(t) k_z}{(k_y^2(t) + k_z^2)^2} \Psi_A(t), \tag{7.36}$$

$$\left\{ \frac{\mathrm{d}^2}{\mathrm{d}t^2} + 2A \frac{k_x k_y(t)}{k_y^2(t) + k_z^2} \frac{\mathrm{d}}{\mathrm{d}t} + \left(V_A^2 k_x^2(t) + 2A^2 k_x^2 \frac{k_y^2(t) - k_z^2}{(k_y^2(t) + k_z^2)^2} \right) \right\} \Psi_A(t) =$$

$$= 2A \frac{k_x^2 k_z}{k_y^2(t) + k_z^2} \frac{\mathrm{d}\Psi_f(t)}{\mathrm{d}t} + 4A^2 \frac{k_x^3 k_y(t) k_z}{(k_y^2(t) + k_z^2)^2} \Psi_f(t). \tag{7.37}$$

When we compare these equations with Eqs. (7.29,30) we note that the mean flow velocity shear modifies the MHD waves (see the homogeneous parts of Eqs. 7.36,37) and results in their linear interaction (the inhomogeneous terms of these equations). When the frequencies of these waves are approximately equal a linear resonance occurs. As a result wave modes exchange energy. If only one wave was present before the resonance, then the second one will be generated. Naturally, the details of the transformation process depend on the eigenfrequencies as well as on the values of the coupling coefficients. As it has been shown by Chagelishvili, Rogava and Tsiklauri 1996 transformations of waves in shear flows may be studied in analogy with a model mechanical system. Below we employ the same approach.

7.3.2 Mechanical analogy

We define the following normalized physical variables:

$$\Phi_1(t) \equiv \frac{k_x \Psi_f(t)}{\sqrt{k_y^2(t) + k_z^2}} = \frac{\mathrm{i}k_x \tilde{b}_x(t)}{B_0 \sqrt{k_y^2(t) + k_z^2}}, \tag{7.38}$$

$$\Phi_2(t) \equiv \frac{\Psi_A(t)}{\sqrt{k_y^2(t)+k_z^2}} = \frac{\mathrm{i}k_y(t)\tilde{b}_z(t) - \mathrm{i}k_z\tilde{b}_y(t)}{B_0\sqrt{k_y^2(t)+k_z^2}}, \tag{7.39}$$

and rewrite Eqs. (7.36,37) as follows:

$$\frac{\mathrm{d}^2\Phi_1(t)}{\mathrm{d}t^2} + \omega_1^2(t)\Phi_1(t) = -\mathbf{\Lambda}\Phi_2(t), \tag{7.40}$$

$$\frac{\mathrm{d}^2\Phi_2(t)}{\mathrm{d}t^2} + \omega_2^2(t)\Phi_2(t) = \mathbf{\Lambda}\Phi_1(t), \tag{7.41}$$

where

$$\omega_1^2(t) = V_A^2k^2(t) - \frac{A^2k_x^2k_z^2}{(k_y^2(t)+k_z^2)^2}, \tag{7.42}$$

$$\omega_2^2(t) = V_A^2k_x^2(t) - \frac{A^2k_x^2k_z^2}{(k_y^2(t)+k_z^2)^2}, \tag{7.43}$$

and

$$\mathbf{\Lambda} = \frac{2Ak_xk_z}{k_y^2(t)+k_z^2}\left\{\frac{\mathrm{d}}{\mathrm{d}t} + \frac{Ak_xk_y(t)}{k_y^2(t)+k_z^2}\right\}. \tag{7.44}$$

Equations (7.40,41) describe a mechanical system of two coupled pendulums with varying lengths: $\omega_1^2(t)$ and $\omega_1^2(t)$. The oscillations of the first pendulum $\Phi_1(t)$ correspond to the fast magnetosonic waves. The second pendulum $\Phi_2(t)$ mimics the Alfvén waves. The oscillations are dynamically coupled and $\mathbf{\Lambda}$ is the coupling form. When the frequencies of these pendulums strongly differ from one another then despite of the coupling there is not any noticable energy exchange in between. If the frequencies are close to each other, the coupling becomes important, the pendulums start to exchange energy. When this process occurs there is no clear identification between two oscillatory systems. Therefore this temporal area is called "degeneracy region". Hence we may outline two necessary conditions for effective energy exchange between oscillations (see Chagelishvili et al. 1996):

1. the system should have a the degeneracy region, where

$$|\omega_1^2(t) - \omega_2^2(t)| < \left|\frac{\mathbf{\Lambda}\Phi_i(t)}{\Phi_i(t)}\right|, \tag{7.45}$$

2. the degeneracy region should be crossed slowly:

$$\left|\frac{\mathrm{d}\omega_i(t)}{\mathrm{d}t}\right| \ll \left|\frac{\mathbf{\Lambda}\Phi_i(t)}{\Phi_i(t)}\right|, \tag{7.46}$$

where $i = 1,\ 2$. The existence of the degeneracy region indicates the possibility of a two waves resonance in the system. The second condition

implies that waves should be in resonance long enough to allow energy to be transferred from one branch to another.
Using the approximate form of the derivative: $|\mathrm{d}\Phi_i(t)/\mathrm{d}t| \simeq |\omega_i(t)\Phi_i(t)|$ in Eqs. (7.45-46) we may derive conditions for the existence of the degeneracy region:

$$k_y(t) \simeq 0, \quad |k_z^3| < 2A\frac{|k_x\omega_i(t)|}{V_A^2}. \tag{7.47}$$

We focus on $|\omega_2| < |\omega_1|$. At low shear parameters ($A^2 < \omega_A^2$) the latter equation yields the following condition:

$$\left(\frac{k_z}{k_x}\right)^3 < \left|\frac{2A}{\omega_A}\right|. \tag{7.48}$$

Equation (7.46) is automatically fulfilled at low value of the shear parameter. The transformation of fast magnetosonic and Alfvén waves should occurs for perturbations with mainly horizontal wave-vector. Clearly, Eq. (7.48) verifies the qualitatively derived condition (iii).
To illustrate the transformation we solve numerically Eqs. (7.40,41) for initial conditions exciting only oscillations of the second pendulum: $\Psi_1(0) = \mathrm{d}/\mathrm{d}t\Psi_1(0) = \mathrm{d}/\mathrm{d}t\Psi_2(0) = 0$ and $\Psi_2(0) = 1$. Figures 7.3 and 7.4 show the evolution of the displacements of the pendulums as well as as their derivatives and the total energy and frequencies of oscillations, respectively. A transformation of the oscillations clearly occurs in the time interval when the frequencies are in the degeneracy region, in the vicinity of $t = t^*$, where $k_y(t^*) = 0$. Outside the degeneracy region the oscillations are not coupled and vary only due to the frequency variation. In physical terms this process describes the transformation of the Alfvén into the fast magnetosonic wave mode.

7.4 Numerical analysis

The resonant wave transformations in parallel shear flow are in general studied with the use of numerical computations. We solve Eqs. (7.10-15) for initial conditions that excite only one particular MHD wave SFH.

7.4.1 Transformations of fast magnetosonic and Alfvén waves

In the cold plasma approximation we have already seen that the fast magnetosonic and Alfvén waves can be transformed into one another due to the velocity shear. In this subsection we verify this result when a background flow is present, where the thermodynamic pressure may

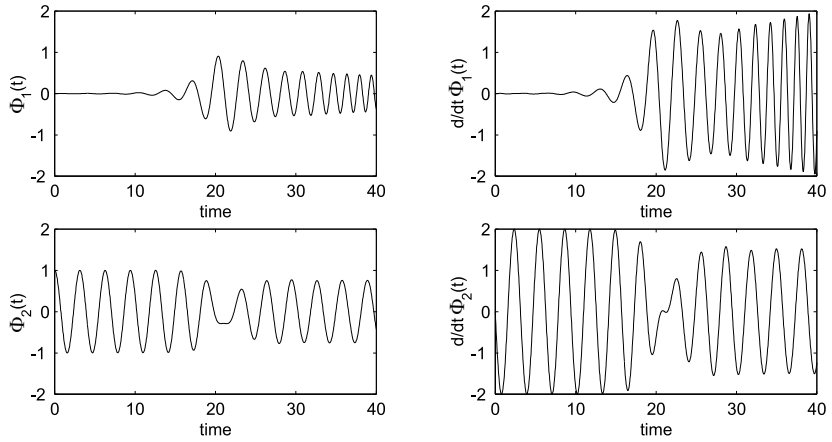

Figure 7.3: Dynamics of the system of the two coupled oscillations. Only the second mode oscillations are present initially. Clearly, the resonance occurs in the vicinity of the $t = 40$. As a result part of energy of the second oscillations is transferred into the first one. In the described example $k_y(0)/k_x = 2$, $k_z/k_x = 0.25$, and $A/(V_A k_x) = 0.025$.

not be neglected and $\beta \neq 0$. We choose initial conditions to excite only Alfvén wave oscillations: $\Phi_f(0) = \mathrm{d}_t\Phi_f(0) = \Phi_s(0) = \mathrm{d}_t\Phi_s(0) = 0$ and $\Phi_A(0) = 1$. Figure 7.5 shows the evolution of the physical quantities and the energy of the perturbations. The energies of the fast magnetosonic and Alfvén wave may be calculated outside the degeneracy region using the following approximate equations:

$$E_f(t) = \frac{\rho_0 v_A^2}{2}\left(\left|\frac{\mathrm{d}\Phi_f(t)}{\mathrm{d}t}\right|^2 + \omega_f^2(t)|\Phi_f(t)|^2\right), \tag{7.49}$$

$$E_A(t) = \frac{\rho_0 v_A^2}{2(k_y^2(t)+k_z^2)}\left(\left|\frac{\mathrm{d}\Phi_A(t)}{\mathrm{d}t}\right|^2 + \omega_A^2|\Phi_A(t)|^2\right) . \tag{7.50}$$

The temporal evolution of the fast wave frequency $\omega_f^2(t)$ is due to the time dependent wave-number $k_y = k_y(t)$ in Eq. (7.24). The energies of the wave modes are plotted on the Fig. 7.6. The transformation of the fast magnetosonic into the Alfvén wave SFH is clearly seen in the evolution of the physical quantities as well as in energy. The wave frequencies identify the existence of the degeneracy region, where the resonance and the wave transformation occur. We can identify several signs of the transformation process:

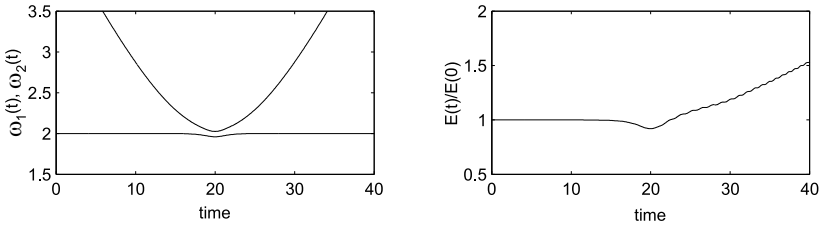

Figure 7.4: Dynamics of frequencies $\omega_1(1)$, $\omega_2(t)$ and the normalized total energy of oscillations. Existence of the degeneracy region at $t \sim 40$ is revealed by the vicinity of frequencies of oscillations. Total energy of oscillations clearly demonstrates the excitation of the higher frequency oscillations - after the degeneracy region energy of the excited oscillations grows proportionally to the frequency of oscillations – $\omega_1(t)$.

Compressibility: Mainly incompressible Alfvénic perturbations generate density oscillations (see D graph in Fig. 7.5).

Polarization: The transverse perturbations that are characteristic for the Alfvén waves (i.e. perpendicular to the magnetic filed: Y and Z directions in our notations) gain longitudinal components after the resonance area (see U_x and B_x graphs in Fig. 7.5).

Frequency variation: The waves have a constant frequency of before the resonance area, while afterwards the frequency increases, just like the frequency of the fast magnetosonic mode (see Fig. 7.5).

Energy variation: The total energy of the perturbation SFH is nearly constant before the resonance area, and it grows nearly proportional to the fast magnetosonic wave frequency afterwards. The wave energies individually clearly demonstrate the transformation phenomenon.

The transformation of the fast magnetosonic into the Alfvén waves is very similar. The energy of the initially generated wave is partially transformed into the second wave during the resonance. Numerical calculations also show that the transformation rate is similar to that of the reverse process. The resonant interaction of these waves exhibit a reciprocal symmetry.
The transformation rate strongly depends on parameters of the system – the relative positioning of the dispersion curves in the resonance area. Complete transformation occurs only when the frequencies of the MHD modes match exactly: i.e. in the $\beta = 0$ approximation for the SFH with $k_z = 0$. In reality the transformation is always partial – both waves remain in shear flow after the resonant interaction. The transformation

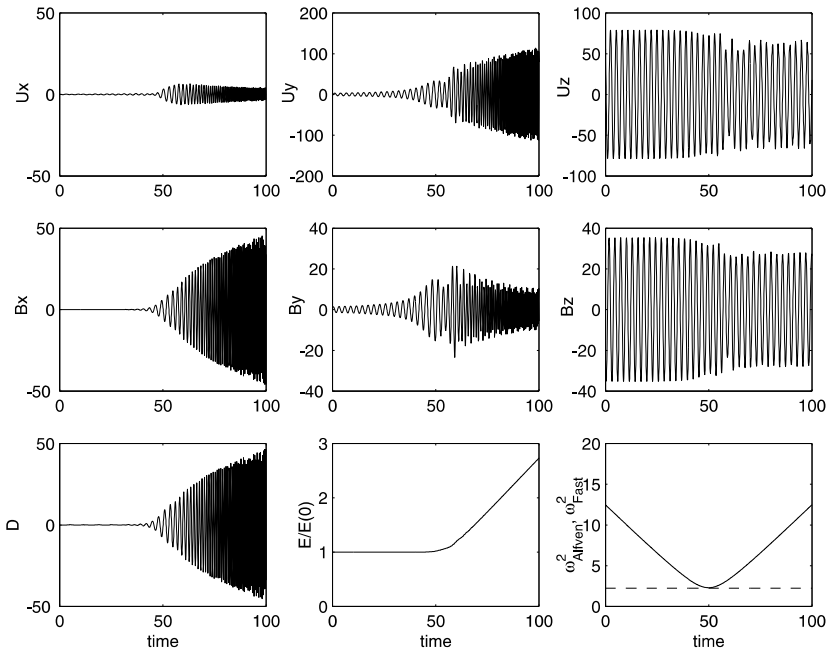

Figure 7.5: Transformation of the Alfvén into the fast magnetosonic wave. Here $A/(c_s k_x) = 0.1$, $\beta = 0.2$, $k_y(0)/k_x = 5$, $k_z/k_x = 0.2$ and initial conditions correspond to the SFH of the purely alfvénic perturbations. Figure illustrates the evolution of the normalized velocity ($\mathbf{U}(t) \equiv \tilde{v}(t)/c_s$), magnetic field ($\mathbf{B}(t) \equiv \mathrm{i}\tilde{b}(t)/B_0$), density ($D(t) = \mathrm{i}\tilde{\rho}(t)/\rho_0$), total energy ($E(t)/E(0)$) and frequencies of the perturbation modes. Dashed is the frequency of the Alfvén wave. Frequencies of oscillations fall into the resonance area in the vicinity of the $t = 50$, where $k_y(50) = 0$. As a result of the two wave resonance part of the energy of the Alfvén wave is transferred into the fast magnetosonic wave. Generated wave exhibits strong compressibility (D), longitudinal variation (U_x, B_x) and the high frequency of oscillations.

of the fast magnetosonic and Alfvén waves is prolonged in time but more efficient for lower shear parameters, while this process weakens at moderate shear rates: $A/(c_s k_x) > 0.2$.

7.4.2 Transformations of slow magnetosonic and Alfvén waves

We investigate the resonant interaction of the Alfvén and slow magnetosonic waves for the system parameters specified in Sec 3. condition (ii). In other words we study the evolution of Alfvén and slow magnetosonic modes individually in plasma flows with $c_s^2 < V_A^2$. Similarly to

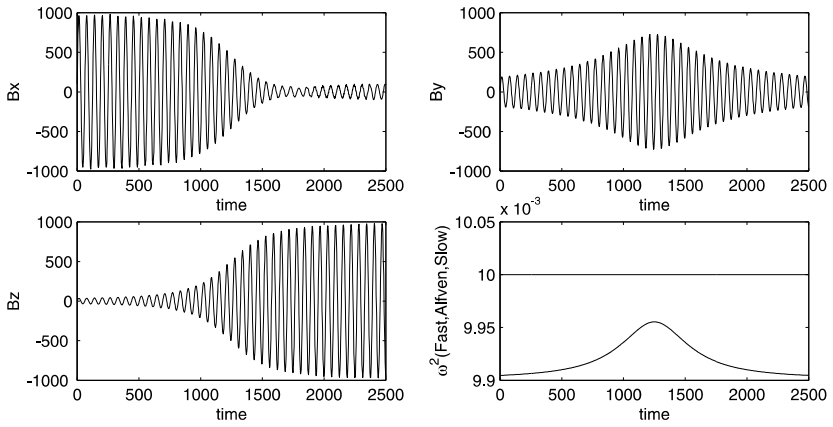

Figure 7.6: Transformation of the slow magnetosonic into the Alfvén wave. Here $A/(c_s k_x) = 0.04$, $\beta = 100$, $k_y(0)/k_x = 5$, $k_z/k_x = 0.9$ and initial conditions correspond to the SFH of the purely slow magnetosonic perturbations. Figure illustrates the evolution of the normalized magnetic field ($\mathbf{B}(t) \equiv \mathrm{i}\tilde{b}(t)/B_0$) and frequencies of the perturbation modes. A significant energy transfer from the slow magnetosonic into the Alfvén wave occurs in the resonance area near $t \sim 1250$ and the longitudinal oscillations of the magnetosonic wave (B_x) generate the transverse Alfvén oscillations (B_z).

the previous problem we choose the initial values of the perturbations using Eqs. (7.26-28). The energy of the slow magnetosonic wave may be calculated with the following approximate expression:

$$E_s(t) = \frac{\rho_0}{2k_x^2}\left(\left|\frac{\mathrm{d}\Phi_s(t)}{\mathrm{d}t}\right|^2 + \omega_s^2(t)|\Phi_s(t)|^2\right), \tag{7.51}$$

The transformation of slow magnetosonic into the Alfvén wave is shown in Fig. 7.6. the generation of the incompressible transverse components together with the mode energies clearly demonstrate the transformation.

7.4.3 Double transformations

Triple transformations can occur when $c_s^2 = V_A^2$. The flat SFH with $k_z = 0$ and $k_y(0) > 0$ falls in the resonance area when $k_y(t) = 0$ and the frequencies of the three MHD modes are exactly equal:

$$\omega_f^2(t^*) = \omega_A^2(t^*) = \omega_s^2(t^*) = V_A^2 k_x^2. \tag{7.52}$$

In this case each MHD mode undergoes a double transformation. We illustrate the double transformations for a less constrained case, when

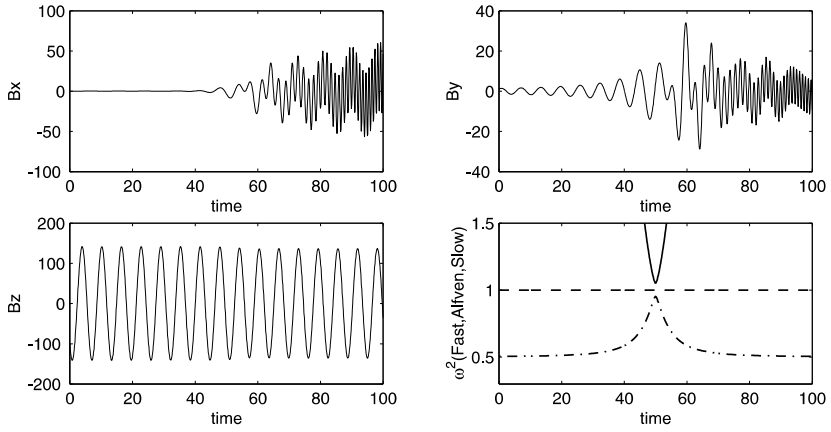

Figure 7.7: The case of the double transformation. Here $A/(c_s k_x) = 0.1$, $\beta = 1$, $k_y(0)/k_x = 5$, $k_z/k_x = 0.05$ and initial conditions correspond to the SFH of the purely Alfvénic perturbations. Figure illustrates the evolution of the normalized magnetic field ($\mathbf{B}(t) \equiv i\tilde{b}(t)/B_0$) and frequencies of the perturbation modes. Solid, dashed and dashed-dotted lines correspond to the fast magnetosonic, Alfvén and slow magnetosonic wave frequencies, respectively. The double excitation of the fast and slow magnetosonic waves occurs in the resonant area, where $t \sim 50$. Generated longitudinal magnetic field (B_x) reveals both, oscillations of the high frequency fast, as well as lower frequency slow magnetosonic wave.

$k_z \neq 0$. For this purpose we chose the Alfvén wave SFH initially and trace its evolution. Numerical solution of this problem is shown in Fig. 7.7, where the evolution of the magnetic field perturbations as well as the variation of the wave frequencies are shown. Clearly, the Alfvén wave resonates with the fast and slow magnetosonic waves simultaneously in the resonance area and a double transformation occurs. The triple point resonance is clearly seen on the graph where the dispersion curves are plotted (see Fig. 7.7).
The three wave resonance occurs for the perturbation SFH with $k_z/k_x \ll 1$ and for low or moderate shear rates: $A/(c_s k_x) \ll 1$.

7.5 Amplification and transformation of slow magnetosonic waves

In this section we look at the transformation of the slow magnetosonic waves into Alfvén waves in a weakly magnetized plasmas: $V_A^2 \ll c_s^2$. The importance of this limit is that together with the resonant interaction of the MHD waves the non-modal mechanism of the transient amplification

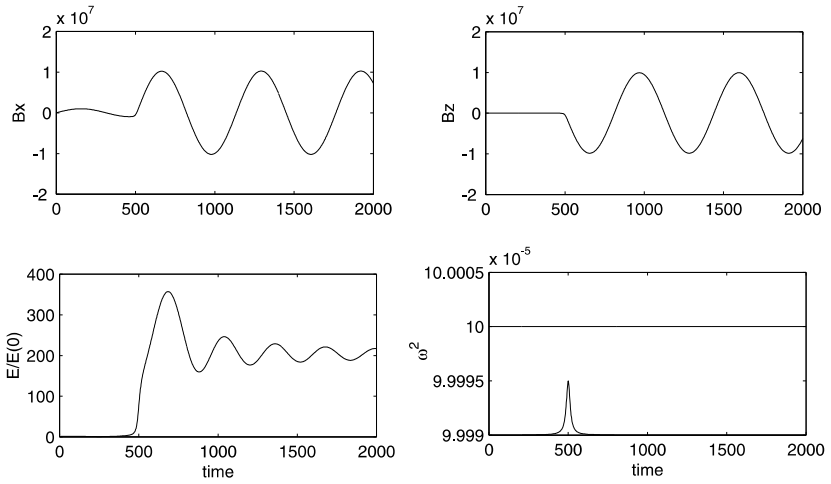

Figure 7.8: Evolution of the initially excited slow magnetosonic wave SFH at the following parameters of the system: $A/(c_s k_x) = 0.1$, $\beta = 10^4$, $k_y(0)/k_x = 50$ and $k_z/k_x = 1$. Figure illustrates the evolution of the normalized magnetic field ($\mathbf{B}(t) \equiv \mathrm{i}\tilde{b}(t)/B_0$), Total energy of perturbations and frequencies of the perturbation modes. Slow magnetosonic wave is amplified by several orders of magnitude as well as partially transformed into an Alfvén waves.

of perturbation may be at work. Conditions for the slow magnetosonic wave to be amplified transiently by the background velocity shear is that it should be aperiodic on the shearing time scales. In other words the slow magnetosonic wave should not oscillate during the time interval when the effective shearing occurs. This yields the following condition:

$$\frac{1}{\omega_s^2(t)} > \frac{1}{A^2}. \tag{7.53}$$

If the condition (7.53) is fulfilled, then in the vicinity of $k_y(t) \sim 0$ the momentum exchange between the vortical velocity field of the slow magnetosonic wave and the background shear flow will be intrinsically anisotropic and transient non-modal growth will occur. The numerical solution of Eqs. (7.10-15) for a weakly magnetized plasmas ($\beta = 0.01$) and an initially excited slow magnetosonic wave is shown on Fig. 7.8. This figure demonstrates that a significant non-modal growth occurs at $t \sim 500$. When together with the amplification of the slow magnetosonic waves, it is simultaneously transformed into the Alfvén wave (see oscillations of the transverse magnetic filed perturbations B_z). As a result both, slow magnetosonic and Alfvén waves are generated and amplified.

7.6 Discussion

The transformation of waves in MHD shear flows presents a novel channel for resonant energy exchange between modes. This process might have important consequences in many astrophysical situations.

An interesting example is solar MHD flows, which exhibit strong spatial inhomogeneities. Wave transformations may play an important role in the energy transfer trough the solar atmosphere also (see Poedts et al. 1999). Important are modifications to the solar wind dynamics (see Poedts et al. 1998).

The influence of a magnetically structured medium on the coupling and the resonant transformation of the MHD waves have been described in Rogava et al. 2000. It appears that the magnetic flux tubes leave their imprints on the wave transformation phenomenon.

Even more tempting is the example of galactic plasma flows, where the evolution of the spiral MHD waves is directly observable. In this case it should be possible to directly identify the reciprocal transformation of MHD waves (see Rogava et al. 1999, Poedts et al. 2002).

An exotic plasma with velocity inhomogeneity was considered in Mahajan et al. 1997. It is proposed that resonant wave transformations may play a key role in the formation of the pulsar radio emission.

Terrestrial plasma should exhibit similar features. The possibility of wave transformations in the ionosphere have been demonstrated by Rogava et al. 1997, Didebulidze 1997.

The Analysis described in the present chapter concerns the simplest possible velocity shear. The picture of the resonant interaction of waves should be modified when the flow velocity has a more complicated inhomogeneity. Effects introduced by the kinematic complexity of the velocity inhomogeneity are considered in Rogava et al. 2001.

Analytic study of the MHD wave transformations in shear flows can be found in Gogoberidze et al. 2005. With the use of asymptotic analysis authors have obtained the wave coupling coefficients for two-wave processes and have described the swing amplification of waves in terms of the wave over-reflection phenomenon.

In the above mentioned literature as well as in the present chapter the effect of the wave transformations are illustrated qualitatively in the wave-numbers space. First complex simulations (DNS) of this process have been worked out by Bodo et al. 2001, where the spatial appearance of the resonant transformations in the 2D MHD shear flows have been investigated.

7.7 Summary

We have described the linear resonant interactions of the MHD wave modes in a flow with sheared velocity. We have shown that a reciprocal transformation of the MHD wave modes may occur symmetrically. Depending on the wave-numbers, the mutual transformation of Alfvén and fast magnetosonic waves is possible in strongly magnetized plasmas. Transformations of the Alfvén and the slow magnetosonic waves are expected in weakly magnetized plasmas. Plasmas with equal magnetic and thermal pressure ($\beta = 1$) may exhibit transformations of all three MHD waves simultaneously.

An important property of the described phenomenon is that it is resonant by nature. In contrast to the mode conversion phenomenon described in Chapters (3-6) the amplitude of waves generated during the transformations do not generally grow with the growth of the shear parameter. In addition the existence of the resonance and an effective energy exchange between the MHD wave modes requires low values of a shear parameters. Finally we note that the transformations due to the velocity shear qualitatively differ from the well-known transformation of waves induced by the spatial inhomogeneities of the background pressure, density or magnetic field. These processes have a different evolution in space and time. Transformation of waves in shear flows occur in a definite time interval, depending on the perturbations themselves all over the spatial domain. The non-kinematic inhomogeneities couple waves at locations of their existence while the process may occur continuously in time.

Chapter 8

Summary

This thesis has concentrated on a non-modal analysis of flows with velocity inhomogeneities. Various astrophysical applications have been considered.

In Chapter 2 we have studied a simple shear flow in order to demonstrate the non-modal method as well as basic properties of flows with inhomogeneous velocity fields. We illustrated the mathematical formalism on a parallel flow with a constant linear velocity shear. The effect of the shearing background on the different types of modes was demonstrated separately.

In Chapter 3 we studied linear mode conversion and sound production in uniform shear flows. The flows under consideration were two dimensional, planar, inviscid, unbounded, and had uniform density/pressure and constant shear of velocity. We studied the aerodynamic production of acoustic waves in inhomogeneous hydrodynamic flows. A qualitative analysis of the wave excitation amplitudes in wave-number space are followed by direct numerical simulations on the vortex package dynamics in shear flows. We have derived the formalism for the separation of linear modes in flows with constant velocity shear. Hence, we carried out numerical analysis to study the wave generation and confirm the theoretical results obtained with the non-modal method.

In Chapter 4 we have extended the theory of Chapter 3 to the MHD waves. We have studied 2D linear perturbations in 3D unbounded ideal MHD shear flows. In this case the linear spectrum consists of the magnetosonic wave mode and two aperiodic modes with zero frequency. These modes are a vortex mode with intrinsic vortical perturbations and a magneto-mechanical mode which has transient vortical characteristics in the sheared medium. Both aperiodic modes are able to excite magnetosonic waves with similar wave-numbers when the wave-number in the direction of the velocity shear becomes zero. It turns out that the

vortex modes are the main source of the waves in flows with weak or moderate magnetic fields. The magneto-mechanical mode may generate more waves in strongly magnetized plasma for stronger velocity shear.

In Chapter 5 we have studied compressible convection in shear flows. In particular we have focused on linear small-scale perturbations in unstably stratified flows with constant shear of velocity. We have found that the mode conversion originates from the velocity shear of the flow. Exponentially growing perturbations of convection are able to excite acoustic waves. At particular wave-numbers g-mode perturbations (perturbations of buoyancy) feed the acoustic radiation of the turbulent convection. The generated oscillations are spatially correlated with the source flow. These process may be important for convection in astrophysical objects. We discussed the solar convective envelope as an example. Generating waves in high shear regions of a stratified turbulent flow, this non-resonant phenomenon can contribute to the production of sound in the solar convection zone.

In Chapter 6 we have investigated non-axisymmetric perturbations in differentially rotating hydrodynamic flows in a gravitational field. The aim here was twofold: Firstly, shear flows commonly occur in many astrophysical situations and they are thought to be the key to the explanation of accretion disk phenomena. Secondly, it gives us an opportunity to study vortex-wave mode conversion in a medium, where two intrinsically different wave modes are present: sound waves as well as internal gravity-spiral waves.

We found that vortices are able to generate gravity-spiral waves in flows with Keplerian shear. Higher shear rates are necessary to trigger the double excitation of density spiral and acoustic waves.

We have analyzed the dynamics of accretion disks and based on our results promote the hydrodynamic model of the turbulence. Firstly, we describe the general balances in the rotating disk flows in 2D and show that the stabilizing effect of the Coriolis force can be overcome by a substantial increase of the Reynolds number. Secondly we study 3D perturbations where we contribute to the bypass transition scenario and derive a possible mechanism for the hydrodynamic turbulence in accretion disks.

In Chapter 7 we have studied the resonant interactions of the MHD wave modes in shear flows. We have shown that the reciprocal transformation of the MHD wave modes may occur symmetrically. Depending on the wave-numbers, the mutual transformation of the Alfvén and fast magnetosonic waves is possible in strongly magnetized plasmas. Transformations of the Alfvén and the slow magnetosonic waves are expected in weakly magnetized plasmas. Plasmas with equal magnetic and thermal pressure ($\beta = 1$) may exhibit the transformations of all three MHD waves simultaneously. An important property is that this process is resonant

by nature: in contrast with the mode conversion phenomenon described in Chapters (3-6) the amplitude of waves generated during transformations do not generally grow when the shear parameter increases. It is quite the opposite. The resonance and effective exchange of energy between the MHD wave modes require low value of shear parameters. We have discussed astrophysical consequences of our study. Among these are applications in the solar atmosphere and wind, galactic spiral arms, pulsar magnetosphere and Earth's atmosphere.

Overall, the main frame of investigation throughout this thesis lies on the non-modal analysis of perturbations, recovering short time transient phenomena that originate from the non-normal character of the shear flows. We hope that our efforts contribute to a better understanding of the kinematically inhomogeneous astrophysical objects.

Bibliography

Afshordi, N., Mukhopadhyay, B., Narayan, R., 2005, *Turbulence in Hydrodynamic Accretion: Lagrangian Analysis of Energy Growth*, Astrophys. J. **629** 373.

Baggett, J. S., Driscoll, T. A. and Trefethen, L. N. 1995, *"A mostly linear model of transition to turbulence"*, Phys. Fluids, **7**, 833

Balbus, S. A., & Hawley, J. F. 1991, *"A powerful local shear instability in weakly magnetized disks. I - Linear analysis. II - Nonlinear evolution"*, Astrophys. J. **376**, 214.

Balbus, S. A. and Hawley, J. F., 1992, *"A Powerful local shear instability in weakly magnetized disks. IV. Nonaxisymmetric perturbations"*, Astrophys. J. **400**, 610.

Balbus, S. A., Hawley, J. F., and Stone, J. M. 1996, *"Nonlinear Stability, Hydrodynamical Turbulence, and Transport in Disks"*, Astrophys. J. **467**, 76.

Balbus, S. A., and Hawley, J. F. 1998, *"Instability, turbulence, and enhanced transport in accretion disks"*, Rev. Mod. Phys., **70**, 1.

Balmforth, N. J. 1992a, *"Solar pulational stability – I. Pulsation-mode thermodynamics"*, Mon. Not. R. Astr. Soc., **255**, 603.

Balmforth, N. J. 1992b, *"Solar pulational stability – III. Acoustical excitation by turbulent convection"*, Mon. Not. R. Astr. Soc., **255**, 639.

Bayly, B. J. 1986, *"Three-dimensional instability of elliptical flow"*, Phys. Rev. Lett., **57**, 2160.

Bayly, B.,J., Orszag, S. A. and Herbert, T. 1988, *"Instability mechanisms in shear-flow transition"*, Ann. Rev. Fluid Mech., **20**, 359.

Berry, M. V., 1990, *"Waves near Stokes lines"*, Proc. R. Soc. London Ser. A, **427**, 265.

Bodo, G., Poedts, S., Rogava, A. D., and Rossi, P., 2001, *"Spatial aspect of wave transformations in astrophysical flows"*, Astron. and Astrophys. **374**, 337.

Bottin, S., Dauchot, O., Daviaud, F. and Manneville, P. 1998, *"Experimental evidence of streamwise vortices as finite amplitude solutions in transitional plane Couette flow"*, Phys. Fluids, **10**, 2597.

Broberg, L. and Brosa, U. 1988, Z. Naturforschung Teil, **43a**, 697.

Butler, K. M. and Farrell, B. F. 1992, *"Three-dimensional optimal perturbations in viscous shear flow"*, Phys. Rev A, **4**, 1637

Chagelishvili, G. D., Khristov, T. S., Chanishvili, R. G., and Lominadze, J. G. 1993, Phys. Rev. E, **47**, 366.

Chagelishvili G. D., Rogava A. D., & Segal I. N. 1994, *"Hydrodynamic stability of compressible plane Couette flow"*, Phys. Rev. E **50**, R4283.

Chagelishvili, G. D. and Chkhetiani, O. G., 1995, *"Linear transformation of Rossby waves in shear flows"*, JETP Letters **62**, 301.

Chagelishvili, G. D., Chanishvili, R. G., & Lominadze, J. G. 1996, *"Physics of the amplification of vortex disturbances in shear flows"*, JETP Letters, **63**, 543.

Chagelishvili, G. D., Rogava, A. D., and Tsiklauri, D. G., 1996, *"Effect of Coupling and Linear Transformation of Waves in Shear Flows"*, Phys. Rev. E **53**, 6028.

Chagelishvili, G. D., Khujadze G. R., Lominadze, J. G. and Rogava, A. D. 1997, *"Acoustic waves in unbounded shear flows"*, Phys. Fluids **9**, 1955.

Chagelishvili, G. D., Rogava, A. D. and Tsiklauri, D. G., 1996a, *"Effect of coupling and linear transformation of waves in shear flows"*, Phys. Rev. E **53**, 6028.

Chagelishvili, G. D., Chanishvili, R. G., Lominadze, J. G. and Tevzadze, A. G. 1997, *"Magnetohydrodynamic waves linear evolution in parallel shear flows: Amplification and mutual transformations"*, Phys. Plasmas **4**, 259.

Chagelishvili, G. D., Tevzadze, A. G., Bodo, G. and Moiseev, S. S. 1997, *"Linear mechanism of wave emergence from vortices in smooth shear flows"*, Phys. Rev. Letters **79**, 3178.

Chagelishvili, G. D., Tevzadze, A. G. and Goossens, M. 1999, *"Generation of oscillations in solar convection zone: linear mechanism of mode conversion in shear flows"*, Proceedings of the conference: 9th European Meeting on Solar Physics, "Magnetic Fields and Solar Processes", Florence, Italy 1999, ESA SP-448, pp. 75-80.

Chagelishvili, G. D., Tevzadze, A. G. and Goossens, M. 2000, *"Linear dynamics of the solar convection zone: excitation of waves in unstably stratified shear flows"*, Proceedings of the conference: Waves in Dusty, Solar and Space Plasmas, Leuven, Belgium 2000, Ed. by F. Verheest, et al. AIP CP-**537**, pp. 200–207.

Chagelishvili, G. D., Tevzadze, A. G., Bodo, G, Rossi, P. and Gogoberidze, G. T. 2000, *"Vortex-wave conversion in high shear flows"*, Advances in Turbulence – VIII, Barcelona, Spain, 2000, Ed. by C. Dopazo, (CIMNE, 2000), pp. 737–740.

Chagelishvili, G. D., Chanishvili, R. G., Hristov, T. S. and Lominadze, J. G. 2002, *"A Turbulence Model in Unbounded Smooth Shear Flows: The Weak Turbulence Approach"*, JETP, **94**, 434.

Chagelishvili G. D., Zahn, J.-P., Tevzadze A. G., and Lominadze J. G., 2003, *"On hydrodynamic shear turbulence in Keplerian disks: via transient growth to bypass transition"*, Astron. Astrophys. **402**, 401.

Chapman, S. J. 2002, *"Subcritical transition in channel flows"*, J. Fluid Mech., **451**, 35.

Cowling, T. G., 1941, *"The non-radial oscillations of polytropic stars"*, Mon. Not. R. Astr. Soc., **101**, 367.

Coles, D. 1965, J. Fluid Mech., **21**, 385.

Cox, J. P., Cox, A. N., Olsen, K. H., King, D. S. and Eilers, D. D. 1966, *"Self excited radial oscillations in the stelllar Envelopes"*, Astrophys. J. **144**, 1038.

Craik, A. D. D. and Criminale, W. O., 1986, *"Evolution of Wavelike Perturbations in Shear Flows: A Class of Exact Solutions of the Navier-Stokes Equations,"*, Proc. R. Soc. of London, Ser. A **406**, 13.

Crighton, D. G., 1981, *"Acoustics as a brunch of fluid mechanics,"*, J. Fluid Mech. **106**, 261.

Criminale, W. O., and Drazin, P. G. 1990, *"The Evolution of Linearized Perturbations of Parallel Flows "*, Studies Appl. Math., **83**, 123.

Dauchot, O. and Daviaud, F., 1995, *"Streamwise vortices in plane Couette flow"*, Phys. Fluids, **7**, 901.

Didebulidze, G. G., 1997, *"Amplification/damping processes of atmospheric acoustic-gravity waves in horizontal winds with linear shear"*, Physics Letters A, **235**, 65.

Drury, L. O'C. 1980, *"On normal modes of gas sheets and discs"*, Mon. Not. Roy. Ast. Soc., **193**, 337.

Dubrulle, B., Marié, L., Normand, Ch., Richard, D., Hersant, F. and Zahn, J.-P., 2005, Astro. Astrophys. **429**, 1.

Dwarkadas, V. V., and Balbus, S. A. 1996, *"Gasdynamical Stability of Shear Flow in Spiral Arms of Disk Galaxies"* Astrophys. J. **467**, 87.

Eddington, A. S., 1941, *"On the Cepheid pulsation"*, Mon. Not. R. Astr. Soc., **101**, 182.

Farrell, B. F., and Ioannou, P. J. 1993, *"Perturbation growth in shear flow exhibits universality"*, Phys. Fluids, **9**, 883. Phys. Fluids A **5**, 2298.

Farrell, B. F., and Ioannou, P. J. 1994, *"Variance maintained by stochastic forcing of non-normal dynamical systems associated with linearly stable shear flows"*, Phys. Rev. Letters, **72**, 1188.

Ffowcs Williams, J. E. 1977, *"Aeroacoustics,"*, Ann. Rev. Fluid Mech. **9**, 447.

Fjørtøft, R. 1950, Geofis. Publ., **17**, 52.

Fridman A. M., 1989, *"On the Dynamics of a Viscous Differentially Rotating Gravitating Medium"*, Sov. Astr. Letters **15**, 487.

Friedman, J. L., and Schutz, B. F. 1978, *"Lagrangian perturbation theory of nonrelativistic fluids"*, Astrophys. J. **221**, 937.

Gebhardt, T. and Grossmann, S. 1994, *"Chaos transition despite linear stability"*, Phys. Rev. E, **50**, 3705.

Gogoberidze, G. T., Chagelishvili, G. D., Sagdeev, R. Z. and Lominadze, J. G., 2005, *"Linear coupling and overreflection phenomena of magnetohydrodynamic waves in smooth shear flows"*, Phys. Plasmas, **11**, 4672.

Goldreich, P.; Lynden-Bell, D. 1965, *"Spiral arms as sheared gravitational instabilities"*, MNRAS, **130**, 125.

Goldreich, P. and Keele, D. A. 1977, *"Solar seismology. I. The stability of the solar p-modes"*, Apstrophys. J. **212**, 243.

Goldreich, P. and Kumar, P. 1990, *"Wave generation by turbulent convection"*, Astrophys. J. **363**, 694.

Goldreich, P. Murray, N. and Kumar, P. 1994, *"Excitation of solar p-modes"*, Astrophys. J. **424**, 466.

Goldreich, P., and Tremaine, S. D. 1978, *"The excitation and evolution of density waves"*, Astrophys. J. **222**, 850.

Goodman, J., and Balbus, S. A. 2001, arXiv:astro-ph/0110229v1

Grossmann, S. 2000, *"The onset of shear flow turbulence"*, Rev. Mod. Phys., **72**, 603.

Gustavsson, L. H., and Hultgren, L. S. 1980, *"A resonance mechanism in plane Couette flow"*, J. Fluid Mech., **98**, 149.

Gustavsson, L. H., 1991, *"Energy growth of three-dimensional perturbations in plane Poiseuille flow,"*, J. Fluid Mech. **224**, 241.

Hawley, J. F., and Balbus, S. A 1991, *"A powerful local shear instability in weakly magnetized disks. I - Linear analysis. II - Nonlinear evolution"*, Astrophys. J. **376**, 223

Hawley, J. F., and Balbus, S. A 1992, *"A Powerful Local Shear Instability in Weakly Magnetized Disks. II. Nonlinear Evolution"*, Astrophys. J. **400**, 595.

Hawley, J. F., Gammie, C. F., and Balbus, S. A. 1995, *"Local Three-dimensional Magnetohydrodynamic Simulations of Accretion Disks"*, Astrophys. J. **440**, 742.

Henningson, D. S. and Reddy, S. C. 1994, *"On the role of linear mechanisms in transition to turbulence"*, Phys. Fluids, **6**, 1396.

Hill, F. et al. *" The solar acoustic spectrum and eigenmode parameters"*, Science **272**, 1292.

Howe, M. S. 1995, *"Contribution to the theory of aerodynamic sound, with application to excess jet noise and the theory of the flute,"*, Phys. Fluids, **9**, 883.

Ioannou, P. J., and Kakouris, A. 2001, *"Stochastic Dynamics of Keplerian Accretion Disks"*, Astrophys. J. **550**, 931.

Johnson, B. M., Gammie, C. F., 2005, *Linear Theory of Thin, Radially Stratified Disks*, Astrophys. J., **626**, 978.

Klahr, H., 2004, *The Global Baroclinic Instability in Accretion Disks. II. Local Linear Analysis*, Astrophys. J. **606**, 1070.

Klahr, H. H., and Bodenheimer, P. 2002, astro-ph/0211629

Kosovichev, A. G. *et al.* 1997, *"Structure and rotation of the solar interior: Initial results from the MDI medium-l program"*, Solar Phys. **170**, 43.

Landahl, M. T. 1980, *"A note of an algebraic instability of inviscid parallel shear flows"*, J. Fluid Mech. **98**, 243.

Lerche, I. and Parker, E. N. 1967, *"An initial-value oscillations of polytropic stars"*, Astrophys. J. **149**, 559.

Lighthill, J. 1978, *"Waves in fluids"*, Cambridge University Press, Cambridge.

Lighthill, M. J. 1952, *"On sound generated aerodynamically. I. Genral theory"*, Proc. R. Soc. London Ser. A **211**, 564.

Lighthill, M. J., 1954, *"On sound generated aerodynamically. II. Turbulence as a source of sound"*, Proc. R. Soc. London Ser. A **222**, 1.

Lilley, G. M., 1997, *"Generation of sound in a compressible mixing region,"*, AFAPL-TR-72-53, US Air Force Aero Propulsion Laboratory.

Lominadze, J. G., Chagelishvili, G. D. and Chanishvili, R. G., 1988, *"The Evolution of Nonaxisymmetric Shear Perturbations in Accretion Disks,"* Sov. Astron. Lett. **14**, 364 (1988).

Longaretti, P.-Y. 2002, *"On the Phenomenology of Hydrodynamic Shear Turbulence"*, Astrophys. J. **576**, 587.

Lord Kelvin (W. Thomson), 1887, Phil. Mag. **24**, Ser. **5**, 188.

Lynden-Bell, D. 1969, *"Galactic Nuclei as Collapsed Old Quasars"*, Nature, **223**, 690.

Lubow, S. H. and Spruit, H. C., 1995, *"Magnetic interchange instability in accretion disks"*, Astrophys. J. **445**, 337.

Mahajan, S. M., Machabeli, G. Z., and Rogava, A. D., 1997, *"Escaping Radio Emission from Pulsars: Possible Role of Velocity Shear"*, Astrophys. J. **479**, L129.

Marcus, S. and Press, W. H. 1997, *"The evolution of nonaxisymmetric shear perturbations in accretion disks,"*, J. Fluid Mech. **79**, 525.

Moffatt, K. 1967, *"The interaction of turbulence with strong wind shear"*, In: Atmospheric Turbulence and Radio wave Propagation, Ed. by A. M. Yaglom and V. I. Tatarskii, Nauka Press, Moscow.

Morkovin, M. V. 1993, in *"Instabilities and Turbulence in Engineering flows"*, Ed. Ashpis, D. E., Gatski, T. B. and Hirsh, R. S. (New York: Kluwer Academic Press).

Nakagawa, Y., and Sekiya, M. 1992, *"Wave action conservation, over-reflection and over-transmission of non-axisymmetric waves in differentially rotating thin discs with self-gravity"* Month. Not. Roy. Ast. Soc. **256**, 685.

Orr, W. McF. 1907a, Proc. R. Irish Acad. Sci. A **27**, 9.

Orr, W. McF. 1907b, Proc. R. Irish Acad. Sci. A **27**, 69.

Orszag, S. A. 1971, *"Galerkin Approximations to Flows within Slabs, Spheres, and Cylinders"*, Phys. Rev. Letters, **26**, 1100.

Orszag, S. A., and Kells, L. C. 1980, J. Fluid Mech., **96**, 161

Orszag, S. A., and Patera, A. T. 1980, *"Subcritical transition to turbulence in plane channel flows"*, Phys. Rev. Lett., **45**, 989.

Pao, S. P. 1973, *"Aerodynamic noise emission from turbulent shear layers,"*, J. Fluid Mech. **59**, 451.

Phillips, O. M., 1960, *"On the generation of sound by supersonic turbulent shear layers,"*, J. Fluid Mech, **9**, 883.

Poedts S., Rogava, A. D., and Mahajan, S. M, 1998, *"Shear-flow-induced Wave Couplings In The Solar Wind"*, Astrophys. J. **505**, 369.

Poedts S., Rogava, A. D., and Mahajan, S. M, 1999, *"Velocity Shear Induced Phenomena in Solar Atmosphere"*, Space Science Reviews **87**, 295.

Poedts, S., and Rogava, A. D., 2002 *"Does spiral galaxy IC 342 exhibit shear induced wave transformations?"*, Astron. Astrophys. **385**, 32.

Pringle, J. E. 1981, *"Accretion discs in astrophysics"*, Ann. Rev. Astron. Astrophys., **19**, 137.

Rayleigh, Lord 1880, Scientific Papers **1**, 474 (Cambridge Univ. press).

Reddy S. C., Schmidt P. J., and Henningson D. S., 1993, *"Pseudospectra of the Orr-Sommerfeld operator"*, SIAM J. Appl. Math. **53**, 15.

Reddy, S. C. and Henningson, D. S., 1993, *"Energy growth in viscous channel flows"*, J. Fluid Mech. **252**, 209.

Rempfer, D. 2003, *"Low-Dimensional Modeling and Numerical Simulation of Transition in Simple Shear Flows"*, Annu. Rev. Fluid Mech., **35**, 229.

Reshotko, E. 2001,, *"Transient growth: A factor in bypass transition"*, Phys. Fluids, **13**, 1067.

Richard, D., and Zahn, J.-P. 1999, *"Turbulence in differentially rotating flows. What can be learned from the Couette-Taylor experiment"*, Astron. Astrophys. **347**, 734.

Richard D. 2001, Thèse de doctorat, Université de Paris.

Rimmele, T. R., Goode, P. R., Harold, E., and Stebbins, R. T. 1995, *"Dark lanes in granulation and the excitation of solar oscillations"*, Astrophys. J. **444**, L119.

Rogava, A. D. and Mahajan, S. M. 1997, *"Coupling of sound and internal waves in shear flows"*, Phys. Rev. E **55**, 1185.

Rogava, A. D., Chagelishvili, G. D. and Mahajan, S. M. 1998, *"Shear Langmuir vortex: An elementary mode of plasma collective behavior"*, Phys. Rev. E **57**, 7103.

Rogava, A. D., Poedts, P., and Heirman, S., 1999, *"Are Galactic Magnetohydrodynamic Waves Coupled?"*, Mon. Not. Royal Ast. Soc. **307**, L31.

Rogava, A. D., Poedts, S., and Mahajan, S. M., 2000, *"Shear-driven Wave Oscillations in Astrophysical Flux Tubes"*, : Astron. Astrophys. **354**, 749.

Rogava, A. D., Poedts, S., and Mahajan, S. M., 2001, *"Acoustics of Kinematically Complex Shear Flows"*, J. Comp. Acoustics **9**, 869.

Ryu, D. and Goodman, J. 1992, *"Convective instability in differentially rotating disks"* Astrophys. J. **388**, 438.

Shakura, N. I., and Sunyaev, R. A. 1973, *"Black holes in binary systems. Observational appearance."*, Astron. Astrophys. **24**, 337.

Stein, R. F. 1967, *"Generation of acoustic and gravity waves by turbulence in an isothermal stratified atmosphere"*, Solar Physics **2**, 385.

Stein, R. F., 1968, *"Waves in the Solar Atmosphere. I. The Acoustic Energy Flux."*, Astrophys. J. **154**, 297.

Stone, J. M., Hawley J. F., Gammie, C. F., & Balbus, S. A. 1996, *"Three-dimensional Magnetohydrodynamical Simulations of Vertically Stratified Accretion Disks"*, Astrophys. J. **463**, 656.

Strous, L. H., Goode, P. R. and Rimmele, T. 2000, *"The dynamics of the excitation of solar oscillations"*, Astrophys. J. **535**, 1000.

Tevzadze, A. G. 1998, *"Emission of magnetosonic waves by vortices in high shear flows"*, Phys. Plasmas **5**, 1557.

Tevzadze, A. G., Chagelishvili, G. D., Chanishvili, R. G., Lominadze, J. G., and Zahn, J.-P., 2003, *"On hydrodynamic shear turbulence in stratified Keplerian disks: Transient growth of small-scale 3D vortex mode perturbations"*, Astron. Astrophys. **407**, 779.

Taylor, G. I. 1936, Proc. R. Soc. Lond. A, **157**, 546.

Trefethen, L. N., Trefethen, A. E., Reddy, S. C., and Discoll, T. A. 1993, *"Hydrodynamic stability without eigenvalues"*, Science, **261**, 578.

Trefethen, L. N. 1997, *"Pseudospectra of linear operators"*, SIAM Review **39**, 383.

Umurhan, O. M., Regev, O. 2004, *Hydrodynamic stability of rotationally supported flows: Linear and nonlinear 2D shearing box results*, Astron. Astrophys. **427**, 855.

Urpin, V. 2002, *"A comparison study of the vertical and magnetic shear instabilities in accretion discs"*, Astron. Astrophys. **404**, 397.

Van Atta, C. W. 1966, J. Fluid Mech., **25**, 495

Waleffe, F. 1997, *"On a self-sustaining process in shear flows"*, Phys. Fluids, **9**, 883.

Wendt, F. 1933, Ing. Arch., **4**, 577.

Yecko, P. A., 2002, *Accretion disk instability revisited. Transient dynamics of rotating shear flow*, Astron. Astrophys. **425**, 385.

Appendix A.

Dynamics of SFH in the stratified shear flow

In this appendix we give the coefficients of the Eqs. (5.32) - (5.33) given in the Chapter 5. For this purpose first we introduce the following notations:

$$W_1^2(t) = c_s^2\bar{k}^2(t) - N_B^2\frac{k_\perp^2(t)}{\bar{k}^2(t)} + 2A^2\frac{k_x^2}{\bar{k}^2(t} - 4A^2\frac{k_x^2k_y^2(t)\bar{k}_z^2}{k_\perp^2(t)\bar{k}^4(t)}, \qquad (A.1)$$

$$W_2^2(t) = N_B^2\frac{k_\perp^2}{\bar{k}^2(t)} + 2A^2\frac{k_x^2\bar{k}_z^2}{k_\perp^2(t)\bar{k}^2(t)}, \qquad (A.2)$$

$$f_1(t) = 2A\frac{k_xk_y(t)}{\bar{k}^2(t)}, \qquad (A.3)$$

$$f_2(t) = 2A\frac{k_xk_y(t)\bar{k}_z^2}{k_\perp^2(t)\bar{k}^2(t)}, \qquad (A.4)$$

$$a_1(t) = -N_B^2 + 2A^2\frac{k_x^2}{k_\perp^2(t)}, \qquad (A.5)$$

$$a_2(t) = 2A\frac{k_xk_y(t)}{k_\perp^2(t)}, \qquad (A.6)$$

$$b_1(t) = N_B^2\frac{k_\perp^4}{k^4} + 4A^2k_x^2\bar{k}_z^2\frac{k_y^2(t) - k_x^2}{\bar{k}^6(t)} + 4A^2\frac{k_x^4\bar{k}_z^4}{k_\perp^2(t)\bar{k}^6(t)}, \qquad (A.7)$$

$$b_2(t) = -2Ak_xk_y(t)\frac{\bar{k}_z^2}{\bar{k}^4(t)}. \qquad (A.8)$$

We also define small parameters $\epsilon_1(t)$ and $\epsilon_2(t)$:

$$\epsilon_1(t) = N_B^2 \frac{\Omega_c^2(t) - \omega_c^2(t)}{\Omega_c^4(t)}, \tag{A.9}$$

$$\epsilon_2(t) = \frac{\Omega_c^2(t) - \omega_c^2(t)}{N_B^2}, \tag{A.10}$$

which relate pressure and entropy perturbations with characteristic physical variables of the acoustic wave and convective mode perturbations (see Eqs. 5.22 - 5.26):

$$p(t) = \Phi_s(t) + \epsilon_1(t)\Phi_c(t), \tag{A.11}$$

$$\psi(t) = \Phi_c(t) + \epsilon_2(t)\Phi_s(t). \tag{A.12}$$

Hence, using variables defined in Eqs. (A.1) - (A.12) we may derive the explicit form of the coefficients in the Eqs. (5.32) - (5.33):

$$\alpha_1(t) = \frac{1}{1-\epsilon_1\epsilon_2}\left(f_1 + \epsilon_1 b_2 - \epsilon_2 a_2 - \epsilon_1\epsilon_2 f_2 - 2\epsilon_1\frac{\mathrm{d}\epsilon_2}{\mathrm{d}t}\right), \tag{A.13}$$

$$\alpha_2(t) = \frac{1}{1-\epsilon_1\epsilon_2}\left(W_1^2 - \epsilon_1\epsilon_2 W_2^2 + \epsilon_1 b_1 - \epsilon_2 a_1 - \frac{\mathrm{d}\epsilon_2}{\mathrm{d}t}(a_2 + \epsilon_1 f_2) - \epsilon_1\frac{\mathrm{d}^2\epsilon_2}{\mathrm{d}t^2}\right), \tag{A.14}$$

$$\alpha_3(t) = \frac{1}{1-\epsilon_1\epsilon_2}\left(-a_2 + \epsilon_1 f_1 - \epsilon_1 f_2 + \epsilon_1^2 b_2 + 2\frac{\mathrm{d}\epsilon_1}{\mathrm{d}t}\right), \tag{A.15}$$

$$\alpha_4(t) = \frac{1}{1-\epsilon_1\epsilon_2}\left(\epsilon_1(W_1^2 - W_2^2) - a_1 + \epsilon_1^2 b_1 + \frac{\mathrm{d}\epsilon_1}{\mathrm{d}t}(\epsilon_1 b_2 + f_1) + \frac{\mathrm{d}^2\epsilon_1}{\mathrm{d}t^2}\right), \tag{A.16}$$

$$\beta_1(t) = \frac{1}{1-\epsilon_1\epsilon_2}\left(f_2 - \epsilon_1 b_2 - \epsilon_2 a_2 + \epsilon_1\epsilon_2 f_1 - 2\epsilon_2\frac{\mathrm{d}\epsilon_1}{\mathrm{d}t}\right), \tag{A.17}$$

$$\beta_2(t) = \frac{1}{1-\epsilon_1\epsilon_2}\left(W_2^2 - \epsilon_1\epsilon_2 W_1^2 - \epsilon_1 b_1 + \epsilon_2 a_1 - \frac{\mathrm{d}\epsilon_1}{\mathrm{d}t}(b_2 + \epsilon_2 f_1) - \epsilon_2\frac{\mathrm{d}^2\epsilon_1}{\mathrm{d}t^2}\right), \tag{A.18}$$

$$\beta_3(t) = \frac{1}{1-\epsilon_1\epsilon_2}\left(-b_2 + \epsilon_2 f_2 - \epsilon_2 f_1 + \epsilon_2^2 a_2 + 2\frac{\mathrm{d}\epsilon_2}{\mathrm{d}t}\right), \tag{A.19}$$

$$\beta_4(t) = \frac{1}{1-\epsilon_1\epsilon_2}\left(\epsilon_2(W_2^2 - W_1^2) - b_1 + \epsilon_2^2 a_1 + \epsilon_2\frac{\mathrm{d}\epsilon_2}{\mathrm{d}t}a_2 + \frac{\mathrm{d}\epsilon_1}{\mathrm{d}t}f_2 + \frac{\mathrm{d}^2\epsilon_2}{\mathrm{d}t^2}\right), \tag{A.20}$$

$$\xi_1(t) = 2Ac_s^2\frac{k_x^2}{k_\perp^2}\left(1 + \frac{\bar{k}_z^2}{k^2}\epsilon_1\right), \tag{A.21}$$

$$\xi_2(t) = -2Ac_s^2\frac{k_x^2\bar{k}_z^2}{k_\perp^2 k^2}\left(1 + \frac{k^2}{\bar{k}_z^2}\epsilon_2\right). \tag{A.22}$$

Note, that in the the shearless limit, i.e. when $A = 0$ these coefficients tend to the values which lead the Eqs. (5.41), (5.42) into the Eqs. (5.27), (5.28):

$$\alpha_1(t) = \alpha_3(t) = \alpha_4(t) = 0 \quad \text{and} \quad \alpha_2(t) = \omega_s^2. \tag{A.23}$$

$$\beta_1(t) = \beta_3(t) = \beta_4(t) = 0 \quad \text{and} \quad \beta_2(t) = \omega_c^2. \tag{A.24}$$